

HDL

239

Copy
RM L58E26

~~CONFIDENTIAL~~

1502
1411
20 AUG 1958

0144752
2524752



TECH LIBRARY KAFB, NM

NACA RM L58E26

3481



RESEARCH MEMORANDUM

LONGITUDINAL AND LATERAL AERODYNAMIC CHARACTERISTICS AT
COMBINED ANGLES OF ATTACK AND SIDESLIP OF A
GENERALIZED MISSILE MODEL HAVING A
RECTANGULAR WING AT A MACH
NUMBER OF 4.08

By Fred M. Smith, Edward F. Ullmann,
and Robert W. Dunning

Langley Aeronautical Laboratory
Langley Field, Va.

~~CONFIDENTIAL~~
~~This document contains neither recommendations nor conclusions of the National Aeronautics and Space Administration. It is the property of NASA and is loaned to your agency; it and its contents are not to be distributed outside your agency without the express permission of the Administrator. The dissemination or revelation of which in any manner to an unauthorized person is prohibited by law.~~

NATIONAL ADVISORY COMMITTEE
FOR AERONAUTICS

WASHINGTON

August 14, 1958

~~CONFIDENTIAL~~

Classification cancelled (or changed to CLASSIFIED FIG D)
By Authority of A.H.S.P. Tech. P.A. Assignment # FF39
(OFFICER AUTHORIZED TO CHANGE)
By 16 MAR 61
NAME AND
S. I. O. F. OFFICER MAKING CHANGE) K. J. M.
By 16 MAR 61
NAME AND
PAGE

NATIONAL ADVISORY COMMITTEE FOR AERONAUTICS

RESEARCH MEMORANDUM

LONGITUDINAL AND LATERAL AERODYNAMIC CHARACTERISTICS AT
COMBINED ANGLES OF ATTACK AND SIDESLIP OF A
GENERALIZED MISSILE MODEL HAVING A
RECTANGULAR WING AT A MACH
NUMBER OF 4.08*

By Fred M. Smith, Edward F. Ullmann,
and Robert W. Dunning

SUMMARY

An investigation has been conducted in the Langley 9- by 9-inch Mach number 4 blowdown jet on a generalized body-wing-tail missilelike configuration to determine the source of the adverse rolling moment due to yaw experienced by this type of configuration having lifting surfaces and ventral and dorsal tail surfaces. At the same time it was desirable to determine the contribution of the model components (body, wing, and tail) to the aerodynamic characteristics of the complete configuration and to determine whether or not a simple method exists for predicting the longitudinal and lateral aerodynamic characteristics at combined angles of attack and sideslip. It was found that the adverse rolling moment results from unequal pressures on upper and lower fins induced by the wing flow fields at angle of attack, and that in general available engineering methods adequately predict the aerodynamic forces but are less accurate in predicting centers of pressure.

INTRODUCTION

In a number of flight tests of missiles having lifting surfaces and dorsal and ventral tail surfaces, it has been found that a fairly large adverse rolling moment due to yaw (positive $C_{l\beta}$) is imposed on the missiles at combined angles of attack and sideslip. In an effort to determine the cause of this adverse rolling moment, as well as the effects of the various elements of a body-wing-tail configuration upon the rolling

*Title, Unclassified.

moment, various combinations of the components of a generalized missile-like configuration were tested in a blowdown jet.

An additional purpose of the investigation was to determine the adequacy of available engineering methods in predicting the longitudinal and the lateral characteristics for a body alone; a body with one, two, three, or four trapezoidal tails or one or two triangular tails; and a body with a wing in two longitudinal positions and with the aforementioned tail arrangements.

The tests were conducted at a Mach number of 4.08 and an average Reynolds number of 1.6×10^6 , based on the maximum body diameter. Normal force, pitching moment, rolling moment, side force, and (for several configurations) yawing moment were obtained for an angle-of-attack range of 0° to 15° for configurations without lifting surfaces and proportionately smaller ranges for those with lifting surfaces, for angles of sideslip of 0° to 5° .

SYMBOLS

The forces and moments are referred to the body axes, and the reference center of moments is located at 51.4 percent body length (fig. 1).

- A body frontal area, $\pi d^2/4$
c wing chord
 C_l rolling-moment coefficient, M_X/qAd
 C_m pitching-moment coefficient, M_Y/qAd
 C_n yawing-moment coefficient, M_Z/qAd
 C_N normal-force coefficient, $-F_Z/qA$
 C_Y side-force coefficient, F_Y/qA
 $C_{l\beta}$ rate of change of rolling-moment coefficient with angle of sideslip, $\partial C_l / \partial \beta$
 $C_{n\beta}$ rate of change of yawing-moment coefficient with angle of sideslip, $\partial C_n / \partial \beta$

$C_{Y\beta}$ rate of change of side-force coefficient with angle of sideslip,
 $\partial C_Y / \partial \beta$

d maximum body diameter

F_Y force along Y-axis

F_Z force along Z-axis

l body length

M_X moment about X-axis

M_Y moment about Y-axis

M_Z moment about Z-axis

q free-stream dynamic pressure

R radius of curvature

u component of free-stream velocity along X-axis

v component of free-stream velocity along Y-axis

V free-stream velocity

w component of free-stream velocity along Z-axis

x longitudinal distance from body nose to center of pressure

α angle of attack, $\tan^{-1} w/u$

β angle of sideslip, $\sin^{-1} v/V$

CONFIGURATION DESIGNATIONS

B body

H horizontal tail symmetrical about XZ-plane

V_l lower vertical tail

V_u upper vertical tail
 W_f wing in forward position
 W_r wing in rearward position

Subscripts:

trap trapezoidal plan form
tri triangular, or half-delta, plan form

An example of the designations is as follows: $BW_f(HV_lV_u)_{\text{trap}}$ represents a body with wing in the forward position and horizontal, upper vertical, and lower vertical trapezoidal tails.

APPARATUS AND TESTS

The tests were conducted in the Langley 9- by 9-inch Mach number 4 blowdown jet. A description of the jet and a test-section flow calibration is presented in reference 1. The stagnation pressure, which was recorded during each run along with the temperature, was controlled by a pressure-regulating valve. The pressure was held at approximately 13 atmospheres and the temperature during the runs dropped from 75° F to approximately 30° F. This pressure and temperature range gave an average Reynolds number of 1.6×10^6 based on maximum body diameter. The tests were run with air having less than 5×10^{-6} pounds of water vapor per pound of dry air. The test-section static temperature and pressure did not reach the point where liquefaction of air would be expected.

A four-component internal strain-gage balance was used to obtain normal force, pitching moment, rolling moment, and side force for all the configurations, and yawing moment was obtained for several configurations with another balance. Combined angles of attack and sideslip were set by using a combination lens-prism embedded in the model wall to reflect and focus a spot from a light source onto a previously calibrated screen. In this way true angles were set directly. The angle-of-attack range was limited by the design loads of the balance and varied from 0° to 15° for configurations with no lifting surfaces to a minimum range of 0° to 5° for the complete configurations. The nominal angle-of-sideslip range was 0° to 5° for all tests.

[REDACTED]
MODELS

A four-caliber tangent ogive nose was combined with an eight-caliber cylinder to form the body for all configurations. Added to this body in two longitudinal positions was a wing with a rectangular plan form, an aspect ratio of 1.67, and a 3.3-percent-thick wedge-slab section. (See fig. 2 for all model components.) The model was tested with various vertical and horizontal trapezoidal-tail arrangements and various vertical triangular-tail arrangements (fig. 3). The trapezoidal and triangular tails had the same exposed plan-form area and same wedge-slab section, but were dissimilar in plan form, aspect ratio, and thickness ratio.. Complete details are given in figures 2 and 3 and table I.

PRECISION OF DATA

The maximum probable uncertainties involved in measuring the angles, forces, and moments and in determining the aerodynamic coefficients of the present tests are given in the following table:

α , deg	±0.1
β , deg	±0.1
C_N	±0.020
C_m	±0.020
C_l	±0.003
C_n	±0.040
C_y	±0.006

METHODS OF PREDICTION

Longitudinal

The normal force and center of pressure at $\beta = 0^\circ$ for the ogive-cylinder body of this investigation were estimated by the method of Grimminger, Williams, and Young (ref. 2), which is simply a correlation of all the experimental normal-force data available for bodies of revolution in supersonic flow at the time the correlation was made. The method has been used with very good results in references 3 and 4. In the present investigation this method was used for the body-alone results and for the contribution of the body when combined with a wing or a horizontal tail, or both.

[REDACTED]

~~CONFIDENTIAL~~

NACA RM L58E26

Two-dimensional shock-expansion theory (ref. 5), which has been found in references 6 and 7 to give very good lift predictions at the present Mach number for three-dimensional wings having attached leading-edge shocks, was used successfully to predict the wing-alone normal force and center of pressure for the wing of this investigation. It was not unreasonable, therefore, to use the shock-expansion theoretical predictions for the normal-force-curve slopes and centers of pressure of the wing and horizontal tail as a base in calculating the interference forces according to the theory of Pitts, Nielsen, and Kaattari in reference 8. The method of reference 8 is a modification of slender-body theory but it is suggested in the reference that it may be applied to configurations other than slender bodies if a realistic normal-force-curve slope is used for the wing. This was done with good results in references 3, 4, and 6. The method was therefore used to predict the interference effects of the wing on the body and on the tail, and the interference effects of the body on the wing and on the tail, for all the combination configurations of this investigation.

Lateral

The basic lateral force and moment predictions were made by essentially the same methods as the longitudinal predictions. The method of reference 2 was used to calculate the body side force, the method of reference 8 was used to compute the interaction side force of the body in the presence of the vertical tail, and shock-expansion theory with several modifications was used to compute the force on the vertical tails. Since for close-coupled wing and tail configurations of the present type the tails lie in the path of the wing shock and expansion fields, it was necessary to compute boundaries and Mach numbers for these wing fields in order to estimate the tail forces.

In order for the force on the tail to be computed, the tail was first divided into a finite number of horizontal strips and then, to account for the body sidewash, the angle of incidence of each strip was varied across the span according to the equation of reference 9:

$$\alpha' = \alpha \left[1 + \left(\frac{a}{x} \right)^2 \right], \text{ where } \alpha' \text{ is the modified angle of incidence, } \alpha \text{ is the indicated angle of incidence, } a \text{ is the body radius, and } x \text{ is the perpendicular distance from the body center line.}$$

The shock-expansion pressures were then obtained by using the computed angle of incidence for each strip along with the corresponding Mach number of the wing flow field. When the force for each strip had been determined a summation was made of the tail forces and then combined with the other forces of the configuration. This process was repeated for other configuration angles of attack until the desired range was covered.

~~CONFIDENTIAL~~

After determining the forces it was a simple matter to determine the moments, both yawing and rolling, by combining an estimated center of pressure for each element of the configuration (including tail strips) with its force. The predictions in final form are $C_y\beta$, $C_l\beta$, and $C_{n\beta}$ plotted against α , along with the experimental results. Some of the results of this method are also shown in reference 10 at Mach numbers of 4.06 and 6.86.

RESULTS AND DISCUSSION

Longitudinal Characteristics

The basic experimental longitudinal coefficients are presented in figures 4 to 9 as functions of angle of attack for representative angles of sideslip and in figures 10 to 12 as functions of angle of sideslip for representative angles of attack. A complete listing of the experimental results (except for wing-alone data, fig. 8) may be found in table II, and an index of the figures is presented as appendix A.

Effects of angle of sideslip.— In general, the normal force for configurations having a wing is only slightly affected by changing the angle of sideslip from 0° to 4° or 5° . (See figs. 4 to 6 and 10 to 12.) With the wing removed, however, a small but consistent increase is observed in C_N with an increase in β from 0° to 4° or 5° . An explanation for this normal-force increase, which is dependent not on the increased resultant angle but on the nonlinear normal-force curve and the resolution of the resultant forces for bodies of revolution, is given in appendix B.

The pitching moment is affected to a greater extent by the change in β . One possible explanation for this change in pitching moment with increased β is the increased loading on the body due to interference between the body and vertical tail, since the greatest effects are indicated by the configurations having unsymmetrical vertical tails. (See figs. 4(b), (c), (f), and (g), and 5(b) and (c).)

Effects of tail configuration.— A careful examination of figures 4 to 6 reveals that, with one exception, changes in tail arrangement or plan form had very little effect on the normal force. The one exception was the addition or removal of the lifting horizontal tail. Figure 7 shows a sizable shift in the pitching-moment curves with a change in tail configuration from an upper fin to a lower, but there appear to be no significant changes in the slopes. The shift is easily explained by considering the drag force produced by the wedge leading edge of either the upper or lower fin, acting eccentric to the body axis and causing the

initial pitching-moment increment at $\alpha = 0^\circ$. The two tail plan forms tested contributed like effects on the pitching moment.

Effects of wing position.- The only effect of changing the wing position was the change in pitching moment due to moving the point of application of the wing normal force.

Comparison with theory.- Figure 8 shows the experimental results for wing-alone tests compared with two-dimensional shock-expansion theory for normal force and pitching moment. Because of the small values of pitching moment involved, slight inaccuracies in the center-of-pressure prediction cause rather large percentagewise differences in pitching moment. The normal-force prediction is within 5 percent of the experimental results for most of the angle-of-attack range.

Comparisons of experimental and theoretical normal force and pitching moment are shown in figure 9 for various combinations of the wing, body, and cruciform trapezoidal tail. The predictions were quite adequate for the normal force when the following methods were used: two-dimensional shock expansion for the wing and horizontal-tail lift, the method of reference 8 for body upwash, and the hypersonic approximation of reference 2 to predict the nonlinear lift of the body. The predictions for the pitching moment (fig. 9(b)) were not as good as those for the normal force, indicating that the center-of-pressure predictions for the wing and its interactions were not as accurate as the force predictions. The predictions for the body and body-tail configurations were within approximately 10 percent of the experimental values, but in some instances the body-wing and body-wing-tail predictions showed more than a 30-percent variation from experiment.

Lateral Characteristics

The basic lateral data are presented in figures 10 to 12 along with the longitudinal data against angle of sideslip for representative angles of attack. For ease of discussion, configurations with and without the wing will be treated separately.

Wing-off configurations.- The wingless configurations in figures 10 to 12 show no noteworthy trends in C_y or C_l when plotted against β . When plotted against α , however, as shown in figure 13 for $\beta = 4^\circ$, C_y and C_l both indicate a decrease in effectiveness with increasing α for the body with upper tail, whereas a slight increase in effectiveness was indicated for the configurations with a lower tail. It was assumed at first inspection that this was the result of the low-aspect-ratio upper fins being shielded by the body at angles of attack above zero. Figure 14 indicates, however, that the shielding by the body could not

possibly account for all the loss in effectiveness because the side force for the body with upper triangular tail is actually less than that for the body alone at the higher angles of attack, and the rolling moment actually reverses sign at these high angles. The results for the body with upper trapezoidal tail (fig. 15), although not showing the C_l reversal, do show the decreased effectiveness in C_l for the higher angles of attack. The loss in effectiveness and the reversal can be attributed to the body vortices shown in profile in figure 16, which consists of schlieren pictures of the flow over the body alone, body with the upper triangular tail, and body with wing at several angles of attack.

In an attempt to gain a better understanding of this rolling-moment phenomenon, the incremental roll produced on a yawed body by adding an upper vertical tail was obtained and is presented in figure 17 as a function of the vertical location of the vortex core in percent tail span. It should be noted here that because of the differences in span of the triangular and trapezoidal tails, the same vortex location in terms of percent tail span is obtained at different angles of attack (and therefore different vortex strengths) and the moment areas of the tails are different. Both of these characteristic differences should tend to magnify the roll contribution of the trapezoidal tail but, as shown in figure 17, the roll contributions of both tails are approximately the same. This similarity in rolling moment for the two tails indicates that at higher angles of attack, when the vortices reach the tip of the trapezoidal tail, the rolling moment might also reverse sign.

The effectiveness in $C_{y\beta}$ and $C_{l\beta}$ for the two tail plan forms is shown in figure 18. The effectiveness of the tails is presented as the ratio of the incremental $C_{y\beta}$ or $C_{l\beta}$ contributed by the tail at $\alpha \geq 0^\circ$ to that contributed at $\alpha = 0^\circ$. Note the negative effectiveness of the upper triangular tail at the higher angles of attack, indicating a decrement instead of an increment in $C_{y\beta}$ and $C_{l\beta}$ contributed by the tail.

Figures 10 to 12 show the same increase in side force for the wingless configurations at combined angles of sideslip and attack as was pointed out for the normal force in the discussion of longitudinal characteristics. The discussion in appendix B also applies in this instance.

Wing-on configurations. - The most significant change in the lateral characteristics caused by adding a wing is the large increase in rolling moment for the configurations having symmetrical vertical tails. (See figs. 10(a) and 11(a).) In general, the addition of the wing provides an

increment in rolling moment with increasing angle of attack for all configurations with a vertical tail surface but has very little effect on side force. (See the remaining parts of figs. 10 and 11.) Figure 19 shows C_y , C_l , and C_n at $\alpha = 4^\circ$ for the components of a configuration consisting of a body, a wing, and a symmetrical vertical tail including their interactions. It is shown that for this type of configuration the body and the tail actually produce most of the side force and that the small wing contribution actually opposes the resultant force. The tail alone contributes practically all the yawing moment, being opposed by the contribution of the body. The rolling moment is provided by the flow field of the wing over the tail. This is the adverse roll due to yaw to which missilelike configurations with close-coupled wing and symmetrical vertical tails are subjected.

The wing position affects the lateral characteristics only to the extent that it increases or reduces the vertical-tail area exposed to the wing shock and expansion fields. Examples of this wing-position effect are shown in figures 10 and 11, where it can be seen that the trapezoidal tail, which has a higher aspect ratio, experiences larger changes in rolling moment than the triangular tail owing to the greater changes in exposed area. Figure 20, which is presented to demonstrate the effects of angle of attack on a number of configurations at $\beta = 4^\circ$, adequately shows the reduced C_l for the configuration with trapezoidal tails with the wing in the rear position. The rolling moment for the triangular tails and the side force for all the configurations in figure 20 are generally unchanged by the alternate wing position of this investigation. Figure 20 also indicates that an increase in angle of attack generally provides an increment in C_l and an increment in negative C_y .

The efficiencies in $C_{y\beta}$ and $C_{l\beta}$ for the various vertical tails immersed in the flow field from the wing in two longitudinal positions are given in figure 21. These efficiencies (the ratios of the incremental $C_{y\beta}$ or $C_{l\beta}$ produced by the vertical tails in the presence of the body and wing to that produced by the same tails in the presence of the body without the wing) give an indication of the effectiveness of the tails in the presence of the wing flow fields through an angle-of-attack range. Figure 21 indicates that the upper trapezoidal tail generally loses some effectiveness with increasing angle of attack, especially with the wing in the rearward position when the low pressure field from the wing reduces the force on the tails. The upper triangular tail, however, actually gains effectiveness with increasing α when the wing is in the forward position. This is the result of the low-pressure wing flow field moving off the lower-aspect-ratio tail and exposing the tail to the higher pressure flow behind the trailing-edge shock.

Comparison with theory.-- Predictions of $C_{l\beta}$, $C_{n\beta}$, and $C_{Y\beta}$ for the body with wing and trapezoidal tails are shown in figure 22(a); $C_{l\beta}$ and $C_{Y\beta}$ only are given for the configurations with triangular tails (fig. 22(b)). In general, the trends of the experimental $C_{l\beta}$ are adequately predicted, and except for the configuration with two trapezoidal tails, the experimental values are generally predicted within 15 to 20 percent. The predictions for $C_{Y\beta}$ were always within 10 percent of the experimental values. It would seem that the forces can be estimated with much more accuracy than the centers of pressure, since the predictions for $C_{Y\beta}$ are much better than those for $C_{l\beta}$. The predictions for $C_{n\beta}$ are also rather inaccurate; in all cases they are higher than the experimental results.

CONCLUSIONS

A wind-tunnel investigation has been made for a number of body-tail and body-wing-tail missilelike configurations at a Mach number of 4.08 at combined angles of attack and sideslip, and the experimental results have been compared with engineering methods of prediction. The following conclusions were drawn regarding the longitudinal and lateral aerodynamic characteristics of the configurations:

1. Engineering methods exist which give reasonable approximations of the forces for both the longitudinal and lateral results of this investigation but less accurate approximations for the centers of pressure.
2. For angles of attack greater than zero at a given angle of sideslip, the major sources of adverse incremental rolling moment are (a) the wing shock and expansion flow fields acting on the vertical tail and (b) the shed body vortices acting on the upper vertical tail.

Langley Aeronautical Laboratory,
National Advisory Committee for Aeronautics,
Langley Field, Va., May 12, 1958.

APPENDIX A

INDEX OF FIGURES

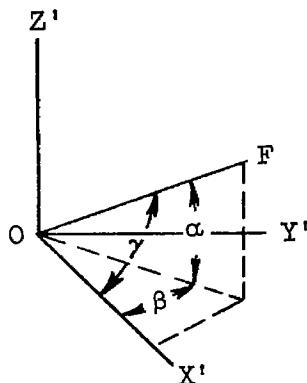
Figure	Description
1	Axis system for tests with direction of forces and moments
2	Schematic diagram of model showing important dimensions
3	Schematic diagram of various tail configurations of tests
4	C_N and C_m against α ($\beta = 0^\circ$ and 4° or 5°) for all configurations having trapezoidal tails
5	C_N and C_m against α ($\beta = 0^\circ$ and 4° or 5°) for all configurations having triangular tails
6	C_N and C_m against α ($\beta = 0^\circ$ and 4°) for configurations having no tail
7	C_m against α ($\beta = 0^\circ$) showing effects of tail arrangements
8	Experimental and theoretical C_N and C_m against α for wing-alone test
9	Experimental and theoretical C_N and C_m against α ($\beta = 0^\circ$) for various combinations of a body, wing, and cruciform trapezoidal tail
10	C_l , C_y , C_n (when available), C_m , and C_N against β ($\alpha = 0^\circ$ and 4°) for all configurations having trapezoidal tails
11	C_l , C_y , C_m , and C_N against β ($\alpha = 0^\circ$ and 4°) for all configurations having triangular tails
12	C_l , C_y , C_n , C_m , and C_N against β ($\alpha = 0^\circ$ and 4°) for configurations having no tail
13	C_y and C_l against α ($\beta = 4^\circ$) for all configurations having no wing

Figure	Description
14	C_Y and C_l against β ($\alpha = 0^\circ, 8^\circ, 12^\circ, 14^\circ$, and 15°) for body alone and body with upper triangular tail to show effects of body vortices
15	C_Y and C_l against β ($\alpha = 0^\circ, 8^\circ$, and 15°) for body with upper trapezoidal tail to show effects of body vortices
16	Schlieren photographs of flow for body alone, body with triangular tails, and body with forward wing at angles of attack of $0^\circ, 5^\circ, 10^\circ$, and 15°
17	Incremental C_l due to α against percent of tail span ($\beta = 1^\circ$ and 5°) for two configurations of body and upper vertical tail
18	Tail effectiveness at α in $C_{Y\beta}$ and $C_{l\beta}$ against α for several tails in combination with a body of revolution
19	Sources of C_Y , C_l , and C_n against β ($\alpha = 4^\circ$) among the various elements of a body with wing and vertical tails
20	C_Y and C_l against α ($\beta = 4^\circ$) for several body-wing and body-wing-tail configurations
21	Tail efficiency in $C_{Y\beta}$ and $C_{l\beta}$ against α for several tail arrangements in combination with a body of revolution and a wing
22	Experimental and theoretical $C_{l\beta}$, $C_{n\beta}$, and $C_{Y\beta}$ against α for a body-wing-tail configuration having several tail arrangements
23	Normal-force and side-force characteristics for a body of revolution at combined angles of attack and sideslip, illustrating equations of appendix B

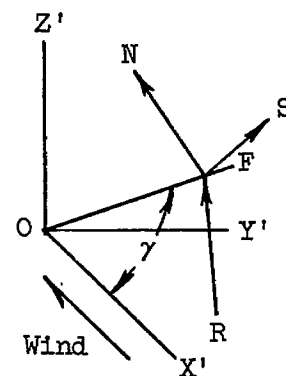
APPENDIX B

FORCES ON A BODY OF REVOLUTION AT COMBINED
ANGLES OF ATTACK AND SIDESLIP

In the rectangular coordinate system of sketch (a) the point F represents the nose of a body of revolution at an angle of attack α



Sketch (a)



Sketch (b)

and an angle of sideslip β . The angle γ resulting from these combined angles and limited by the body FO and the X' (wind) axis can be expressed as

$$\gamma = \cos^{-1} \cos \alpha \cos \beta \quad (1)$$

Curves of this equation are shown in figure 23(a).

The resultant force (RF in sketch (b)) imposed on the body at angle of incidence γ by the airstream can be resolved into two components, NF (normal force) and SF (side force). Upon solving for these two components the normal force is found to be

$$NF = RF \frac{\cos \beta \sin \alpha}{\sin \gamma} \quad (2)$$

and the side force is

$$SF = RF \frac{\sin \beta}{\sin \gamma} \quad (3)$$

If the variation of force on the body is linear with changing angle, then

$$\frac{\partial(RF)}{\partial\gamma} = \frac{\partial(NF)}{\partial\alpha}$$

and

$$(NF)_{\beta \geq 0} = \frac{\partial(NF)}{\partial\alpha} \gamma \frac{\cos \beta \sin \alpha}{\sin \gamma} \quad (4)$$

For a more general form of the equation, the ratio of the normal force for a body with $\beta \geq 0^\circ$ to that for a body with $\beta = 0^\circ$ becomes in coefficient form

$$\frac{(C_N)_{\beta \geq 0}}{(C_N)_{\beta=0}} = \frac{C_{N_\alpha} \gamma}{C_{N_\alpha} \alpha} \frac{\cos \beta \sin \alpha}{\sin \gamma}$$

or

$$\frac{(C_N)_{\beta \geq 0}}{(C_N)_{\beta=0}} = \frac{\gamma \cos \beta \sin \alpha}{\alpha \sin \gamma} \quad (5)$$

and the corresponding ratio for the side force becomes

$$\frac{(C_Y)_{\alpha \geq 0}}{(C_Y)_{\alpha=0}} = \frac{\gamma \sin \beta}{\beta \sin \gamma} \quad (6)$$

The ratios of equations (5) and (6) are plotted in figures 23(b) and (c), respectively, which show that the normal force for a constant α decreases with increasing β and the side force for a constant β increases with increasing α .

The nonlinear force curve, more characteristic of a body of revolution than the previously assumed linear force variation, is shown in figure 23(d). This curve was computed from the results of reference 2 for a body of revolution with an ogival nose and an afterbody with a fineness ratio of 8 for a Mach number of 4. Note the two- and three-fold increase of some of the curves in figures 23(e) and (f) over corresponding curves in figures 23(b) and (c), due entirely to incorporating values from the nonlinear body force curve with equations (5) and (6) to form the new equations

$$\frac{(C_N)_{\beta \geq 0}}{(C_N)_{\beta=0}} = \frac{(C_R)_{\beta \geq 0}}{(C_N)_{\beta=0}} \frac{\cos \beta \sin \alpha}{\sin \gamma} \quad (7)$$

and

$$\frac{(C_Y)_{\alpha \geq 0}}{(C_Y)_{\alpha=0}} = \frac{(C_R)_{\alpha \geq 0}}{(C_Y)_{\alpha=0}} \frac{\sin \beta}{\sin \gamma} \quad (8)$$

where C_R is the resultant force coefficient at angle γ .

The preceding equations and figure 23 explain and demonstrate the increases in normal force and side force that occur when angles of attack and sideslip are combined for a body of revolution. The increases can be significant, depending on the magnitude of the combined angles.

REFERENCES

1. Ulmann, Edward F., and Lord, Douglas R.: An Investigation of Flow Characteristics at Mach Number 4.04 Over 6- and 9-Percent-Thick Symmetrical Circular-Arc Airfoils Having 30-Percent-Chord Trailing-Edge Flaps. NACA RM L51D30, 1951.
2. Grimminger, P., Williams, E. P., and Young, G. B. W.: Lift on Inclined Bodies of Revolution in Hypersonic Flow. Jour. Aero. Sci., vol. 17, no. 11, Nov. 1950, pp. 675-690.
3. Ulmann, Edward F., and Dunning, Robert W.: Some Effects of Fin Plan Form on the Static Stability of Fin-Body Combinations at Mach Number 4.06. NACA RM L52D15a, 1952.
4. Ulmann, Edward F., and Dunning, Robert W.: Normal Force, Center of Pressure, and Zero-Lift Drag of Several Ballistic-Type Missiles at Mach Number 4.05. NACA RM L54D30a, 1954.
5. Ivey, H. Reese, Stickle, George W., and Schuettler, Alberta: Charts for Determining the Characteristics of Sharp-Nose Airfoils in Two-Dimensional Flow at Supersonic Speeds. NACA TN 1143, 1947.
6. Ulmann, Edward F., and Bertram, Mitchel H.: Aerodynamic Characteristics of Low-Aspect-Ratio Wings at High Supersonic Mach Numbers. NACA RM L53I23, 1953.
7. Ulmann, Edward F., and Smith, Fred M.: Aerodynamic Characteristics of a 60° Delta Wing Having a Half-Delta Tip Control at a Mach Number of 4.04. NACA RM L55A19, 1955.
8. Pitts, William C., Nielsen, Jack N., and Kaattari, George E.: Lift and Center of Pressure of Wing-Body-Tail Combinations at Subsonic, Transonic, and Supersonic Speeds. NACA Rep. 1307, 1957.
9. Lagerstrom, P. A., and Van Dyke, M. D.: General Considerations About Planar and Non-Planar Lifting Systems. Rep. No. SM-13432, Douglas Aircraft Co., Inc., June 1949.
10. Ulmann, Edward F., and Ridyard, Herbert W.: Flow-Field Effects on Static Stability and Control at High Supersonic Mach Numbers. NACA RM L55L19a, 1956.

18

~~CONFIDENTIAL~~

NACA RM L58E26

TABLE I.- GEOMETRIC CHARACTERISTICS OF THE MODELS

Body:

Length, in.	12.00
Maximum diameter, in.	1.00
Frontal area, sq in.	0.785
Nose length, in.	4.00
Nose radius of curvature, in.	16.25

Wing:

Span, in.	5.00
Chord, in.	3.00
Area, sq in.	15.00
Aspect ratio	1.67
Taper ratio	1.00
Maximum thickness, in.	0.100
Leading-edge sweepback, deg	0
Dihedral	0

Trapezoidal tail (one only):

Span (exposed), in.	1.68
Root chord, in.	2.126
Tip chord, in.	0.693
Area (exposed), sq in.	2.37
Aspect ratio (exposed)	1.19
Taper ratio	0.313
Maximum thickness, in.	0.100
Leading-edge sweepback, deg	40.7

Triangular tail (one only):

Span (exposed), in.	1.126
Root chord (exposed), in.	4.204
Area (exposed), sq in.	2.37
Aspect ratio (exposed)	0.53
Taper ratio	0
Maximum thickness, in.	0.100
Leading-edge sweepback, deg	75.0

TABLE II.- EXPERIMENTAL RESULTS

β , deg	α , deg	C_N	C_m	$\frac{x_i}{\% l}$	C_l	C_Y	C_n	β , deg	α , deg	C_N	C_m	$\frac{x_i}{\% l}$	C_l	C_Y	C_n
(a) Configuration B								(b) Configuration BW _f							
0	0	-0.0083	-0.0065	-	.0007	-0.0059		0	0	-0.0634	.0001	-	-0.0243	.0004	.0003
0	2	.1051	.3094	27	-.0007	-0.0059		0	2	.7890	.2158	49	-0.0162	-0.0027	.0744
0	4	.2298	.5744	31	.0026	-0.0030		0	4	1.6563	.3938	49	-0.0080	-0.0072	.4251
0	6	.4149	.7368	37	.0013	-0.0074		0	6	2.4907	.5926	30	-0.0182	-0.0116	.2214
0	8	.6684	.7509	42	.0034	-0.0132		0	8	3.5357	.6576	30	-0.0079	-0.0204	.3073
0	10	.9653	.7706	45	.0024	-0.0148									
0	12	1.2550	.8173	46	.0090	-0.0250									
0	14	1.5836	.8629	47	.0083	-0.0268									
0	15	1.7719	.8944	47	.0129	-0.0309									
1	0	-0.0042	-0.0065	-	-.0003	-0.0555		1	0	-0.0591	.0040	-	-0.0173	-0.0519	-1.503
1	2	.1092	.3045	28	-.0009	-0.0060		1	2	.8018	.2201	49	-0.0171	-0.0042	.0970
1	4	.2339	.5705	31	.0020	-0.0056		1	4	1.6478	.3981	49	-0.0190	-0.0028	.0482
1	6	.4174	.7302	37	.0009	-0.0079		1	6	2.4961	.5948	50	-0.0261	-0.0701	.0300
1	8	.6693	.7446	42	.0022	-0.0096		1	8	3.5063	.6762	50	-0.0103	-0.0855	.1203
1	10	.9572	.7679	45	.0031	-0.0104									
1	12	1.2633	.8159	46	.0074	-0.0257									
1	14	1.5792	.8606	47	.0081	-0.0287									
1	15	1.7741	.8638	47	.0110	-0.0451									
2	0	-0.0084	-0.0100	-	-.0013	-0.1168		2	0	-0.0590	-0.0036	-	-0.0112	-0.1055	
2	2	.1134	.3040	29	-.0018	-0.1187		2	2	.8009	.2383	49	-0.0152	-0.1131	
2	4	.2426	.5517	32	-.0007	-0.1543		2	4	1.6437	.4221	49	-0.0208	-0.1259	-0.2133
2	6	.4289	.7001	38	*	-0.1971		2	6	2.4963	.5566	49	-0.0300	-0.1362	-0.1590
2	8	.6776	.7212	42	.0009	-0.1669		2	8	3.5110	.7078	50	-0.0205	-0.1969	
2	10	.9643	.7584	45	.0018	-0.2132									
2	12	1.2715	.8150	46	.0068	-0.2981									
2	14	1.5874	.8498	47	.0074	-0.2988									
2	15	1.7739	.8520	47	.0092	-0.2695									
3	0	-0.0084	-0.0140	-	-.0028	-0.1824		3	0	-0.0631	-0.0026	-	-0.0121	-0.1656	-0.4615
3	2	.1134	.2890	30	-.0023	-0.1890		3	2	.8020	.2519	49	-0.0122	-0.1771	-0.4153
3	4	.2509	.5242	34	-.0002	-0.2102		3	4	1.6416	.4473	49	-0.0200	-0.1917	-0.4022
3	6	.4451	.6715	39	-.0008	-0.2433		3	6	2.4940	.5920	49	-0.0287	-0.2091	-0.3571
3	8	.6985	.6922	43	-.0005	-0.2833		3	8	3.5107	.7405	50	-0.0290	-0.2417	-0.2973
3	10	.9840	.7364	45	.0014	-0.3185									
3	12	1.2857	.7921	46	.0056	-0.3553									
3	14	1.5979	.8355	47	.0052	-0.3803									
3	15	1.7846	.8375	47	.0068	-0.3959									
4	0	-0.0084	-0.0100	-	-.0031	-0.2972		4	0	-0.0588	-0.0057	-	-0.0021	-0.2915	
4	2	.1216	.2731	33	-.0035	-0.2664		4	2	.8020	.2749	48	-0.0058	-0.2505	
4	4	.2684	.4971	36	-.0008	-0.2972		4	4	1.6334	.4702	49	-0.0117	-0.2665	
4	6	.4703	.6194	40	-.0008	-0.3415		4	6	2.5026	.6208	49	-0.0232	-0.2898	
4	8	.7246	.6528	44	-.0005	-0.3889		4	8	3.4808	.7821	49	-0.0366	-0.3258	
4	10	1.0037	.7134	45	-.0006	-0.4280									
4	12	1.2941	.7650	46	-.0034	-0.4693									
4	14	1.6167	.8127	47	-.0037	-0.5043									
4	15	1.7972	.8129	48	-.0044	-0.5249									
5	0	-0.0041	-0.0071	-	-.0046	-0.3449		5	0	-0.0589	-0.0041	-	-0.0118	-0.3126	-0.7113
5	2	.1299	.2606	35	-.0037	-0.3581		5	2	.7809	.2881	48	-0.0081	-0.3328	-0.6819
5	4	.2652	.4660	38	-.0024	-0.3981		5	4	1.6543	.4942	49	-0.0005	-0.3532	-0.3887
5	6	.4955	.5753	42	-.0005	-0.4544		5	6	2.4943	.6483	49	-0.0137	-0.3794	-0.6180
5	8	.7497	.6313	44	-.0006	-0.4971		5	8	3.5042	.6395	49	-0.0409	-0.4805	-0.5984
5	10	1.0317	.6759	46	-.0006	-0.5490									
5	12	1.3209	.7406	47	-.0029	-0.5900									
5	14	1.6334	.7742	47	-.0031	-0.6362									
5	15	1.8247	.7774	48	-.0046	-0.6580									

REF ID: A6425

TABLE II. - EXPERIMENTAL RESULTS - Continued

TABLE II. - EXPERIMENTAL RESULTS - Continued

β , deg	α , deg	C_N	C_m	x_i , $\% l$	C_t	C_Y	C_n	β , deg	α , deg	C_N	C_m	x_i , $\% l$	C_t	C_Y	C_n
(e) Configuration B(V_l) _{trap}								(f) Configuration BW _f (V_l) _{trap}							
0	0	.0168	-.1781	-	.0013	-.0015		0	0	-.0338	-.1787	-	-.0154	-.0041	.1577
0	2	.1346	.1360	49	-.0036	.0001		0	2	.8408	.0264	51	-.0112	-.0086	.2007
0	4	.2557	.3942	38	-.0027			0	4	1.6715	.1788	50	-.0057	-.0161	.2874
0	6	.4461	.5377	41	-.0042	.0030		0	6	2.5779	.3162	50	-.0071	-.0279	.3627
0	8	.6959	.5493	45	-.0029	-.0043		0	8	3.5512	.4249	50	-.0209	-.0388	.4884
0	10	.9829	.5438	47	-.0044	-.0135									
0	12	1.2837	.6008	47	-.0012	.0160									
0	14	1.6124	.6368	48	-.0012	.0162									
0	15	1.7878	.6548	48	-.0034	-.0144									
1	0	.0256	-.1445	-	.0979	-.1491		1	0	-.0162	-.1824	-	.0937	-.1425	.4831
1	2	.1351	.1353	48	.0927	-.1483		1	2	.8403	.0219	51	.1026	-.1586	.5522
1	4	.2650	.3929	39	.0922	-.1510		1	4	1.6457	.1786	50	.1124	-.1755	.6961
1	6	.4461	.5357	41	.0923	-.1571		1	6	2.5498	.3093	50	.1363	-.2014	.8298
1	8	.6930	.5493	45	.0928	-.1743		1	8	3.5293	.4129	50	.1652	-.2253	.9287
1	10	.9864	.5484	47	.1030	-.1989									
1	12	1.2894	.6075	47	.1013	-.2107									
1	14	1.6139	.6431	48	.1118	-.2359									
1	15	1.7893	.6491	48	.1043	-.2312									
2	0	.0271	-.1332	-	.1944	-.2966		2	0	.0022	-.1948	-	.2033	-.2259	.7279
2	2	.1448	.1167	45	.1922	-.2978		2	2	.8327	-.0003	51	.2271	-.3151	.8782
2	4	.2697	.3695	40	.1925	-.3101		2	4	1.6378	.1685	50	.2361	-.3374	1.0912
2	6	.4589	.4959	42	.1937	-.3330		2	6	2.5427	.2907	50	.2762	-.3804	1.2463
2	8	.7049	.5128	45	.1971	-.3619		2	8	3.5381	.3856	50	.3092	-.4261	1.5236
2	10	.9931	.5273	47	.2073	-.3943									
2	12	1.2938	.6208	47	.2196	-.4354									
2	14	1.6142	.6253	48	.2236	-.4534									
2	15	1.7919	.6329	48	.2217	-.4447									
3	0	.0250	-.2170	-	.2918	-.4501		3	0	.0001	-.2146	-	.3070	-.4346	.9505
3	2	.1466	.0691	47	.2938	-.4607		3	2	.8253	-.0271	52	.3417	-.6445	1.2139
3	4	.2836	.3053	42	.2950	-.4799		3	4	1.6471	.1452	51	.3620	-.5129	1.4577
3	6	.4723	.4247	44	.2957	-.5105		3	6	2.5550	.2769	50	.4183	-.5743	1.7218
3	8	.7221	.4559	46	.3015	-.5478		3	8	3.5181	.3663	50	.4634	-.6284	2.0524
3	10	1.0035	.4806	47	.3105	-.5922									
3	12	1.2959	.5385	48	.3231	-.6420									
3	14	1.6168	.5851	48	.3353	-.6821									
3	15	1.7987	.5872	49	.3351	-.6987									
4	0	.0196	-.2464	-	.3874	-.6072		4	0	-.0267	-.2711	-	.4149	-.5844	
4	2	.1488	.0173	50	.3906	-.6227		4	2	.8115	-.0545	52	.4683	-.6300	
4	4	.2980	.2283	45	.3905	-.6511		4	4	1.6421	.1114	51	.4936	-.6831	
4	6	.4933	.3341	46	.3932	-.6974		4	6	2.5414	.2423	51	.5480	-.7610	
4	8	.7384	.3732	47	.3988	-.7399		4	8	3.4994	.3415	51	.6119	-.8414	
4	10	1.0173	.4120	48	.4141	-.7939									
4	12	1.3052	.4742	48	.4314	-.8502									
4	14	1.6183	.5224	49	.4423	-.9072									
4	15	1.8003	.5228	49	.4442	-.9245									
								5	0	-.0411	-.3111	-	.5227	-.7495	1.5904
								5	2	.8000	-.0874	52	.5674	-.8112	1.7025
								5	4	1.6366	-.0774	51	.6172	-.8641	2.2104
								5	6	2.5225	-.1976	51	.7000	-.9513	2.5961
								5	8	3.4906	.3209	51	.7210	-.0543	

TABLE II. - EXPERIMENTAL RESULTS - Continued

TABLE II. - EXPERIMENTAL RESULTS - Continued

β , deg	α , deg	C_N	C_m	$x, %$	C_l	C_Y	C_n	β , deg	α , deg	C_N	C_m	$x, %$	C_l	C_Y	C_n
(i) Configuration B(H) _{trap}								(j) Configuration BW _f (H) _{trap}							
0	0	-0.0373	+1348	-	.0123	.0027		0	0	-0.0380	.0868	-	.0175	-0.0012	
0	2	.4182	-1.1587	74	.0102	-.0046		0	2	1.0203	-.8800	59	-.0181	-0.0026	
0	4	.8514	-2.4375	75	.0190	-.0134		0	4	2.0999	-1.9022	59	-.0001	-0.0058	
0	5	1.0741	-3.0386	75	.0221	-.0120		0	6	3.2632	-3.0196	59	.0040	-0.1339	
1	0	-0.0332	+1268	-	.0122	-.0556		1	0	-.0504	.1072	-	.0116	-0.0509	
1	2	.4175	-1.1684	75	.0060	-.0634		1	2	1.0240	-.8831	59	-.0079	-0.0541	
1	4	.8523	-2.4407	75	.0109	-.0775		1	4	2.0944	-1.8821	59	.0072	-0.0643	
1	5	1.0779	-3.0688	75	.0157	-.0863		1	6	3.2500	-3.0105	59	.0020	-0.0638	
2	0	-0.0291	+1189	-	.0131	-.1154		2	0	-.0503	.1067	-	.0094	-0.1078	
2	2	.4158	-1.1674	75	.0052	-.1247		2	2	1.0284	-.8838	58	.0015	-0.1099	
2	4	.8784	-2.4661	75	.0063	-.1490		2	4	2.1111	-1.8966	59	.0075	-0.1227	
2	5	1.0849	-3.0926	75	.0076	-.1639		2	6	3.2520	-2.9874	59	.0028	-0.1308	
3	0	-0.0292	.0965	-	.0118	-.1854		3	0	-.0753	.1326	-	.0073	-0.1662	
3	2	.4152	-1.1729	75	.0061	-.1953		3	2	1.0354	-.8877	58	.0070	-0.1742	
3	4	.8689	-2.4761	75	.0030	-.2249		3	4	2.1152	-1.8955	59	.0085	-0.1834	
3	5	1.0890	-3.0706	75	.0032	-.2442		3	6	3.2319	-2.9728	59	.0098	-0.1982	
4	0	-0.0252	.0851	-	.0131	-.2572		4	0	-.0795	.1291	-	.0004	-0.2353	
4	2	.4188	-1.1800	75	.0058	-.2735		4	2	1.0437	-.8891	58	.0126	-0.2431	
4	4	.8712	-2.4421	75	.0093	-.3115		4	4	2.1305	-1.8849	59	.0137	-0.2628	
4	5	1.1072	-3.0688	74	.0005	-.3397		4	6	3.2359	-2.9292	59	.0109	-0.2789	
5	0	-0.0283	.0777	-	.0110	-.3491		5	0	-.0754	.1362	-	.0071	-0.3201	
5	2	.4187	-1.1574	74	.0057	-.3641		5	2	1.0602	-.8874	58	.0219	-0.3225	
5	4	.8808	-2.4321	74	.0005	-.4143		5	4	2.1330	-1.8425	59	.0237	-0.3580	
5	5	1.1214	-3.0597	74	-.0038	-.4397		5	6	3.2189	-2.8329	59	.0081	-0.3732	

TABLE II. - EXPERIMENTAL RESULTS - Continued

β , deg	α , deg	C_N	C_m	x_i , % l	C_l	C_Y	C_n	β , deg	α , deg	C_N	C_m	x_i , % l	C_l	C_Y	C_n
(b) Configuration B(HV _u) _{trap}								(d) Configuration BW _f (HV _u) _{trap}							
0 0 0 0	0 2 4 5	-0.0751 +0.3686 +0.6247 1.0593	+0.3374 -0.9409 -2.2986 -2.8652	- 73 74 74	0.0047 0.0107 0.0225 0.0277	-0.0059 +0.0102 +0.0062 -0.0123	-	0 0 0 0	0 2 4 6	-0.0844 +0.9932 2.0127 3.2118	+2.937 -0.6913 -1.7816 -2.8805	- 57 58 59	-0.0151 -0.0043 -0.0011 +0.0026	-0.0012 +0.0060 -0.0044 -0.0074	
1 1 1 1	0 2 4 5	-0.0761 +0.3621 +0.8279 1.0554	+0.3343 -0.9353 -2.2973 -2.8684	- 73 74 74	-0.0941 +0.0783 -0.0779 -0.0643	+0.1423 +0.1385 +0.1506 +0.1434	-	1 1 1 1	0 2 4 6	-0.0849 +0.9899 2.0771 3.2143	+3.006 -0.6770 -1.7411 -2.8490	- 57 58 59 59	-0.1132 -0.0884 -0.0781 -0.0677	-0.1390 +0.1256 -0.1359 -0.1296	
2 2 2 2	0 2 4 5	-0.0734 +0.3638 +0.8355 1.0601	+0.3365 -0.9169 -2.2546 -2.9056	- 72 74 74	-0.1802 +0.1743 +0.1729 +0.1676	+0.2875 +0.2823 +0.2940 +0.3000	-	2 2 2 2	0 2 4 6	-0.0866 +0.9933 2.0914 3.2203	+3.226 -0.6589 -1.7266 -2.8301	- 57 58 58 59	-0.2057 -0.1712 -0.1506 -0.1300	-0.2788 +0.2363 -0.2431 -0.2659	
3 3 3 3	0 2 4 5	-0.0678 +0.3729 +0.8384 1.0733	+0.3598 -0.9080 -2.2236 -2.8459	- 72 73 73	-0.2764 +0.2645 +0.2688 +0.2615	+0.4349 +0.4320 +0.4523 +0.4587	-	3 3 3 3	0 2 4 6	-0.0808 +0.0022 2.1037 3.2319	+3.447 -0.6448 -1.7014 -2.7918	- 57 58 58 59	-0.2941 -0.2572 -0.2272 -0.1858	-0.4222 +0.3995 -0.3960 -0.3954	
4 4 4 4	0 2 4 5	-0.0630 +0.3853 +0.8612 1.0873	+0.3738 -0.8834 -2.2147 -2.8227	- 70 72 73 73	-0.3682 +0.3580 +0.3399 +0.3592	+0.5896 +0.5863 +0.6113 +0.6291	-	4 4 4 4	0 2 4 6	-0.0720 +0.0200 2.1264 3.2165	+3.5883 -0.6228 -1.6699 -2.7189	- 56 58 58 58	-0.3892 -0.3165 -0.2850 -0.2562	-0.5474 +0.5422 -0.5381 -0.5356	
5 5 5 5	0 2 4 5	-0.0542 +0.3981 +0.8754 1.1118	+0.3974 -0.8521 -2.1616 -2.7867	- 69 72 72	-0.4599 +0.4515 +0.4509 +0.4496	+0.7599 +0.7611 +0.7638 +0.8015	-	5 5 5 5	0 2 4 6	-0.0552 +0.0479 2.1469 3.2251	+4.243 -0.5786 -1.5936 -2.6201	- 56 58 58 58	-0.4763 -0.4041 -0.3860 -0.3283	-0.7293 +0.7042 -0.6976 -0.6939	

TABLE II. - EXPERIMENTAL RESULTS - Continued

β , deg	α , deg	C_N	C_m	x_i , $\% l$	C_l	C_Y	C_n	β , deg	α , deg	C_N	C_m	x_i , $\% l$	C_l	C_Y	C_n
(m) Configuration B(HV) _{trap}								(n) Configuration BW _{1(HV)_{trap}}							
0	0	-0.0164	-0.0313	-	.0146	-0.0032		0	0	-0.0590	-0.0676	-	-0.0093	-0.0057	
0	2	.4396	-1.3384	77	.0147	-0.0017		0	2	1.0750	-1.1189	60	-0.0033	-0.0029	
0	4	.8780	-2.6248	76	.0205	-0.0223		0	4	2.1700	-2.1823	60	.0057	-0.0162	
0	5	1.1200	-3.2866	76	.0214	-0.0166		0	6	3.3090	-3.2639	60	.0232	-0.0150	
1	0	-0.0119	-0.0595	-	.1133	-0.1496		1	0	-0.0288	-0.0909	-	.1001	-1.1468	
1	2	.4435	-1.3652	77	.1128	-0.1535		1	2	1.0757	-1.1199	60	.1158	-1.1544	
1	4	.8813	-2.6270	76	.1076	-0.1629		1	4	2.1719	-2.1834	60	.1335	-0.1730	
1	5	1.1140	-3.2725	76	.1054	-0.1637		1	6	3.3047	-3.2698	60	.1685	-0.1914	
2	0	-0.0087	-0.0559	-	.2156	-0.2998		2	0	-0.0314	-0.1127	-	.2026	-0.2878	
2	2	.4440	-1.3741	77	.2071	-0.3034		2	2	1.0720	-1.1313	60	.2456	-0.3105	
2	4	.8831	-2.6561	76	.1983	-0.3257		2	4	2.1706	-2.2030	60	.2559	-0.3329	
2	5	1.1256	-3.3063	76	.1985	-0.3430		2	6	3.2984	-3.2711	60	.3113	-0.3707	
3	0	-0.0132	-0.0829	-	.3120	-0.4524		3	0	-0.0421	-0.1362	-	.3163	-0.4354	
3	2	.4456	-1.4024	78	.3084	-0.4639		3	2	1.0582	-1.1528	60	.3453	-0.4667	
3	4	.8927	-2.6743	76	.2972	-0.4959		3	4	2.1612	-2.2411	60	.3885	-0.5111	
3	5	1.1296	-3.3276	76	.2878	-0.5158		3	6	3.2996	-3.3011	60	.4494	-0.5683	
4	0	-0.0193	-0.1123	-	.4094	-0.6124		4	0	-0.0520	-0.1584	-	.4218	-0.5817	
4	2	.4510	-1.4469	78	.4067	-0.6338		4	2	1.0524	-1.1829	61	.4866	-0.6354	
4	4	.8946	-2.7046	77	.3847	-0.6674		4	4	2.1518	-2.2592	60	.5107	-0.6801	
4	5	1.1348	-3.3550	76	.3863	-0.6980		4	6	3.2774	-3.2985	60	.5800	-0.7559	
5	0	-0.0296	-0.1442	-	.5064	-0.7842		5	0	-0.0671	-0.1703	-	.5915	-0.7526	
5	2	.4595	-1.4558	79	.5034	-0.8120		5	2	1.0360	-1.1992	61	.6050	-0.8082	
5	4	.8918	-2.7168	77	.4813	-0.8552		5	4	2.1323	-2.2624	60	.6407	-0.8626	
5	5	1.1400	-3.3813	76	.4766	-0.8948		5	6	3.2543	-3.2406	60	.6991	-0.9423	

TABLE II.- EXPERIMENTAL RESULTS - Continued

β , deg	α , deg	C_N	C_m	x_i , $\% l$	C_l	C_Y	C_n	β , deg	α , deg	C_N	C_m	x_i , $\% l$	C_l	C_Y	C_n
(a) Configuration $B(HV_uV_l)_{trap}$								(b) Configuration $BW_f(HV_uV_l)_{trap}$							
0	0	-0.0416	.1399	-	.0109	-0.0046		0	0	-0.0632	.0980	-	-0.0072	-0.0043	
0	2	.0407	-1.1363	75	.0159	-0.0003		0	2	1.0500	-0.9429	59	.0019	-0.0015	
0	4	.8358	-2.4134	75	.0101	-0.0293		0	4	2.1505	-2.0196	59	.0159	-0.0105	
0	5	1.0688	-3.0357	75	.0188	-0.0091		0	6	3.2690	-3.1244	59	.0291	-0.0108	
1	0	-0.0461	.1431	-	.0145	-0.2568		1	0	-0.0631	.1054	-	.0052	-0.2308	
1	2	.0461	-1.1528	75	.0195	-0.2316		1	2	1.0568	-0.9396	59	.0418	-0.2283	
1	4	.8356	-2.3952	75	.0114	-0.2131		1	4	2.1556	-2.0114	59	.0683	-0.2436	
1	5	1.0669	-3.0276	75	.0201	-0.2320		1	6	3.2716	-3.1236	59	.0934	-0.2624	
2	0	-0.0469	.1588	-	.0232	-0.4711		2	0	-0.0591	.1190	-	.0062	-0.4587	
2	2	.0463	-1.1470	75	.0254	-0.4608		2	2	1.0533	-0.9282	59	.0751	-0.4578	
2	4	.8406	-2.4134	75	.0115	-0.4661		2	4	2.1606	-2.0336	59	.1147	-0.4833	
2	5	1.0734	-3.0435	75	.0157	-0.4791		2	6	3.2746	-3.1691	59	.1622	-0.5054	
3	0	-0.0477	.1585	-	.0253	-0.7057		3	0	-0.0598	.1261	-	.0170	-0.6858	
3	2	.0428	-1.1650	75	.0290	-0.6987		3	2	1.0452	-0.9299	59	.1078	-0.6961	
3	4	.8485	-2.4155	75	.0138	-0.7173		3	4	2.1626	-2.0383	59	.1681	-0.7289	
3	5	1.0855	-3.0591	75	.0162	-0.7295		3	6	3.2356	-3.1214	59	.2403	-0.7492	
4	0	-0.0487	.1573	-	.0299	-0.9418		4	0	-0.0613	.1339	-	.0274	-0.9248	
4	2	.0498	-1.1536	75	.0354	-0.9430		4	2	1.0527	-0.9407	59	.1498	-0.9373	
4	4	.8563	-2.4131	75	.0159	-0.9568		4	4	2.1554	-2.0282	59	.2301	-0.9738	
4	5	1.0976	-3.0508	74	.0159	-0.9770		4	6	3.2396	-3.0388	59	.3063	-0.9915	
5	0	-0.0564	.1941	-	.0134	-1.1775		5	0	-0.0673	.1449	-	.0373	-1.1662	
5	2	.0240	-1.1530	78	.0209	-1.1880		5	2	1.0614	-0.9345	59	.1600	-1.1843	
5	4	.8637	-2.3843	74	.0192	-1.2139		5	4	2.1349	-1.9885	59	.2790	-1.2160	
5	5	1.1122	-3.0420	74	.0172	-1.2974		5	6	3.2502	-2.8957	59	.3447	-1.1261	

TABLE II. - EXPERIMENTAL RESULTS - Continued

S , deg	α , deg	C_N	C_m	x_i $\% l$	C_l	C_Y	C_n	β , deg	α , deg	C_N	C_m	x_i $\% l$	C_l	C_Y	C_n
(w) Configuration BW _r (V _u) _{trap}								(x) Configuration BW _r (V _u) _{tri}							
0	0	.0088	.0816	-	.0165	.0056		0	0	-.0797	.1713	-	.0040	.0131	
0	1	.3306	-.3360	60	.0202	-.0048		0	1	.3346	-.3643	60	.0104	.0043	
0	2	.7267	-.8913	62	.0166	.0129		0	2	.7400	-.9271	62	.0106	.0072	
0	3	1.2303	-.5565	62	.0240	.0118		0	3	1.1939	-.15260	62	.0203	.0118	
0	4	1.6294	-.2184	62	.0209	.0260		0	4	1.5829	-.2,0720	62	.0188	.0114	
0	5	2.0902	-.2,7146	62	.0325	.0292		0	5	2.0600	-.2,6853	62	.0289	.0054	
0	6	2.5406	-.3,3370	62	.0200	.0246		0	6	2.4795	-.3,2713	62	.0206	-.0003	
1	0	.0078	.0935	-	-.0794	-.1322		1	0	-.0593	.1462	-	-.0567	-.1177	
1	1	.3672	-.3767	60	-.0700	-.1346		1	1	.3342	-.3576	60	-.0453	-.1160	
1	2	.7382	-.8926	61	-.0719	-.1160		1	2	.7352	-.9271	62	-.0401	-.1138	
1	3	1.1886	-.1,4940	62	-.0640	-.1127		1	3	1.1973	-.1,5258	62	-.0340	-.1176	
1	4	1.6220	-.2,0832	62	-.0663	-.1060		1	4	1.5842	-.2,0556	62	-.0354	-.1109	
1	5	2.0759	-.2,6801	62	-.0574	-.0922		1	5	2.0605	-.2,6932	62	-.0293	-.1088	
1	6	2.5553	-.3,3348	62	-.0685	-.1001		1	6	2.4996	-.3,2927	62	-.0322	-.1118	
2	0	.0099	.1222	-	-.1715	-.2730		2	0	-.0840	.1623	-	-.1113	-.2505	
2	1	.3691	-.3558	59	-.1603	-.2747		2	1	.3471	-.3694	60	-.0986	-.2477	
2	2	.7367	-.8499	61	-.1613	-.2526		2	2	.7412	-.9181	62	-.0915	-.2394	
2	3	1.1901	-.1,4548	62	-.1568	-.2471		2	3	1.2006	-.1,5201	62	-.0820	-.2376	
2	4	1.6171	-.2,0456	62	-.1520	-.2355		2	4	1.6207	-.2,1136	62	-.0824	-.2351	
2	5	2.0701	-.2,6402	62	-.1462	-.2295		2	5	2.0709	-.2,7009	62	-.0769	-.2303	
2	6	2.5600	-.3,2963	62	-.1519	-.2296		2	6	2.5027	-.3,2808	62	-.0743	-.2285	
3	0	.0151	.1518	-	-.2638	-.4226		3	0	-.0341	.1621	-	-.1649	-.3948	
3	1	.3736	-.3251	59	-.2523	-.4231		3	1	.3499	-.3557	60	-.1542	-.3913	
3	2	.7374	-.8039	60	-.2542	-.4037		3	2	.7774	-.9305	61	-.1398	-.3811	
3	3	1.1928	-.1,4116	61	-.2451	-.3869		3	3	1.2098	-.1,5096	62	-.1319	-.3690	
3	4	1.6215	-.1,9973	62	-.2430	-.3809		3	4	1.6354	-.2,0985	62	-.1279	-.3437	
3	5	2.0462	-.2,5577	62	-.2387	-.3781		3	5	2.0827	-.2,6938	62	-.1219	-.3589	
3	6	2.5516	-.3,2242	62	-.2352	-.3752		3	6	2.5297	-.3,2794	62	-.1194	-.3506	
4	0	.0280	.1875	-	-.3535	-.5812		4	0	-.0328	.2003	-	-.2148	-.5400	
4	1	.3851	-.2822	57	-.3367	-.5697		4	1	.3577	-.3083	59	-.2008	-.5255	
4	2	.7544	-.7562	60	-.3420	-.5468		4	2	.7755	-.8787	61	-.1800	-.5134	
4	3	1.1902	-.1,3514	61	-.2313	-.5352		4	3	1.2198	-.1,4792	61	-.1728	-.5047	
4	4	1.6137	-.1,9138	61	-.3255	-.5228		4	4	1.6512	-.2,0797	62	-.1653	-.4933	
4	5	2.0543	-.2,5130	62	-.3187	-.5162		4	5	2.1041	-.2,6837	62	-.1620	-.4872	
4	6	2.5455	-.3,1576	62	-.3120	-.5179		4	6	2.5452	-.3,2639	62	-.1599	-.4787	
5	0	.0491	.2204	-	-.4475	-.7503		5	0	.0109	.2524	-	-.2660	-.6938	
5	1	.3887	-.2252	56	-.4296	-.7373		5	1	.3380	-.2182	57	-.2473	-.6800	
5	2	.7749	-.7049	59	-.4359	-.7156		5	2	.7834	-.8195	60	-.2290	-.6656	
5	3	1.2257	-.1,3156	60	-.4248	-.7050		5	3	1.2714	-.1,4754	61	-.2182	-.6570	
5	4	1.6335	-.1,8634	61	-.4177	-.6919		5	4	1.6772	-.2,0425	61	-.2058	-.6474	
5	5	2.0863	-.2,4758	61	-.4069	-.6827		5	5	2.1357	-.2,6615	62	-.1975	-.6278	
5	6	2.5306	-.3,0656	61	-.4058	-.6892		5	6	2.5825	-.3,2396	62	-.1967	-.6252	

TABLE II. - EXPERIMENTAL RESULTS - Continued

β , deg	α , deg	C_N	C_m	x_i , $\% l$	C_l	C_y	C_n	β , deg	α , deg	C_N	C_m	x_i , $\% l$	C_l	C_y	C_n
(y) Configuration $BW_r(V_l)_{trap}$								(z) Configuration $BW_r(V_l)_{tri}$							
0	0	.1260	-.3376	-	.0026			0	0	.0335	-.1646	-	-.0027	.0030	
0	1	.4240	-.7293	66	.0081	-.0061		0	1	.3947	-.6353	65	.0019		
0	2	.8021	-1.2677	65	.0032	-.0059		0	2	.7937	-1.1956	64	.0061	-.0001	
0	3	1.2548	-1.8755	64	.0080	-.0105		0	3	1.2386	-1.7739	63	.0131	.0058	
0	4	1.6585	-2.4243	64	.0082	.0101		0	4	1.6738	-2.3896	63	.0195	.0055	
0	5	2.1527	-3.0525	63	.0239	-.0004		0	5	2.1200	-2.9466	63	.0307	.0128	
0	6	2.5329	-3.6006	63	.0032	-.0030		0	6	2.3653	-3.5942	63	.0292	.0098	
1	0	.1308	-.3466	-	.1099	-.1499		1	0	.0340	-.1615	-	.0572	-.1298	
1	1	.4323	-.7458	66	.1115	-.1570		1	1	.3941	-.6428	65	.0448	-.1414	
1	2	.8034	-1.2782	65	.1153	-.1678		1	2	.7866	-.16892	64	.0740	-.1509	
1	3	1.2600	-1.8809	64	.1194	-.1820		1	3	1.2362	-.17729	63	.0793	-.1590	
1	4	1.6547	-2.4191	64	.1109	-.1689		1	4	1.6652	-.23744	63	.0864	-.1702	
1	5	2.1369	-2.9857	63	.1185	-.1763		1	5	2.1209	-.29558	63	.0902	-.1714	
1	6	2.5692	-3.6300	63	.1116	-.1968		1	6	2.5936	-.35894	63	.0924	-.1749	
2	0	.0692	-.2530	-	.2122	-.2912		2	0	.0410	-.1874	-	.1240	-.2703	
2	1	.4411	-.7751	66	.2202	-.3076		2	1	.4280	-.6872	65	.1326	-.2866	
2	2	.8041	-1.2933	65	.2224	-.3222		2	2	.8013	-.12050	64	.2446	-.3055	
2	3	1.2846	-1.9117	64	.2234	-.3451		2	3	1.2586	-.17947	63	.1490	-.3180	
2	4	1.6760	-2.4525	64	.2099	-.3485		2	4	1.6624	-.23773	63	.1541	-.3298	
2	5	2.1562	-3.0659	63	.2138	-.3607		2	5	2.1235	-.29670	63	.1599	-.3509	
2	6	2.5636	-3.6463	63	.2271	-.3868		2	6	2.5980	-.35931	63	.1618	-.3662	
3	0	.0668	-.3030	-	.3183	-.4441		3	0	.0416	-.2189	-	.1870	-.4155	
3	1	.4421	-.8120	67	.3340	-.4689		3	1	.4371	-.7408	65	.2034	-.4389	
3	2	.8432	-1.3696	65	.3408	-.4936		3	2	.8511	-.12897	64	.2184	-.4615	
3	3	1.2730	-1.9418	64	.3378	-.5147		3	3	1.2628	-.18322	63	.2182	-.4836	
3	4	1.6743	-2.4536	64	.3146	-.5248		3	4	1.6716	-.24008	63	.2310	-.5079	
3	5	2.1403	-3.0821	63	.3157	-.5534		3	5	2.1272	-.30016	63	.2325	-.5329	
3	6	2.5693	-3.6696	63	.3461	-.5832		3	6	2.6044	-.36255	63	.2312	-.5313	
4	0	.0687	-.3491	-	.4276	-.6038		4	0	.0444	-.26352	-	.2498	-.5603	
4	1	.4429	-.8307	67	.4368	-.6321		4	1	.4520	-.7848	66	.2660	-.5856	
4	2	.8363	-1.3893	65	.4367	-.6539		4	2	.8207	-.12952	64	.2753	-.6115	
4	3	1.2714	-1.9744	64	.4443	-.6867		4	3	1.2733	-.18795	64	.2813	-.6442	
4	4	1.6606	-2.4596	64	.4068	-.7048		4	4	1.7017	-.24525	63	.2947	-.6736	
4	5	2.1489	-3.1183	63	.4116	-.7363		4	5	2.1610	-.30879	63	.2980	-.7078	
4	6	2.5755	-3.7078	63	.4624	-.7688		4	6	2.6209	-.36678	63	.2944	-.7348	
5	0	.0579	-.3890	-	.5264	-.7828		5	0	.0578	-.3254	-	.3001	-.7211	
5	1	.4306	-.8728	68	.5372	-.8109		5	1	.4472	-.8348	67	.3221	-.7474	
5	2	.8282	-1.4240	66	.5483	-.8450		5	2	.8371	-.13420	65	.3274	-.7814	
5	3	1.3012	-2.0604	65	.5577	-.8878		5	3	1.3077	-.19684	64	.3426	-.8254	
5	4	1.6517	-2.4936	64	.5057	-.9064		5	4	1.7187	-.25278	64	.3523	-.8608	
5	5	2.1492	-3.1570	64	.5080	-.9429		5	5	2.1960	-.31712	63	.3597	-.8989	
5	6	2.5828	-3.7534	63	.5836	-.9824		5	6	2.6466	-.37169	63	.3529	-.9371	

TABLE II. - EXPERIMENTAL RESULTS - Continued

β , deg	α , deg	C_N	C_m	$x_{\% l}$	C_l	C_Y	C_n	β , deg	α , deg	C_N	C_m	$x_{\% l}$	C_l	C_Y	C_n
(aa) Configuration BW _r (V _u V _p) _{trap}								(bb) Configuration BW _r (V _u V _p) _{tri}							
0	0	-0.0042	-0.0145	-	.0005	0.0059		0	0	-0.0377	.0231	-	.0001	.0263	
0	1	.3664	-.5130	63	.0075	0.0073		0	1	.3452	-.4953	63	.0024	.0312	
0	2	.7865	-1.1174	63	.0106	0.0057		0	2	.7757	-1.0905	63	.0064	.0072	
0	3	1.2343	-1.7128	63	.0154	0.0101		0	3	1.2410	-1.6810	63	.0129	.0116	
0	4	1.6483	-2.2958	63	.0215	0.0128		0	4	1.6331	-2.2650	63	.0054	-.0001	
0	5	2.1340	-2.9373	63	.0437	0.0067		0	5	2.0913	-2.8231	63	.0157	.0042	
0	6	2.5772	-3.5407	63	.0414	0.0155		0	6	2.5150	-3.4276	63	.0060	.0043	
1	0	-0.0084	-0.0030	-	.0084	-0.2188		1	0	-0.0209	.0020	-	.0016	-.1914	
1	1	.3554	-.5008	63	.0212	-.2249		1	1	.3512	-.4893	63	.0106	-.1966	
1	2	.7818	-1.1061	63	.0342	-.2295		1	2	.7716	-1.0906	63	.0258	-.2132	
1	3	1.2288	-1.7057	63	.0444	-.2345		1	3	1.2373	-1.6814	63	.0394	-.2211	
1	4	1.6372	-2.2800	63	.0561	-.2287		1	4	1.6351	-2.2577	63	.0348	-.2207	
1	5	2.1383	-2.9464	63	.0731	-.2225		1	5	2.1004	-2.8421	63	.0472	-.2230	
1	6	2.5674	-3.5225	63	.0755	-.2498		1	6	2.5315	-3.4369	63	.0485	-.2233	
2	0	-0.0131	-0.0025	-	.0158	-.4522		2	0	-0.0127	-.0069	-	.0070	-.4098	
2	1	.3794	-.5269	63	.0349	-.4564		2	1	.3793	-.5294	63	.0207	-.4113	
2	2	.7812	-1.0896	63	.0563	-.4652		2	2	.7804	-.1080	63	.0524	-.4366	
2	3	1.2294	-1.7022	63	.0669	-.4753		2	3	1.2424	-.1481	63	.0650	-.4428	
2	4	1.6265	-2.2655	63	.0820	-.4671		2	4	1.6374	-2.2601	63	.0707	-.4487	
2	5	2.1312	-2.9359	63	.0991	-.4708		2	5	2.1065	-.2887	63	.0847	-.4499	
2	6	2.5677	-3.5242	63	.1105	-.4771		2	6	2.5661	-.4979	63	.0915	-.4491	
3	0	.0068	-.0137	-	.0278	-.6984		3	0	-0.0090	-.0005	-	.0125	-.6937	
3	1	.3944	-.5495	63	.0500	-.7104		3	1	.3825	-.5460	63	.0309	-.6457	
3	2	.7835	-1.0891	63	.0789	-.7143		3	2	.8070	-.1233	63	.0777	-.6733	
3	3	1.2372	-1.7038	63	.0910	-.7155		3	3	1.2501	-.7161	63	.0937	-.6757	
3	4	1.6290	-2.2521	63	.1075	-.7183		3	4	1.6629	-.2307	63	.1070	-.6855	
3	5	2.0927	-2.8892	63	.1292	-.7294		3	5	2.1203	-.9158	63	.1220	-.6945	
3	6	2.5668	-3.4940	63	.1424	-.7292		3	6	2.5882	-.4952	63	.1361	-.6905	
4	0	.0092	-.0147	-	.0409	-.9349		4	0	-0.0057	-.0037	-	.0195	-.8545	
4	1	.3960	-.5428	63	.0651	-.9423		4	1	.3930	-.5513	63	.0418	-.8642	
4	2	.7925	-1.0896	63	.0977	-.9476		4	2	.8257	-.1474	63	.0969	-.8905	
4	3	1.2446	-1.7080	63	.1216	-.9639		4	3	1.2692	-.7456	63	.1204	-.8962	
4	4	1.6549	-2.2843	63	.1401	-.9629		4	4	1.6828	-.3393	63	.1347	-.9059	
4	5	2.1002	-2.8980	63	.1617	-.9706		4	5	2.1452	-.5957	63	.1574	-.9153	
4	6	2.5763	-3.5124	63	.1789	-.9799		4	6	2.6039	-.5518	63	.1761	-.9169	
5	0	.0118	-.0089	-	.0452	-1.1910		5	0	-0.0019	-.0021	-	.0189	-.1059	
5	1	.3838	-.5126	62	.0763	-.1975		5	1	.3950	-.5510	63	.0469	-.1084	
5	2	.8049	-1.1007	63	.1068	-.2149		5	2	.8308	-.1442	63	.1050	-.1184	
5	3	1.2620	-1.7346	63	.1431	-.2311		5	3	1.3163	-.8203	63	.1411	-.1337	
5	4	1.6624	-2.2781	63	.1657	-.2390		5	4	1.7039	-.3644	63	.1610	-.1429	
5	5	2.1237	-2.8892	63	.1919	-.1846		5	5	2.1669	-.0094	63	.1894	-.1478	
5	6	2.5983	-3.4369	62	.2093	-.1512		5	6	2.6357	-.5683	63	.2060	-.1993	

TABLE II. - EXPERIMENTAL RESULTS - Concluded

β , deg	α , deg	C_N	C_m	$x,$ $\% l$	C_l	C_Y	C_n	β , deg	α , deg	C_N	C_m	$x,$ $\% l$	C_l	C_Y	C_n
(cc) Configuration BW _R															
0	0	-0.0043	-0.0219	-	-0.0066	.0045									
0	1	.3859	-1.4931	63	-0.0018	-0.0029									
0	2	.7693	-1.0592	63	.0017										
0	3	1.2257	-1.6466	63	.0089	-0.0016									
0	4	1.6420	-2.2420	63	.0110	-0.0002									
0	5	2.0812	-2.7710	62	.0194	-0.0093									
0	6	2.5367	-3.4143	63	.0143	.0071									
1	0	-0.0001	-0.0224	-	-0.0061	.0048									
1	1	.3776	-0.5044	62	-0.0080	.0050									
1	2	.7692	-1.0516	63	-0.0043	.0042									
1	3	1.2230	-1.6459	63	.0064	.0005									
1	4	1.6374	-2.2191	63	.0040	.0046									
1	5	2.0836	-2.7781	62	.0066	.0083									
1	6	2.5320	-3.4058	63	.0139	.0074									
2	0	.0042	-0.0225	-	.0008	.0026									
2	1	.3756	-0.4988	62	-0.0097	.0045									
2	2	.7702	-1.0574	63	.0110	.0000									
2	3	1.2213	-1.6359	62	.0152	.0027									
2	4	1.6396	-2.2030	63	.0101	.0064									
2	5	2.0920	-2.7871	62	.0219	.0089									
2	6	2.5312	-3.3841	62	.0909	.0431									
3	0	.0084	-0.0230	-	.0033	.0044									
3	1	.3751	-0.5008	62	.0100	.0070									
3	2	.7745	-1.0305	62	-0.0086	.0076									
3	3	1.2249	-1.6302	62	.0182	.0071									
3	4	1.6397	-2.1916	62	.0193	.0096									
3	5	2.1035	-2.7852	62	.0365	.0188									
3	6	2.5475	-3.3633	62	.0446	.0238									
4	0	.0054	-0.0280	-	.0083	.0035									
4	1	.3794	-0.4979	62	-0.0071	.0066									
4	2	.7799	-1.0211	62	.0118	.0070									
4	3	1.2327	-1.6095	62	.0251	.0033									
4	4	1.6525	-2.1783	62	.0204	.0076									
4	5	2.1209	-2.7908	62	.0439	.0092									
4	6	2.5649	-3.3569	62	.0568	.0316									
5	0	.0124	-0.0314	-	.0157	.0216									
5	1	.3705	-0.4780	62	.0034	.0262									
5	2	.7927	-1.0198	62	.0143	.0426									
5	3	1.2777	-1.6462	62	.0266	.0386									
5	4	1.6722	-2.1793	62	.0366	.0371									
5	5	2.1398	-2.7972	62	.0521	.0360									
5	6	2.5829	-3.3360	62	.0747	.0455									

CONFIDENTIAL

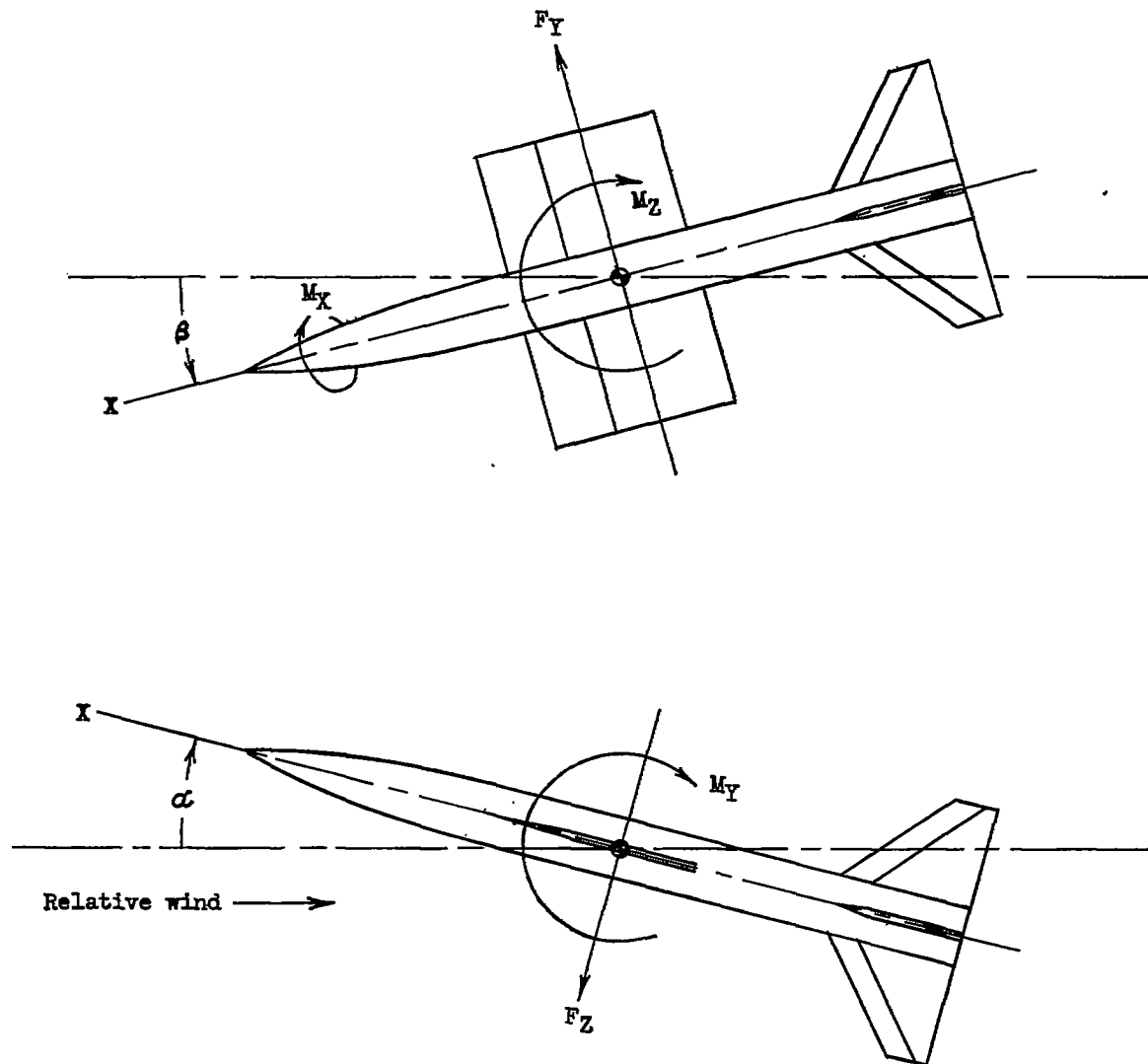


Figure 1.- System of body axes for tests. Arrows indicate positive angles, forces, and moments.

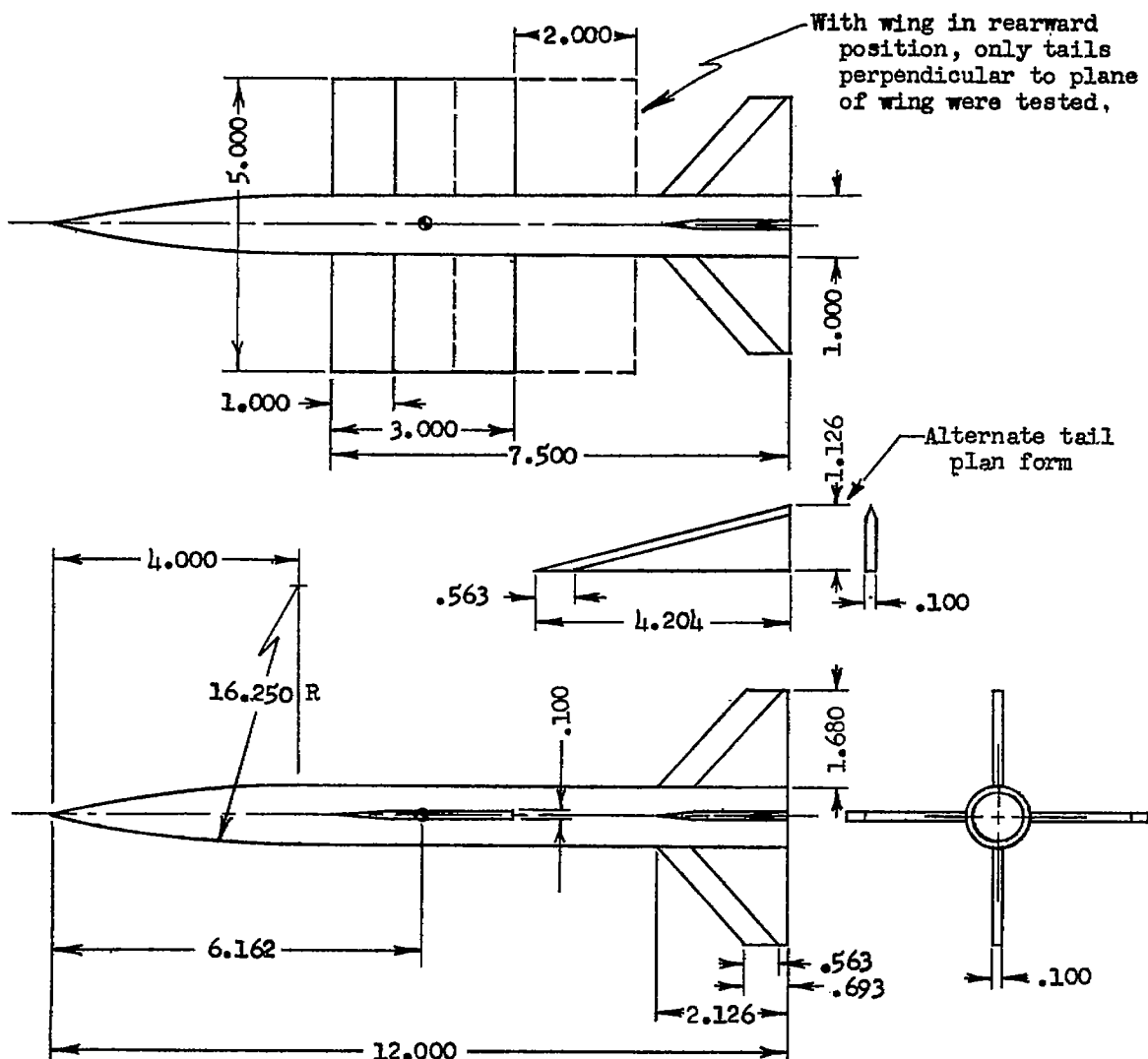
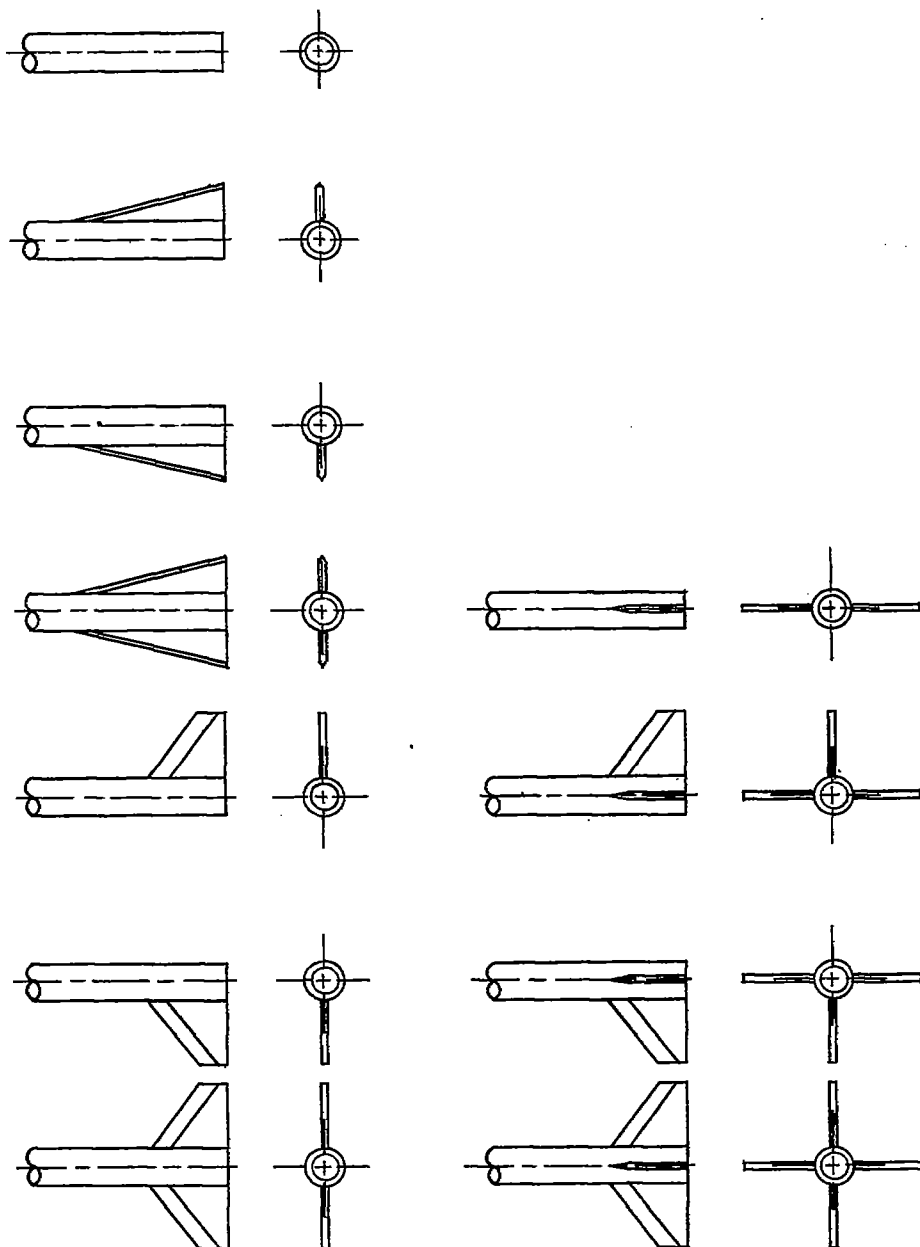


Figure 2.- Schematic diagram of typical configuration showing wing in both longitudinal positions. All dimensions are in inches.



(a) Tail configurations tested with wing off, forward, and rearward.

(b) Tail configurations tested with wing off and forward.

Figure 3.- Schematic diagram of tails tested on configurations with and without wings.

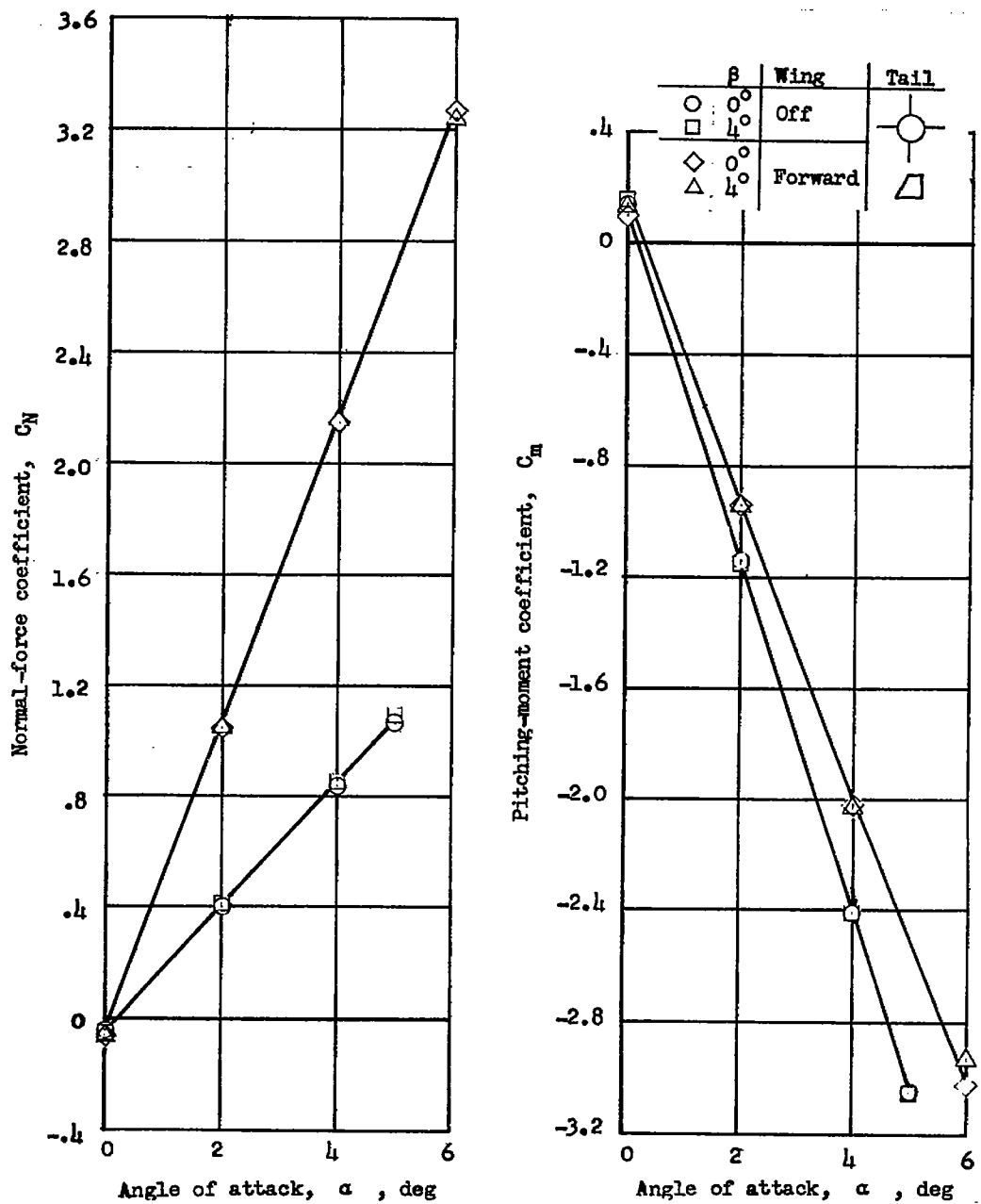
(a) Tail configuration $(HV_uV_l)_{trap}$.

Figure 4.- Effects of presence of wing and wing position on longitudinal aerodynamic characteristics of configurations with various trapezoidal tails.

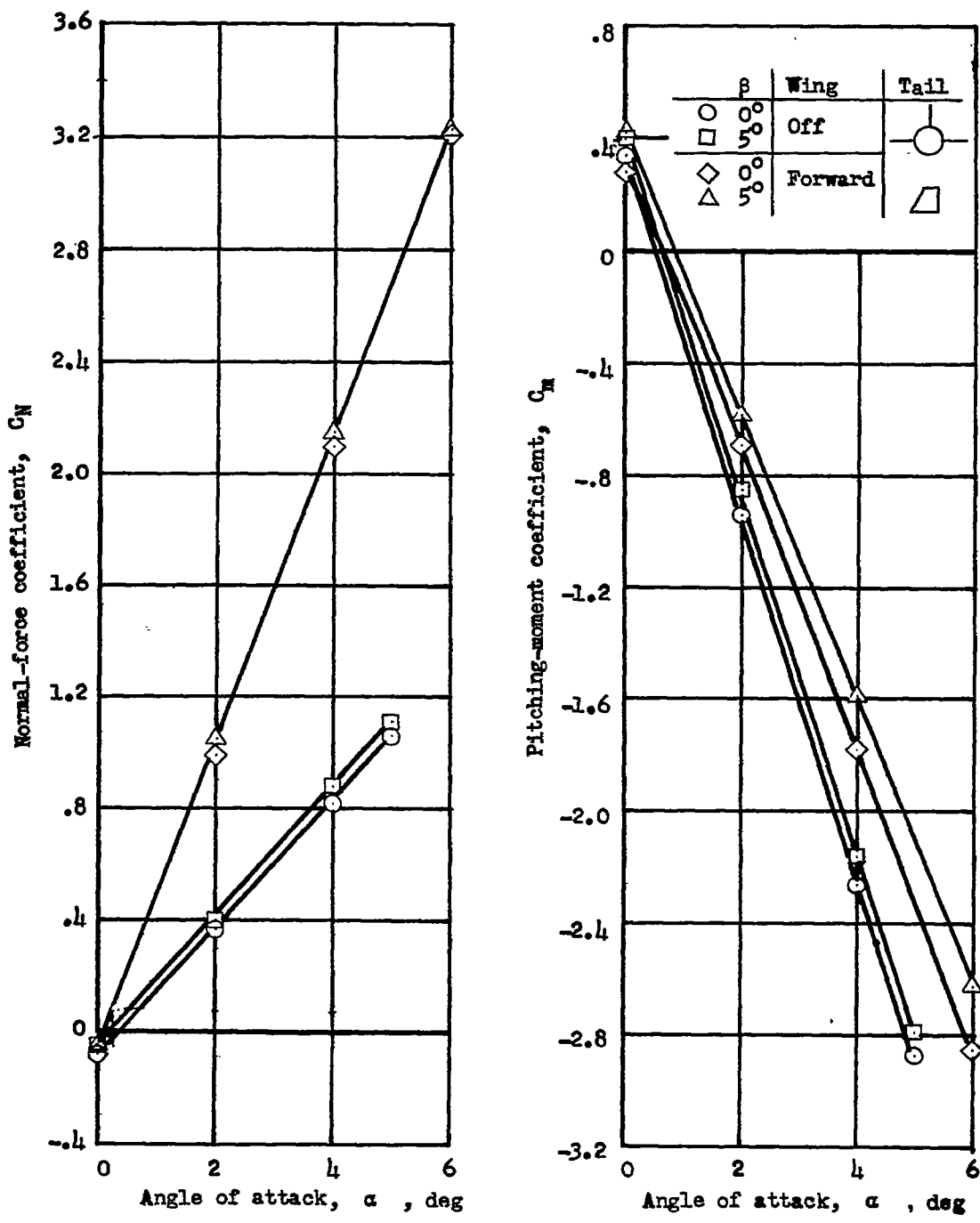
(b) Tail configuration $(HV_u)_{trap}$.

Figure 4.- Continued.

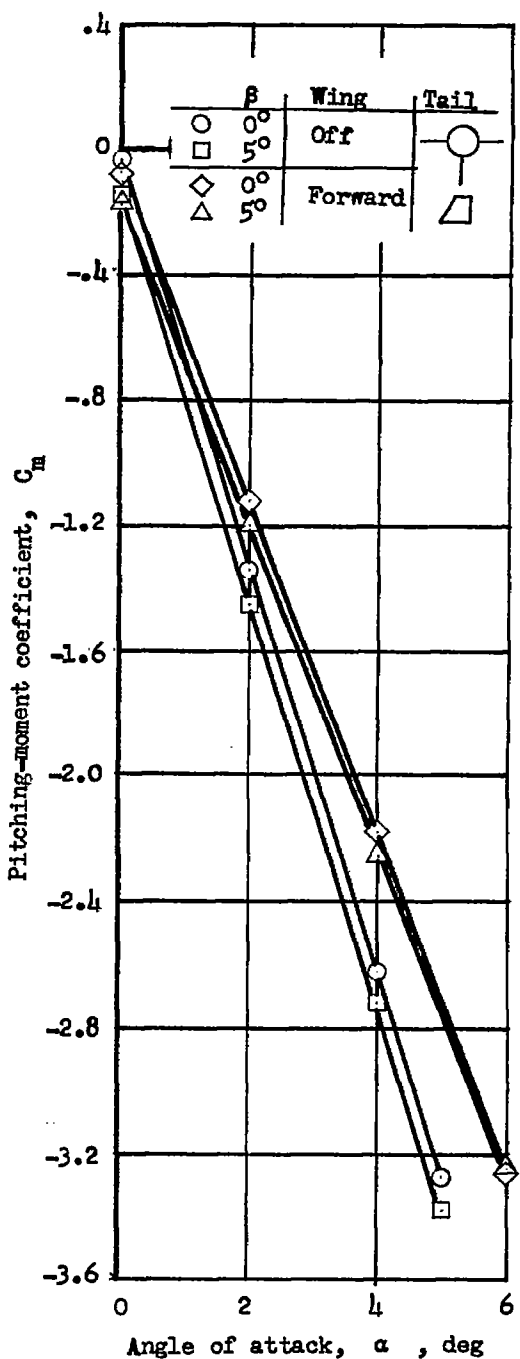
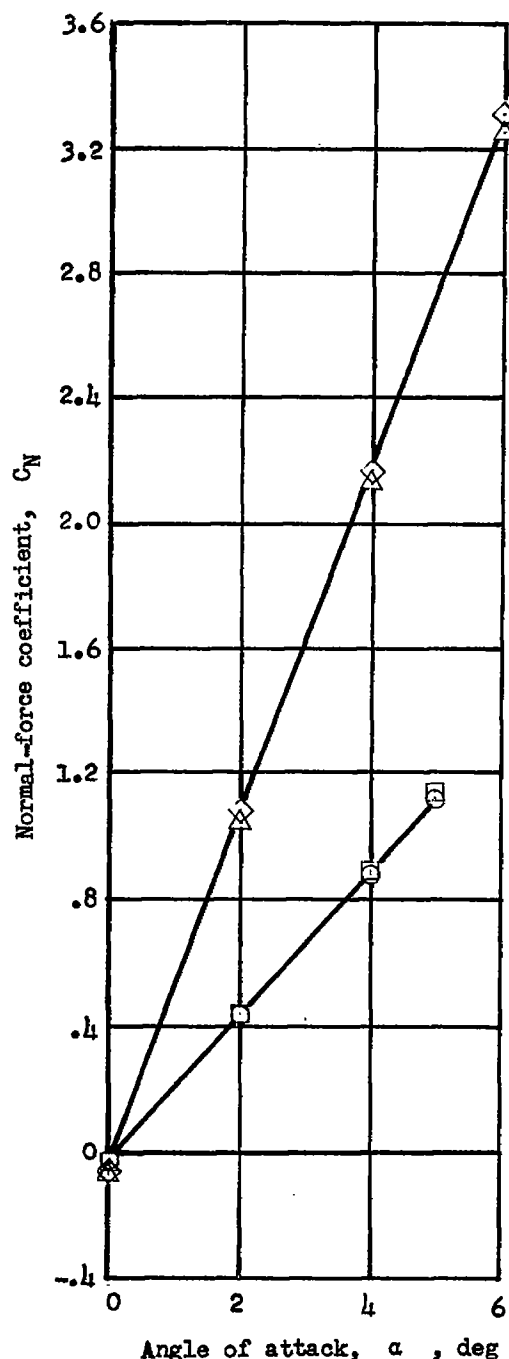
(c) Tail configuration $(HV_l)_{\text{trap}}$.

Figure 4.- Continued.

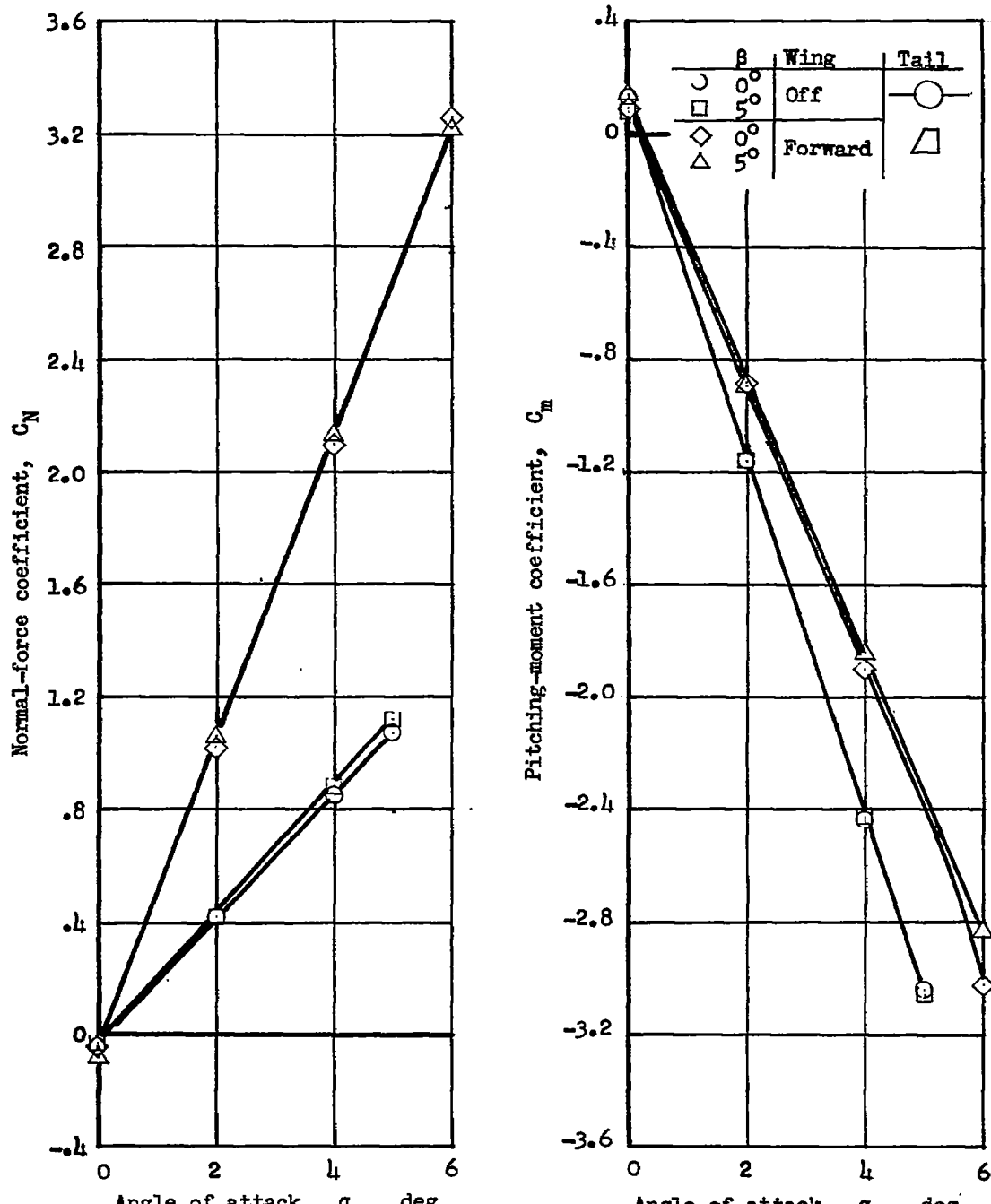
(d) Tail configuration $(H)_{trap}$.

Figure 4.- Continued.

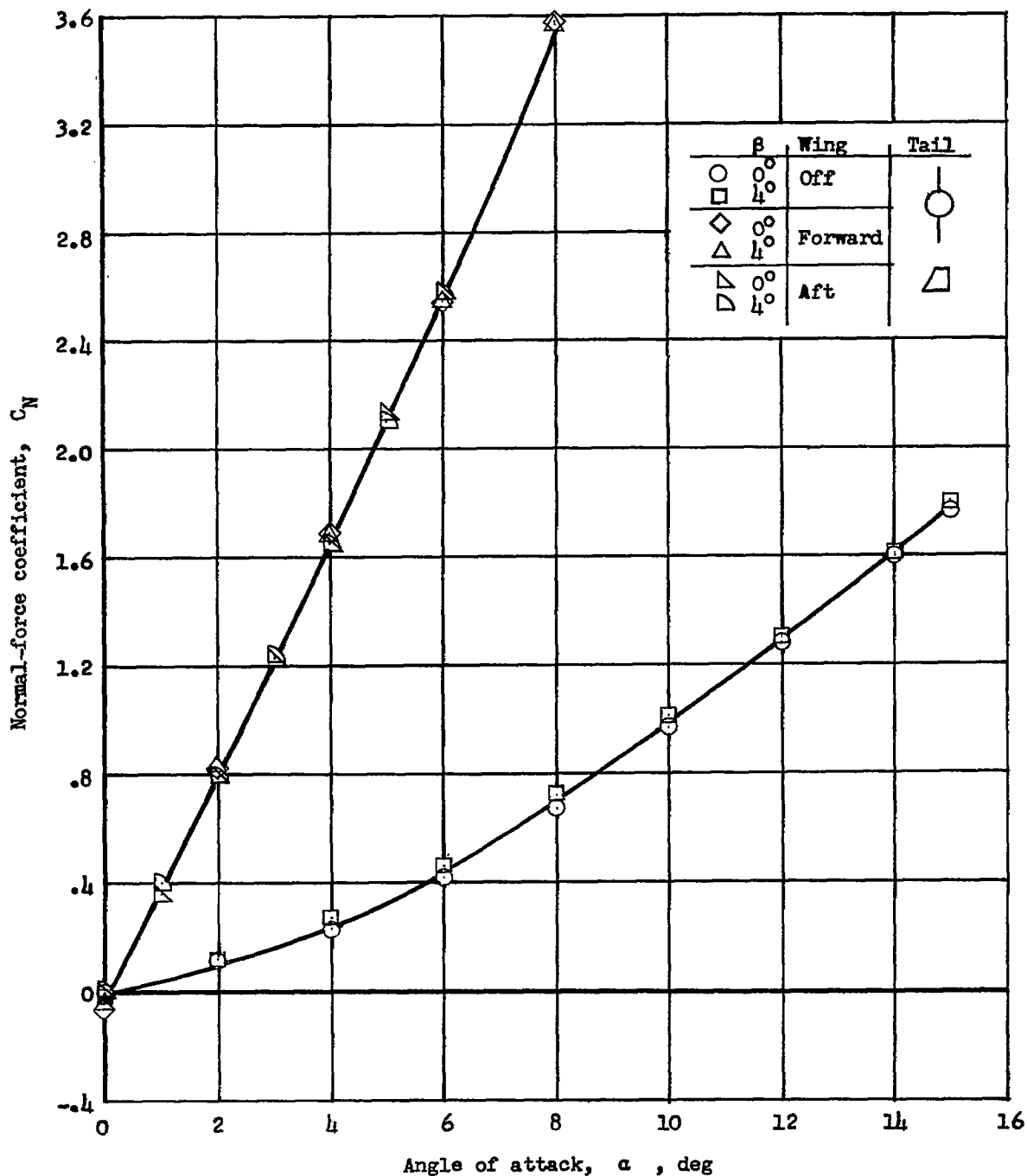
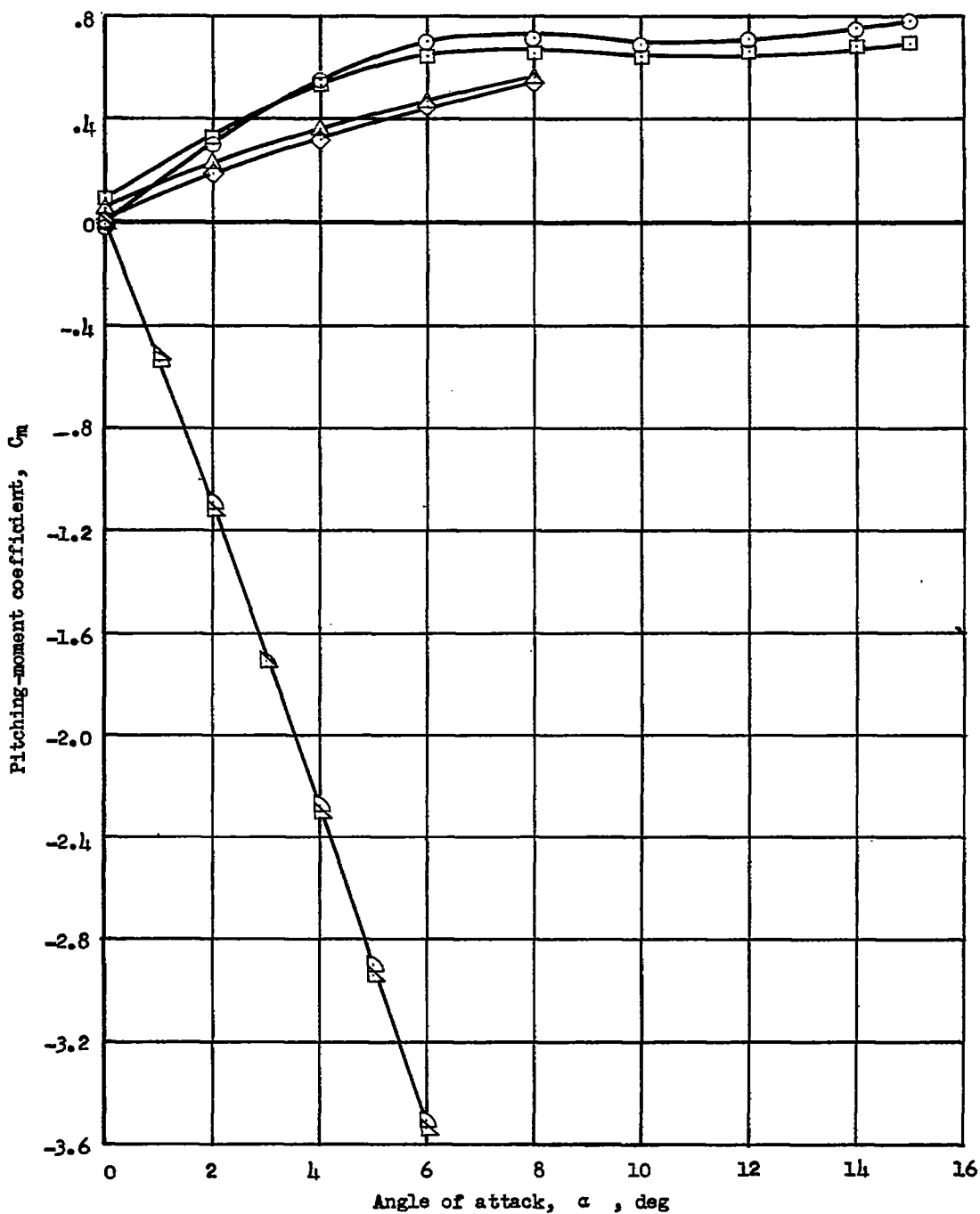
(e) Tail configuration $(V_u V_l)_{trap}$.

Figure 4.- Continued.



(e) Concluded.

Figure 4.- Continued.

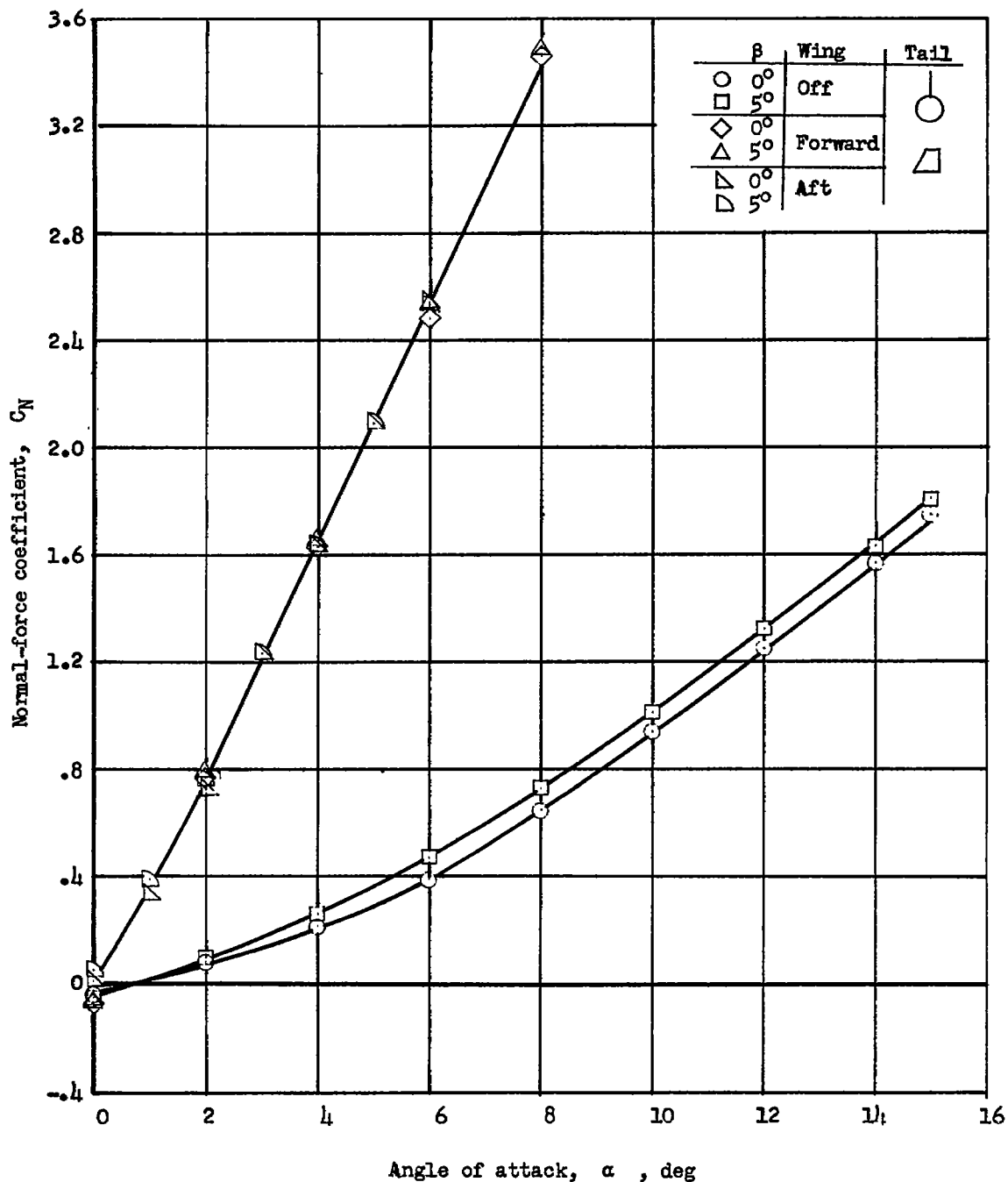
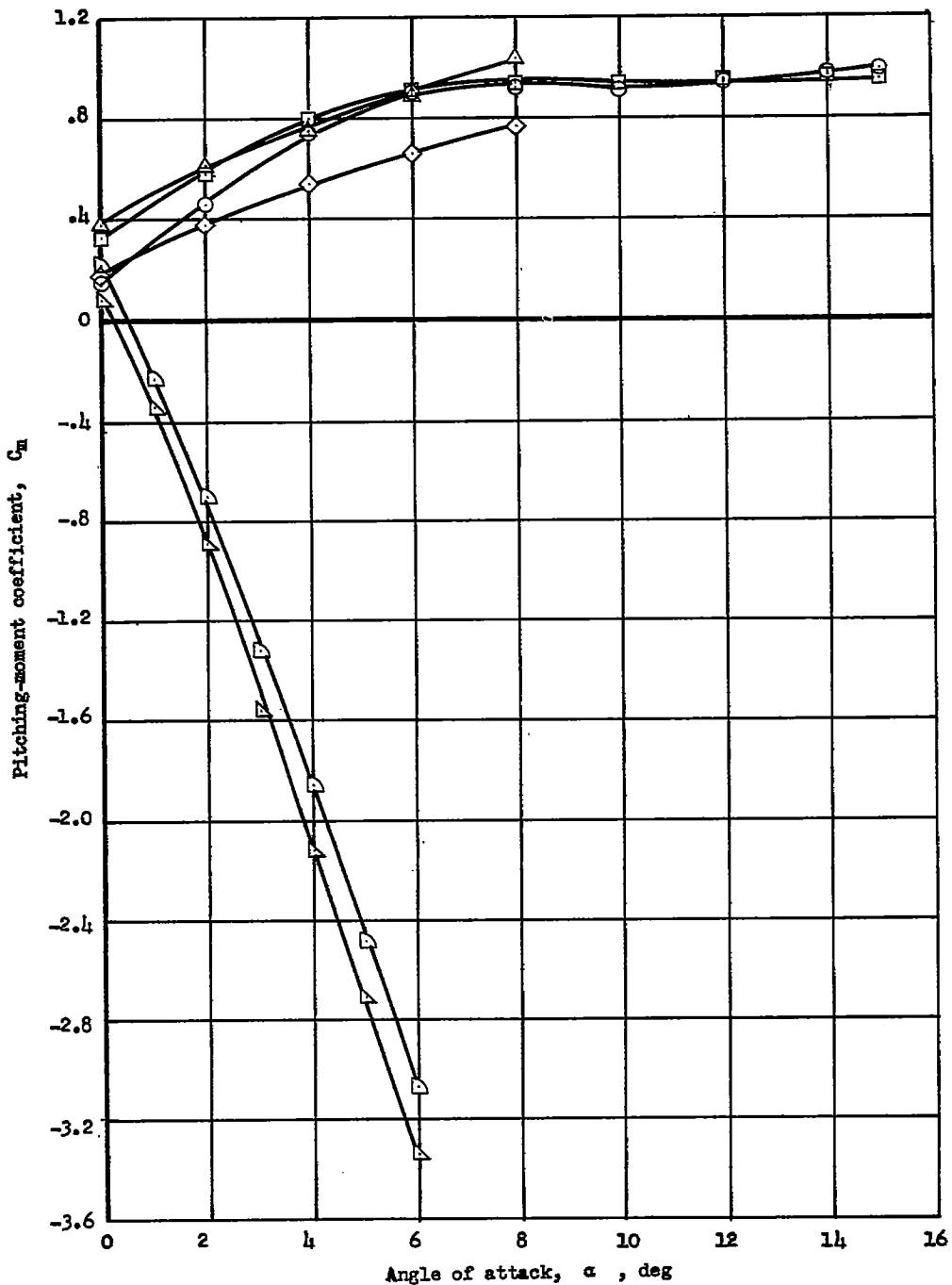
(f) Tail configuration $(V_u)_{trap}$.

Figure 4.- Continued.



(f) Concluded.

Figure 4.- Continued.

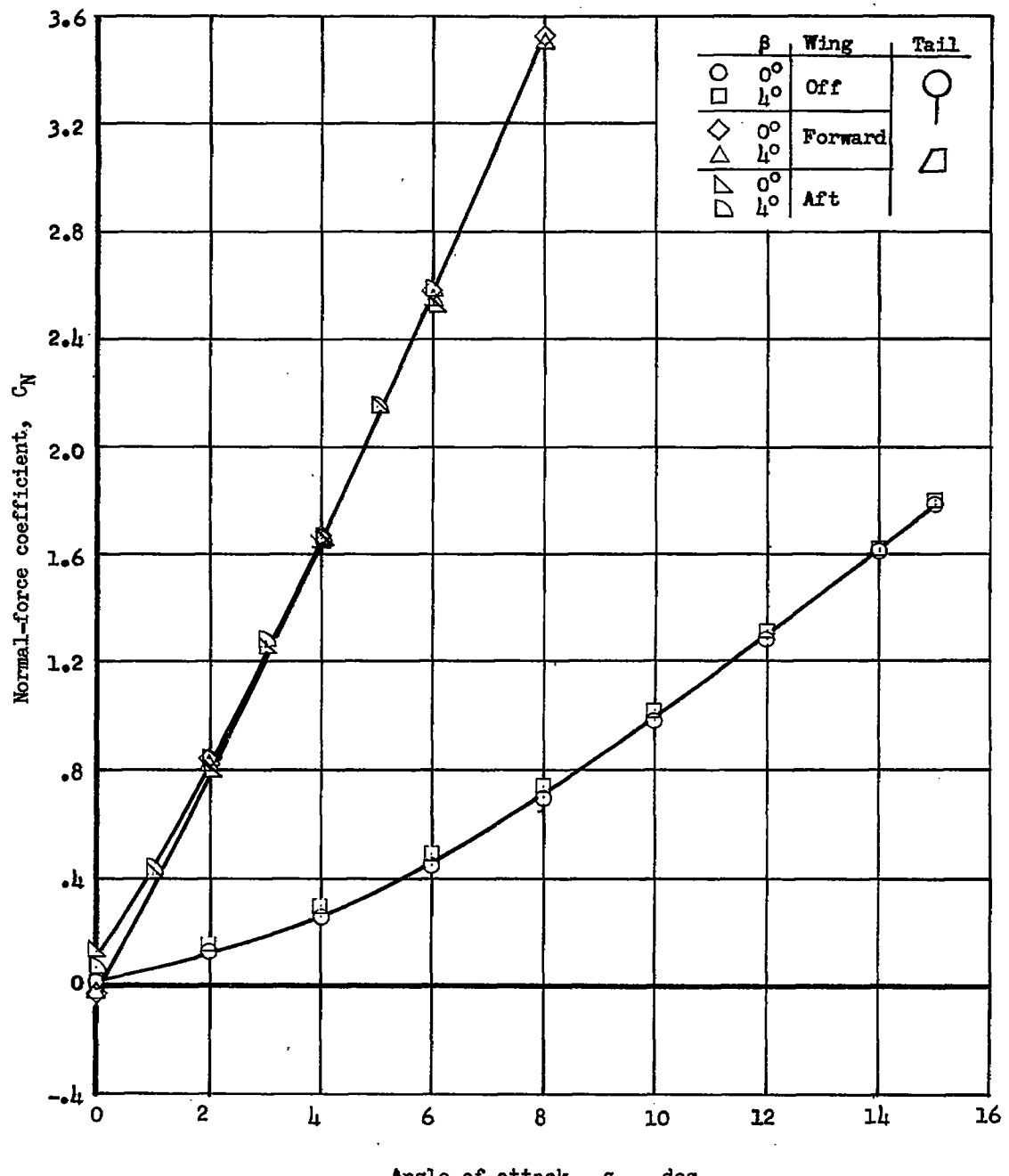
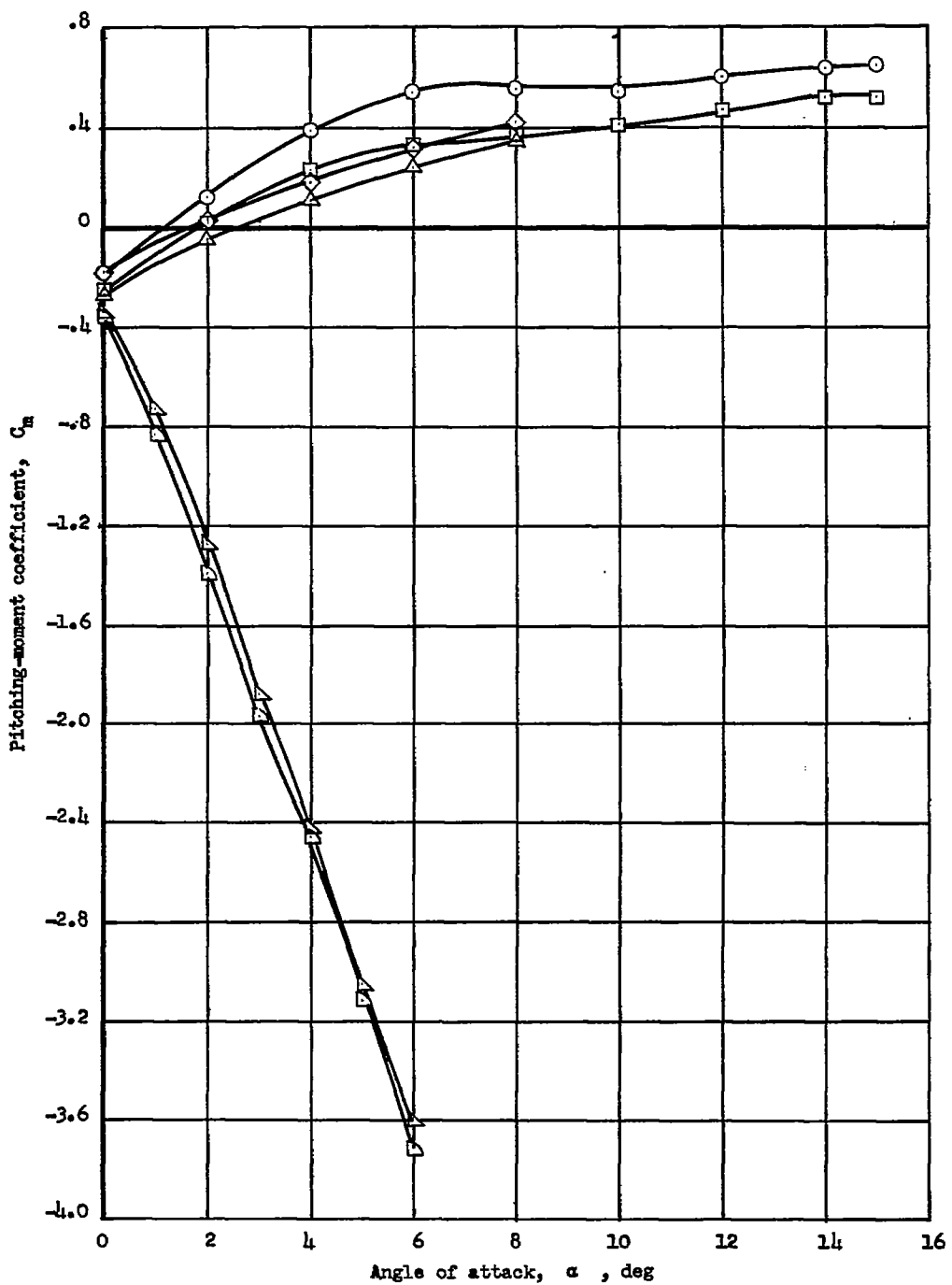
~~CONFIDENTIAL~~(g) Tail configuration $(V_l)_{trap}$.

Figure 4.- Continued.

~~CONFIDENTIAL~~



(g) Concluded.

Figure 4.- Concluded.

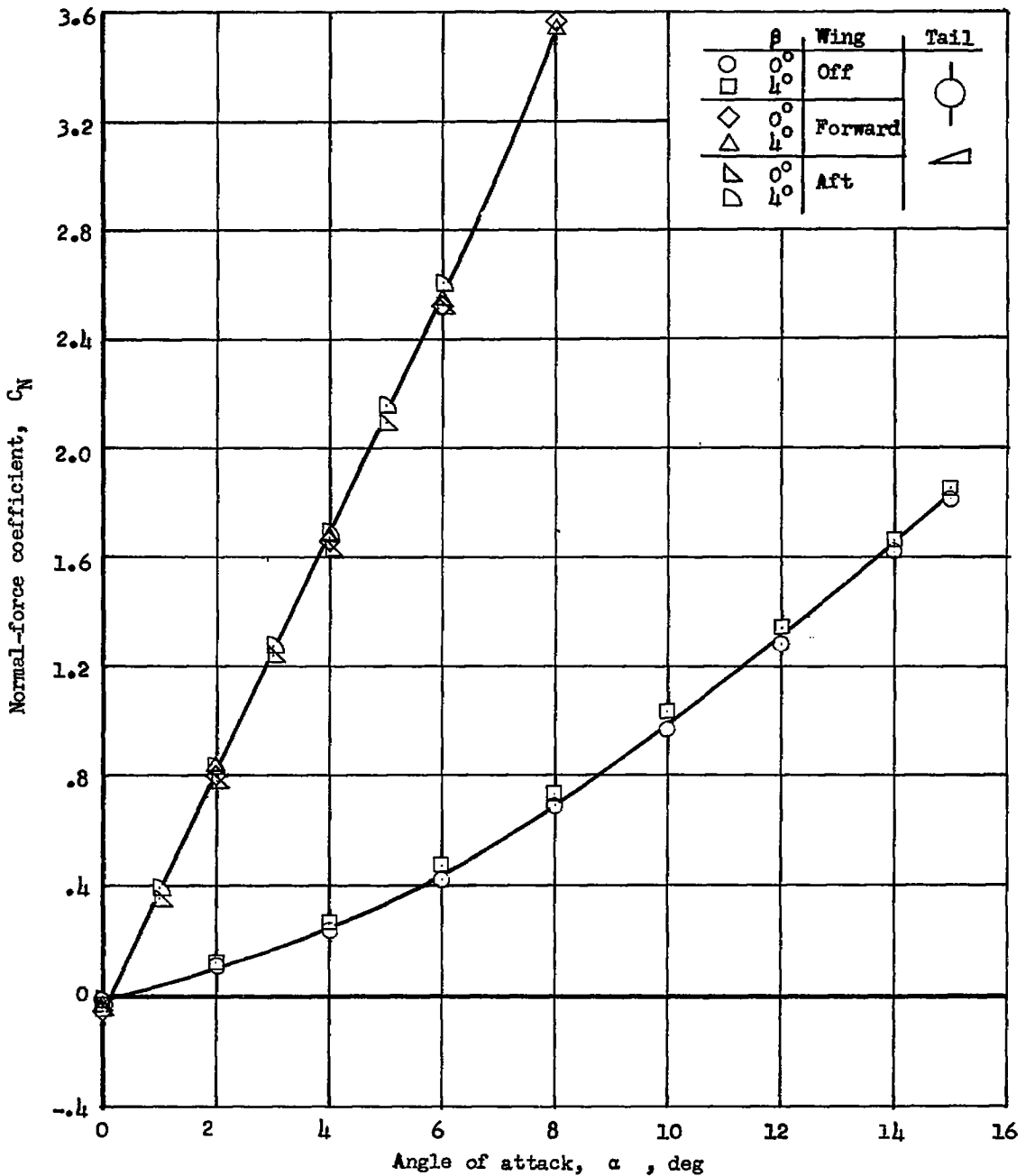
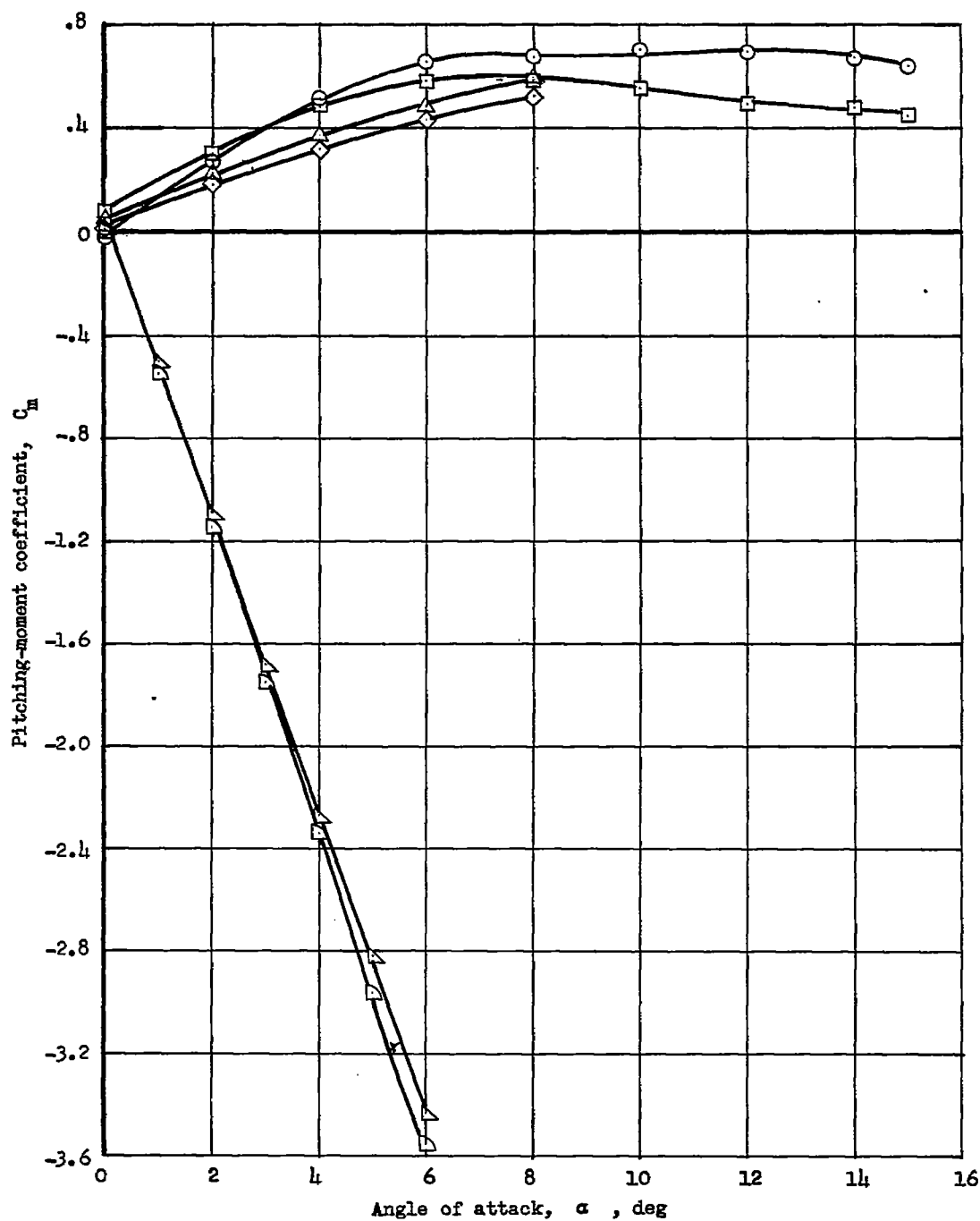
(a) Tail configuration $(V_u V_l)_{tri}$.

Figure 5.- Effects of presence of wing and wing position on longitudinal aerodynamic characteristics of configurations with vertical triangular tails.



(a) Concluded.

Figure 5.- Continued.

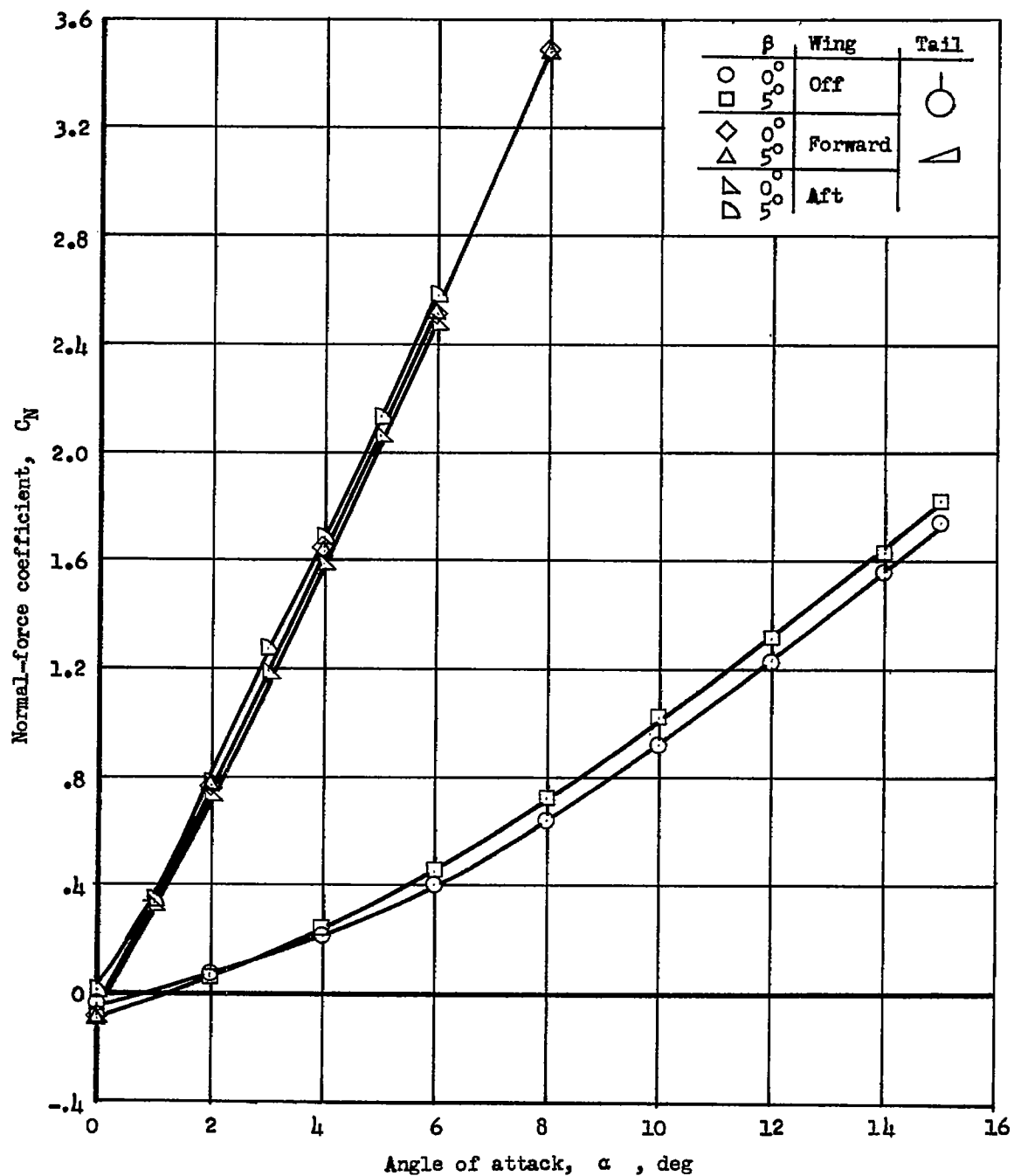
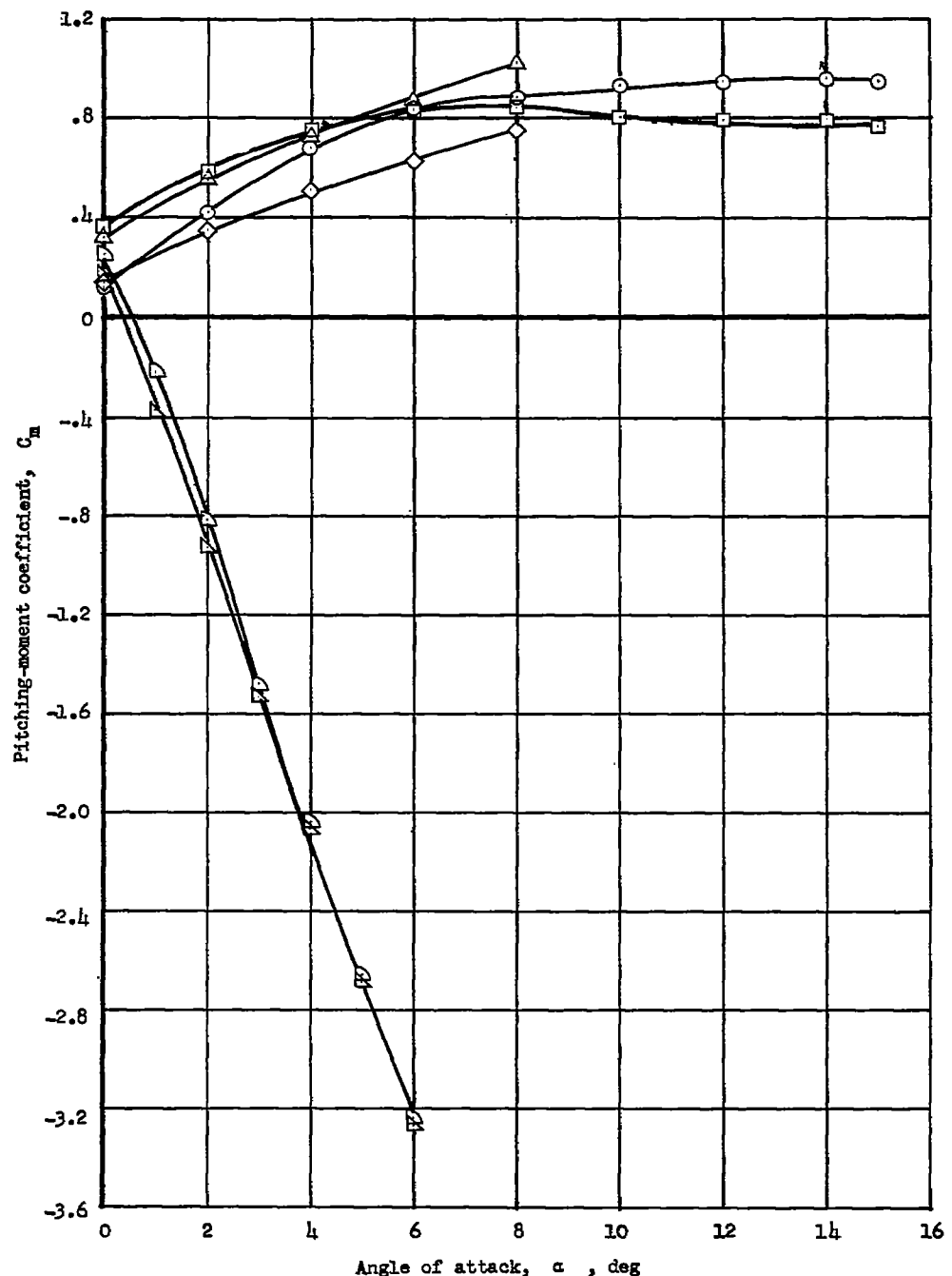
(b) Tail configuration $(V_u)_{tri}$.

Figure 5.- Continued.



(b) Concluded.

Figure 5.- Continued.

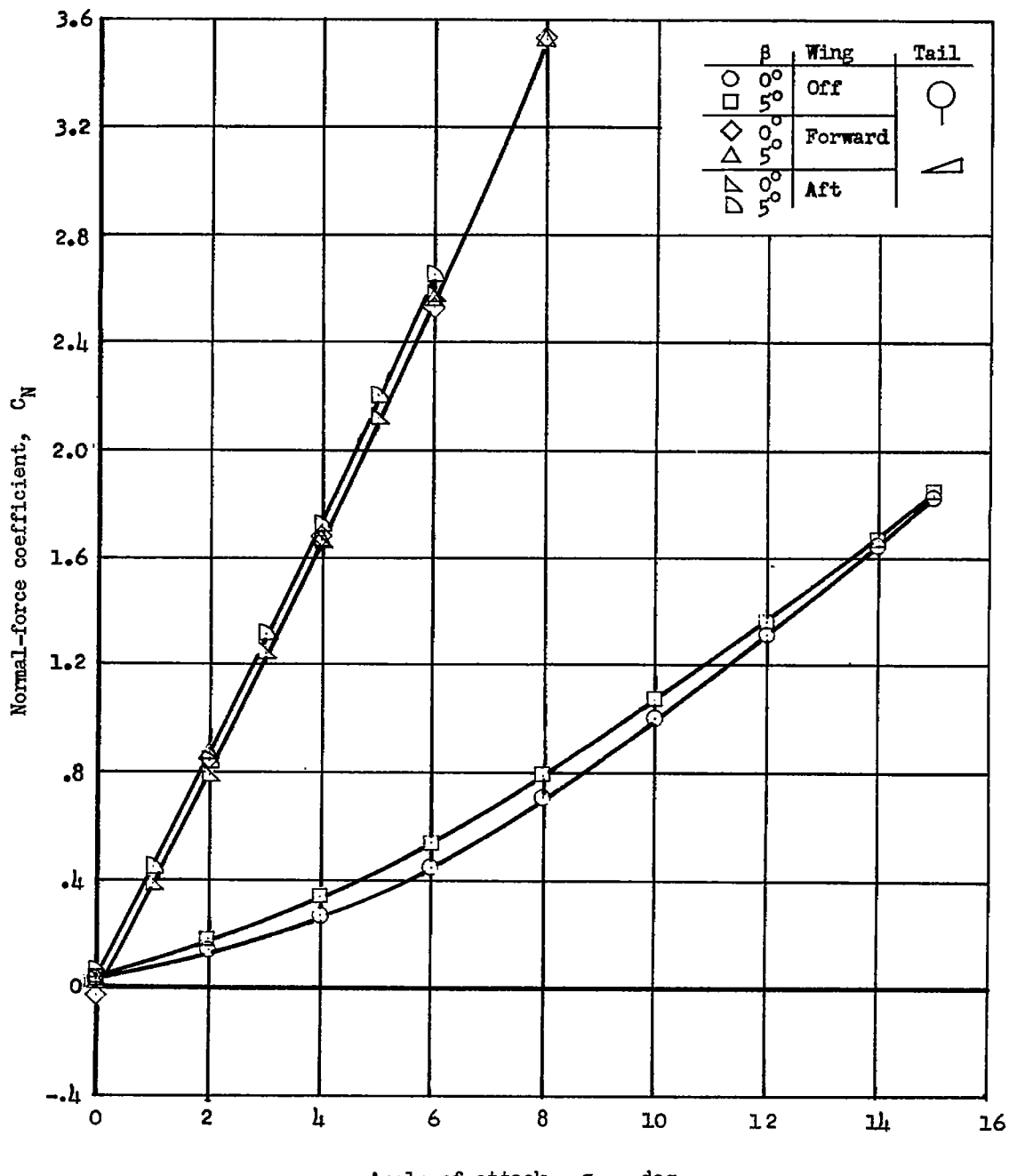
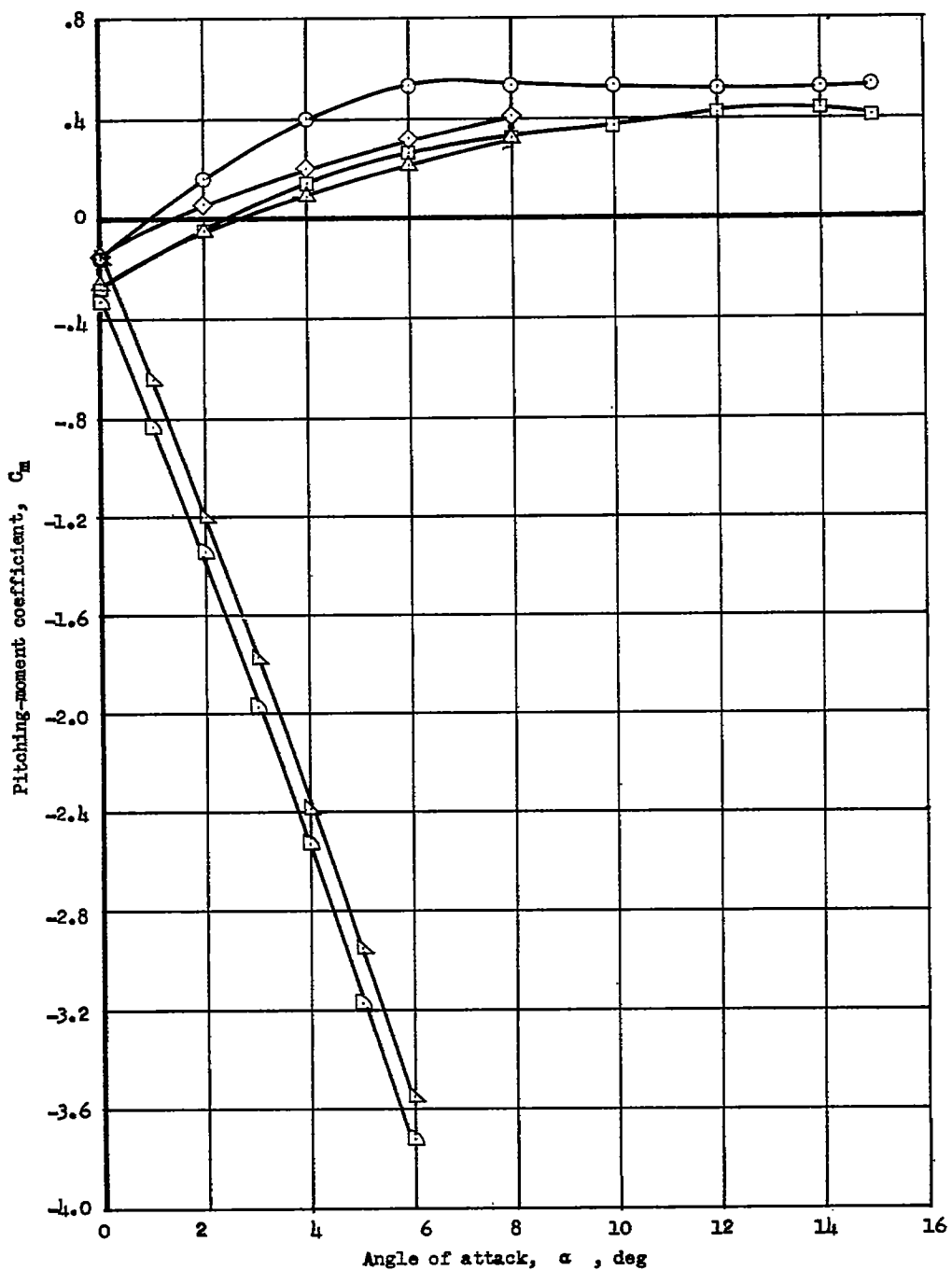
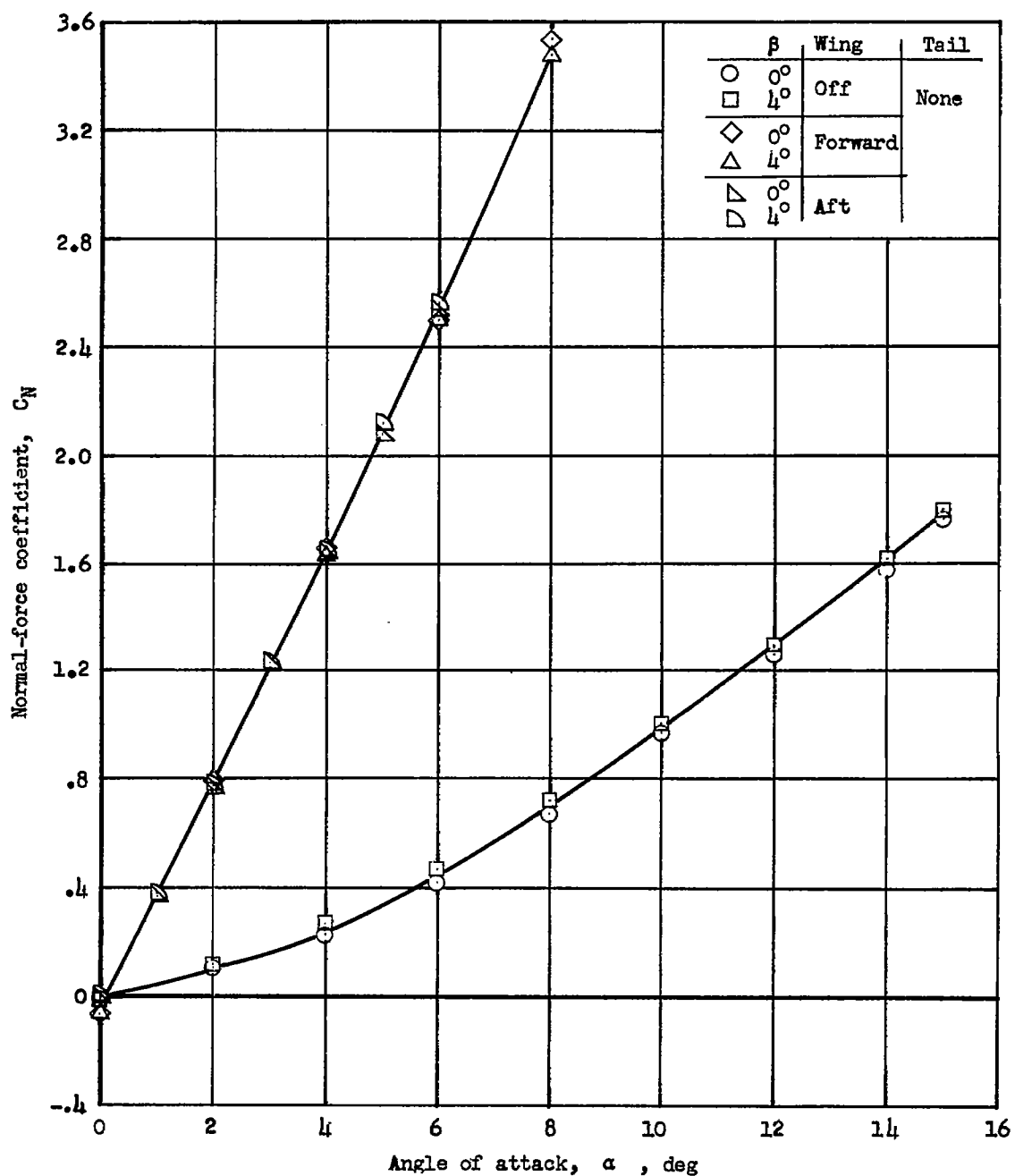
(c) Tail configuration $(V_l)_{tri}$.

Figure 5.- Continued.



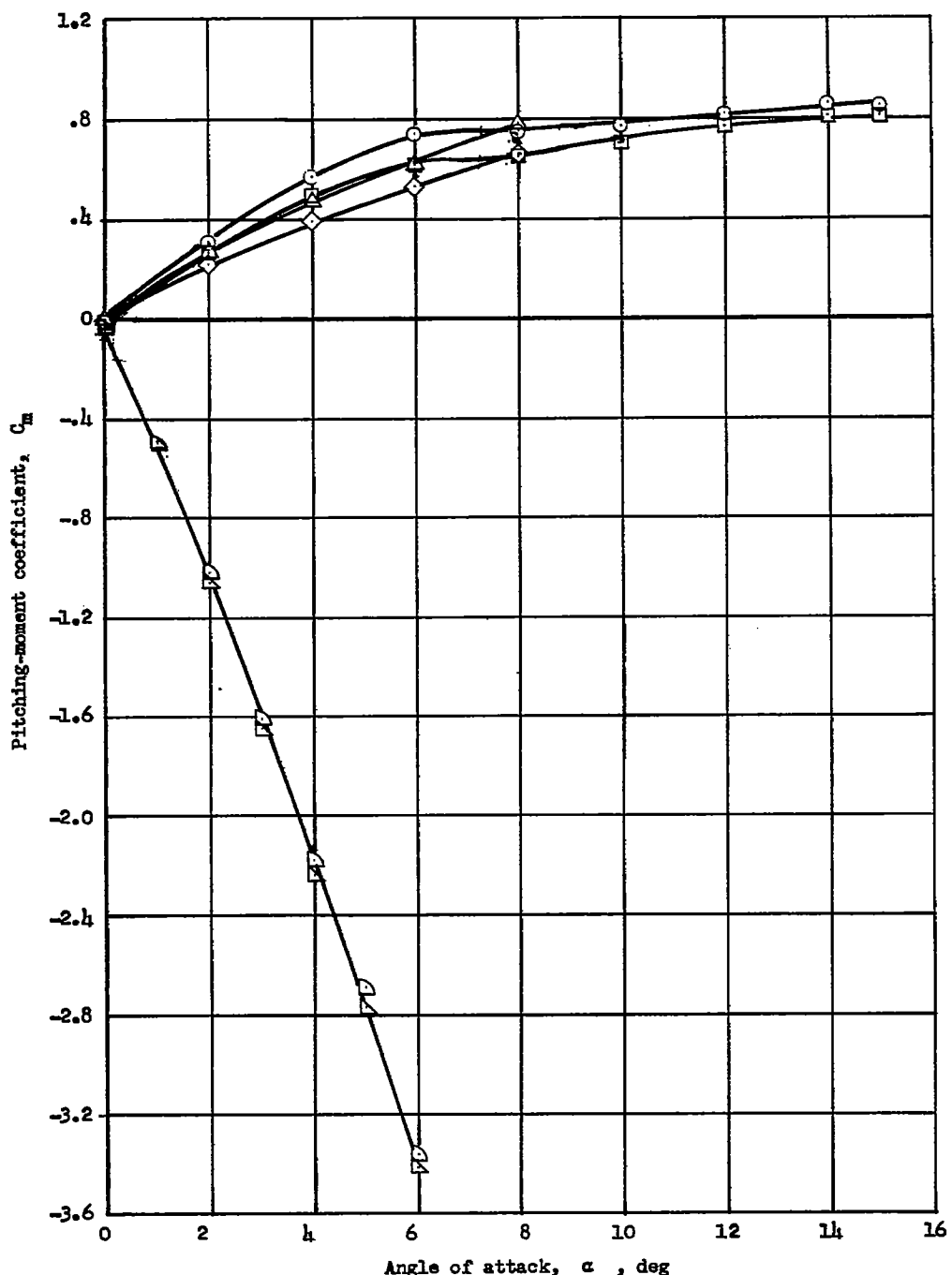
(c) Concluded.

Figure 5.- Concluded.



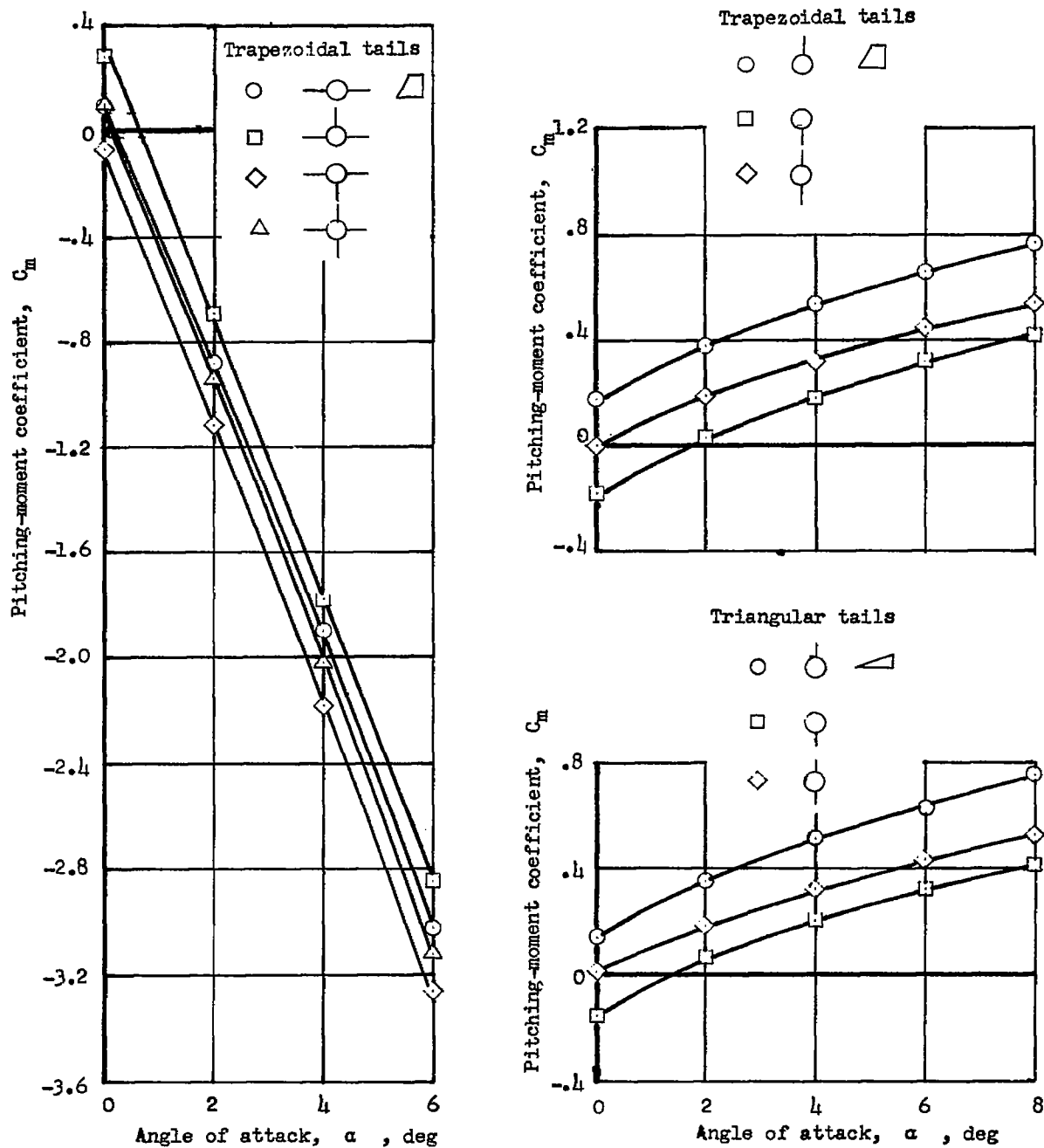
(a) Normal-force coefficient.

Figure 6.- Effects of presence of wing and wing position on longitudinal aerodynamic characteristics of a configuration with no tail.



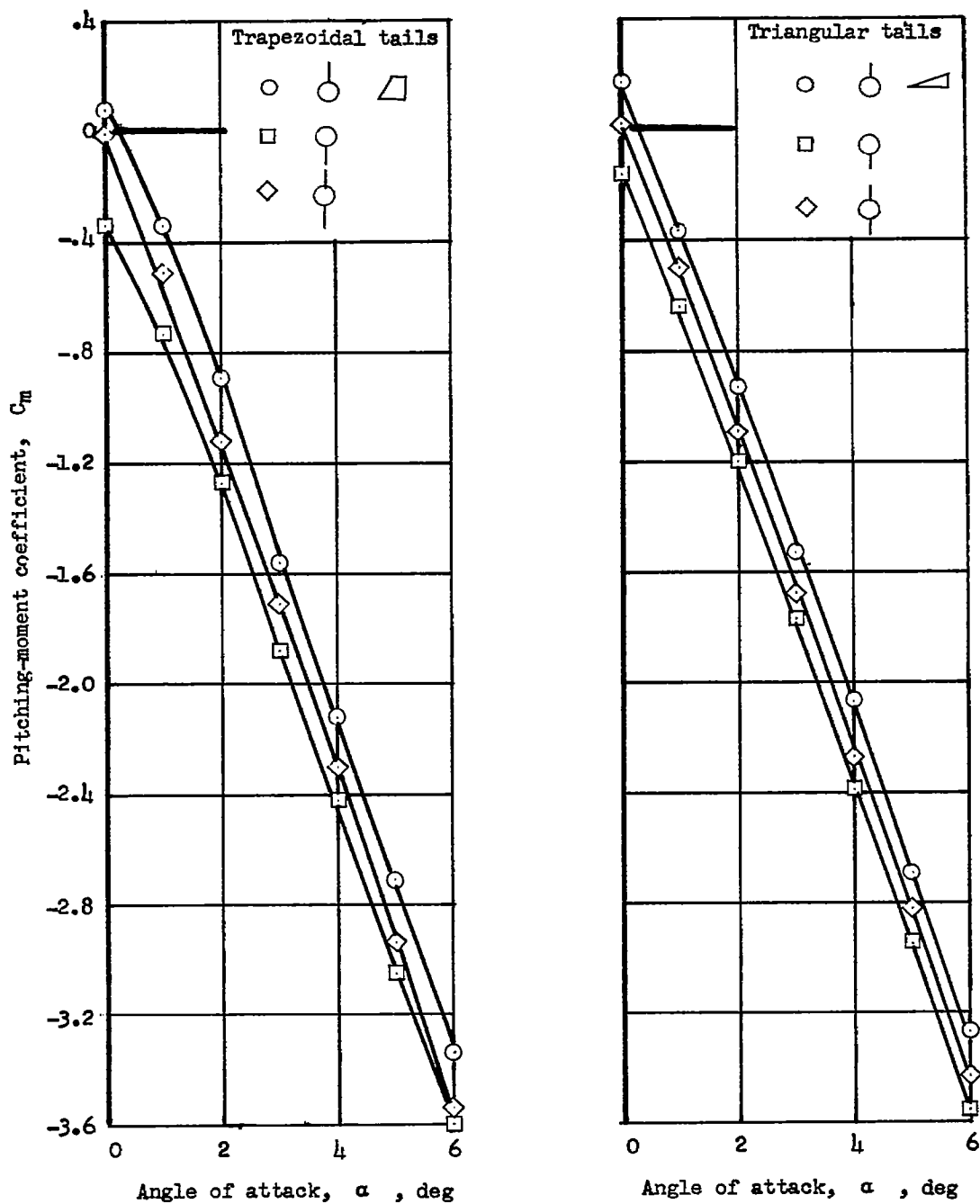
(b) Pitching-moment coefficient.

Figure 6.- Concluded.



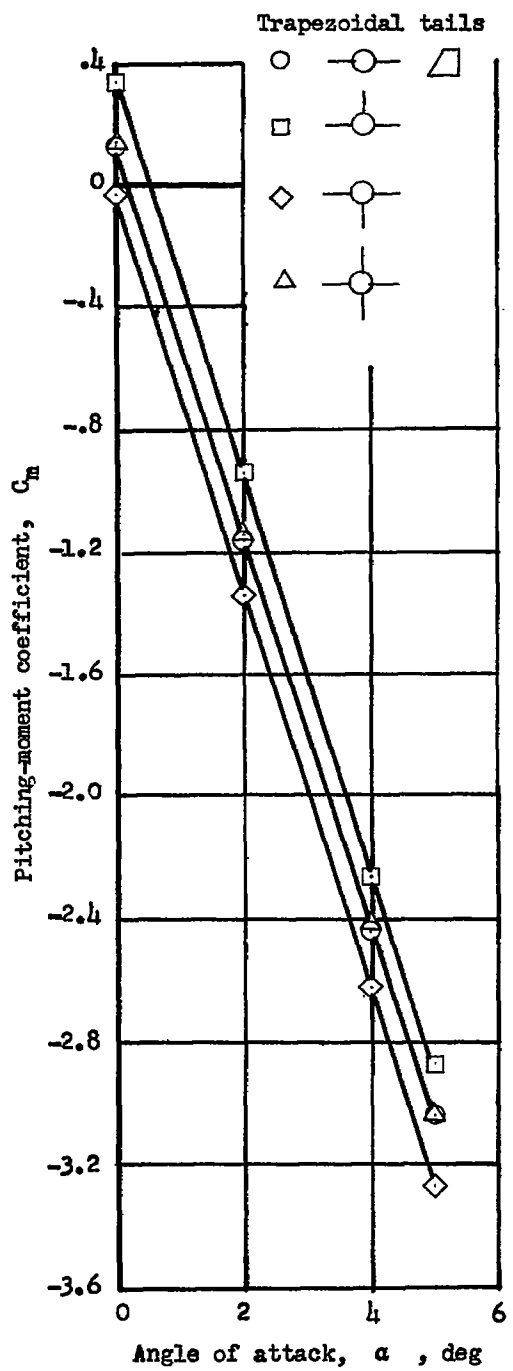
(a) Wing in forward position.

Figure 7.- Effects of various tail arrangements on the wing-on and wing-off pitching moment of a generalized missile at $\beta = 0^\circ$.



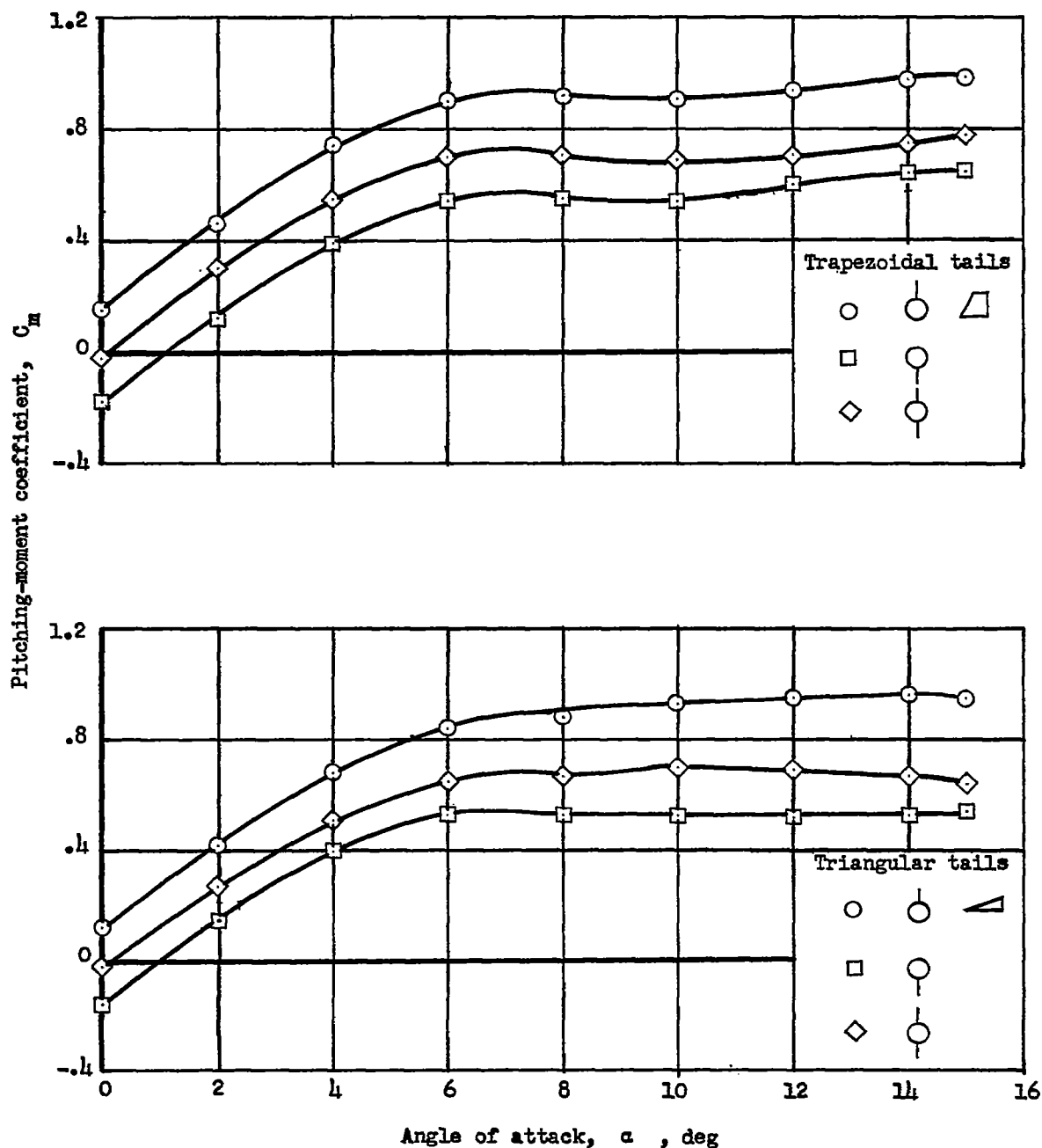
(b) Wing in rear position.

Figure 7.- Continued.



(c) Wing off.

Figure 7.- Continued.



(c) Concluded.

Figure 7.- Concluded.

~~CONFIDENTIAL~~

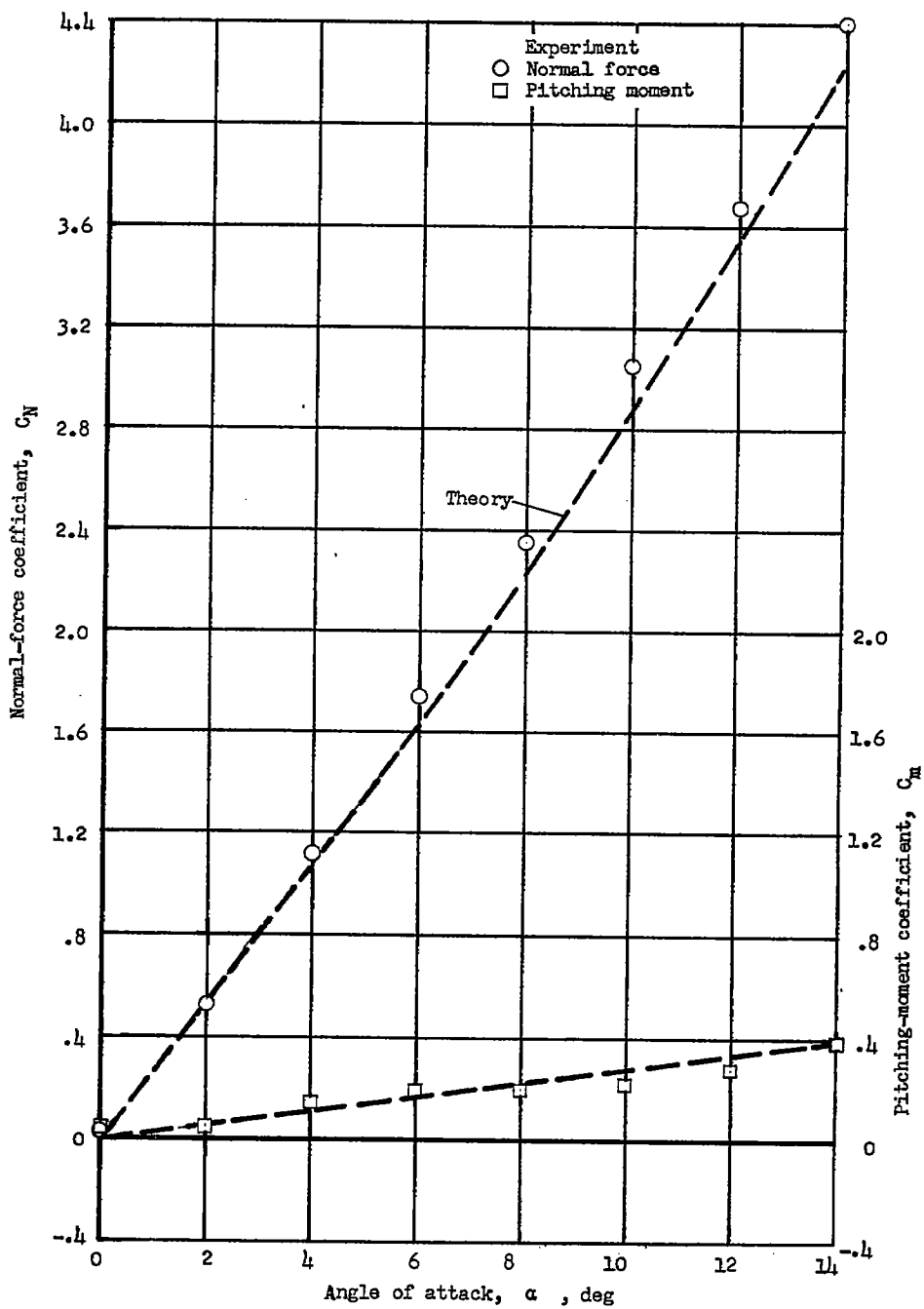
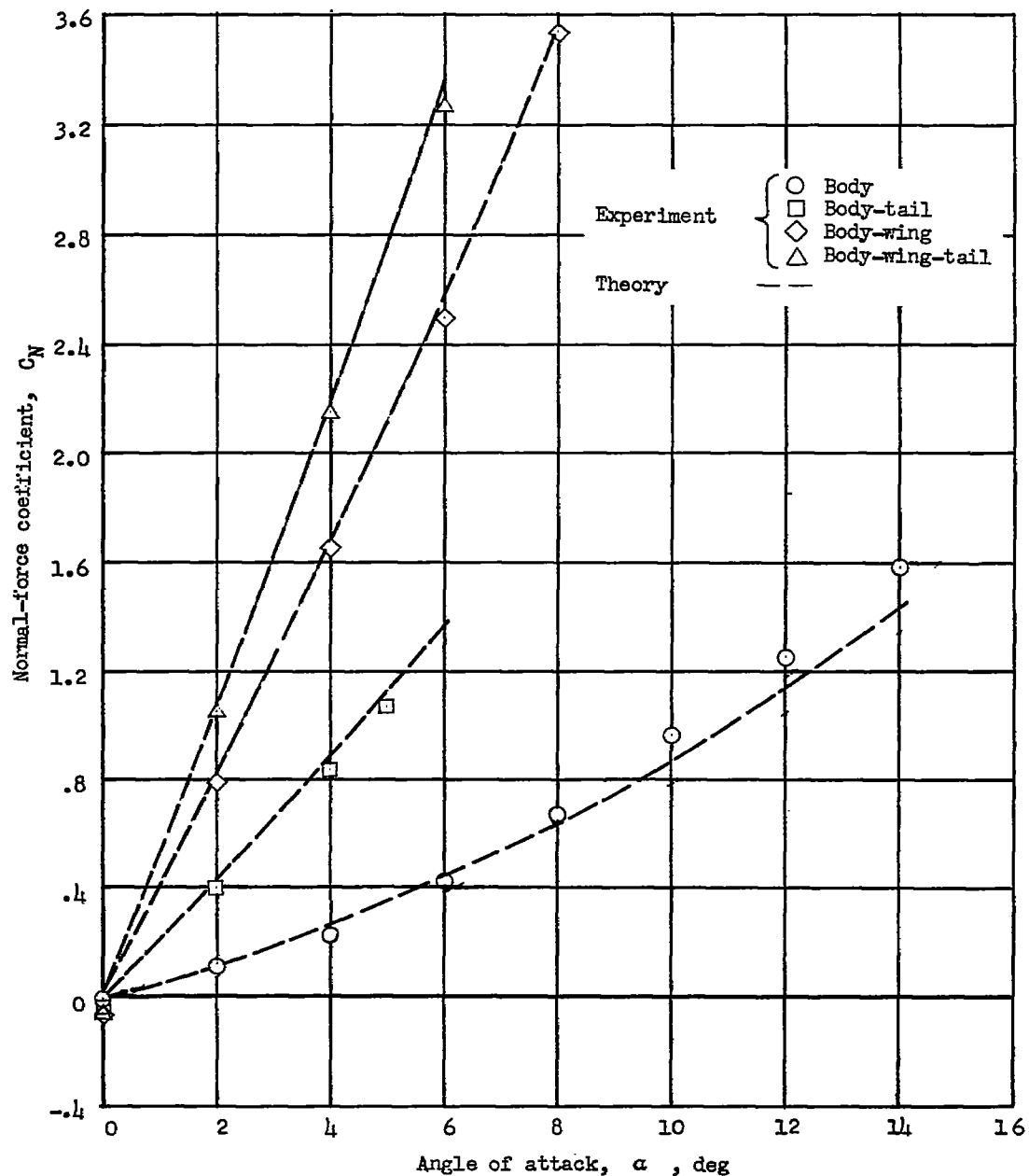
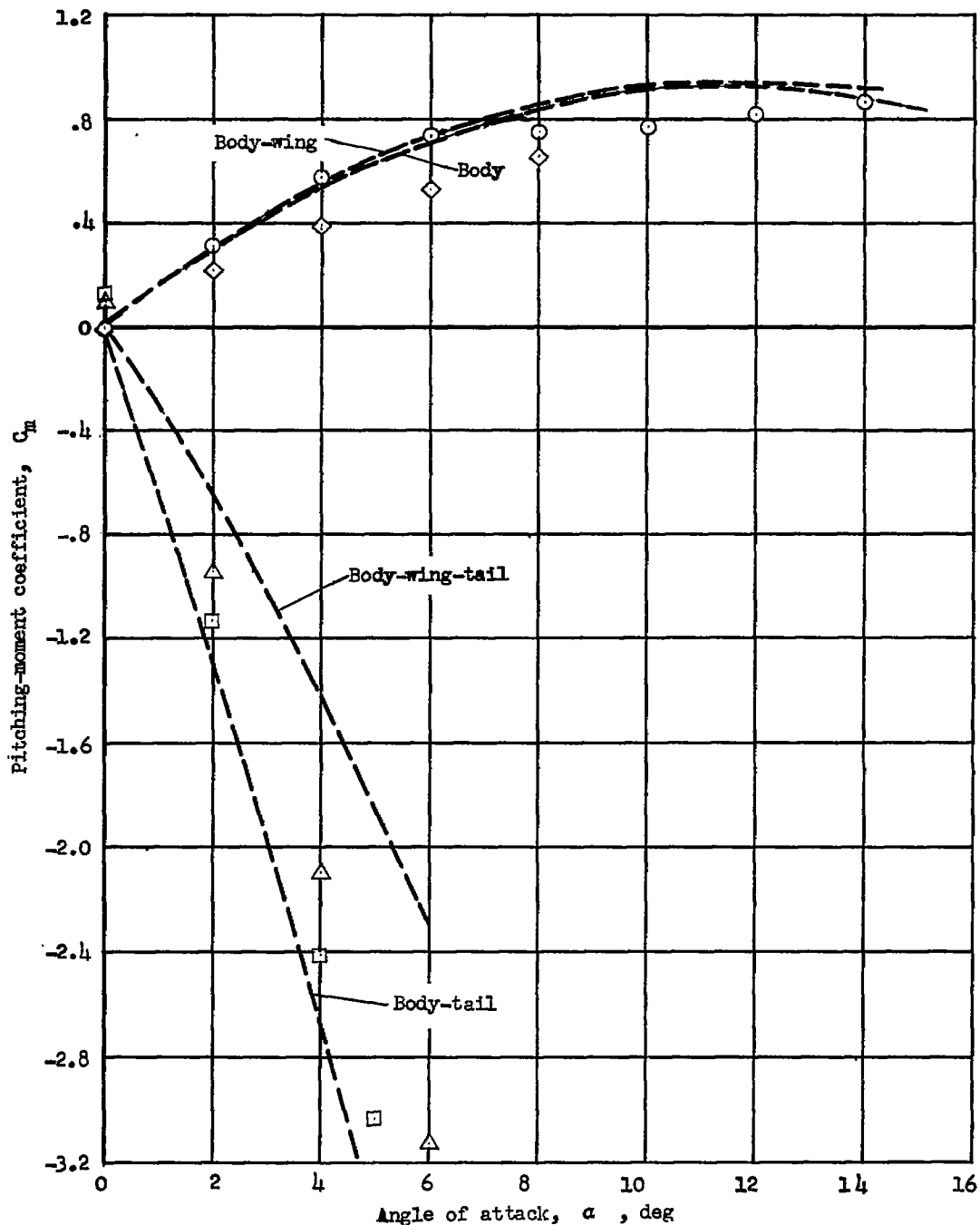


Figure 8.- Experimental and theoretical wing-alone normal force and pitching moment for the rectangular wing of the present configurations.



(a) Normal force.

Figure 9.- Experimental and theoretical normal-force and pitching-moment coefficients for various combinations of a body, a cruciform trapezoidal tail, and a wing in the forward position. $\beta = 0^\circ$.



(b) Pitching moment.

Figure 9.- Concluded.
~~CONFIDENTIAL~~

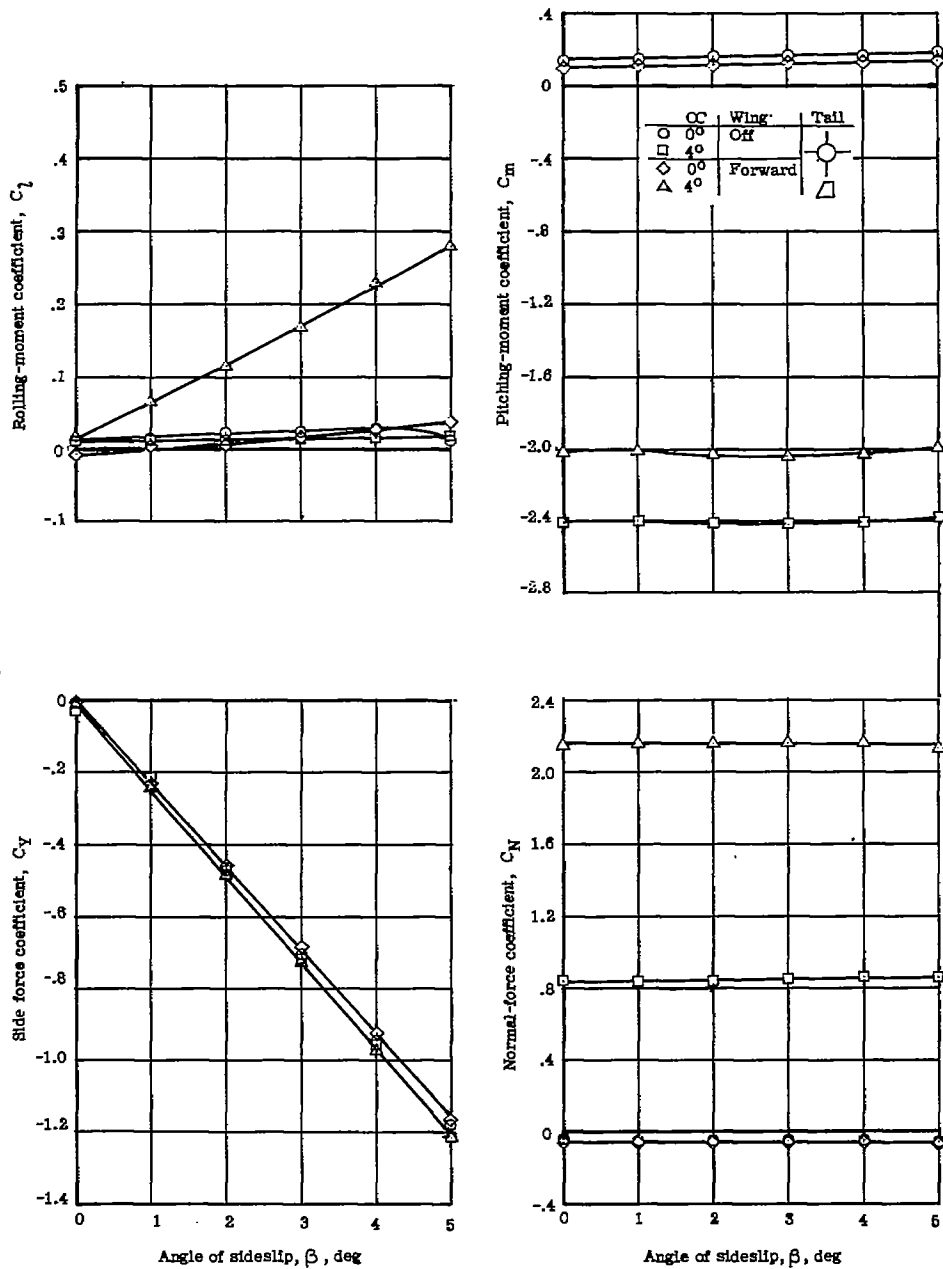
(a) Tail configuration $(HV_uV_l)_{trap}$.

Figure 10.- Effects of angle of attack and wing position on the variation of aerodynamic characteristics with angle of sideslip for configurations with trapezoidal tails.

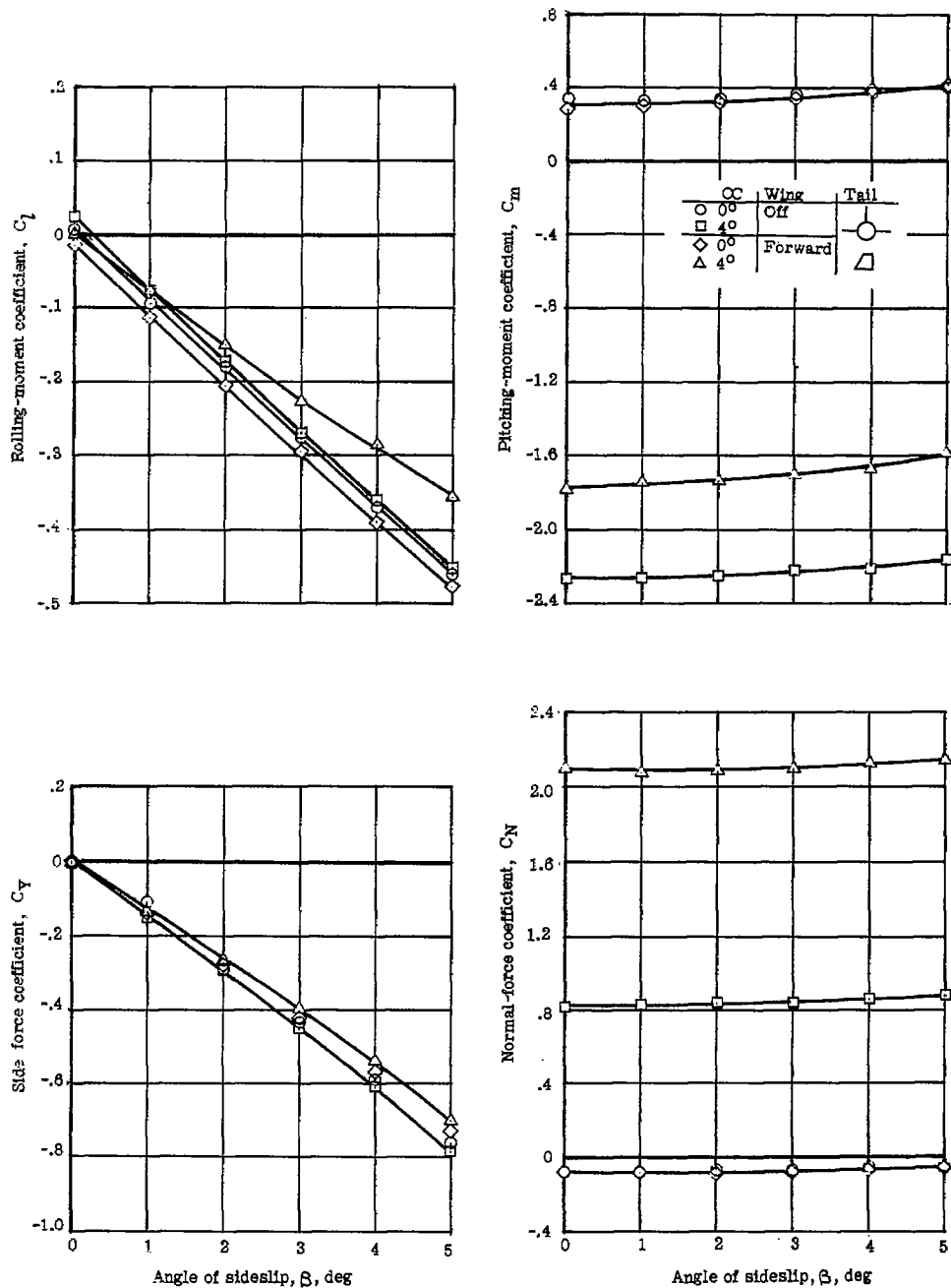
(b) Tail configuration $(HV_u)_{trap}$.

Figure 10.- Continued.

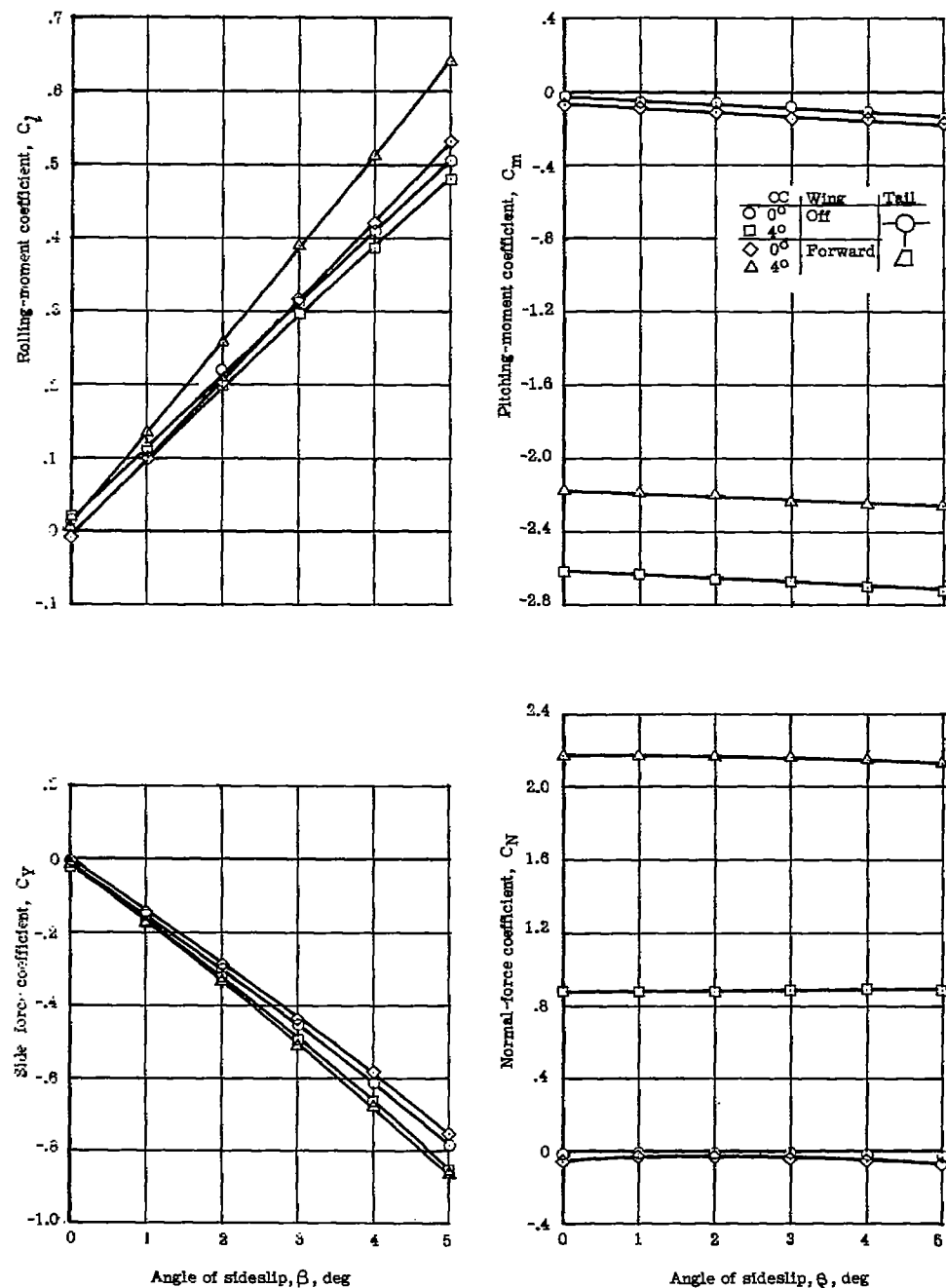
(c) Tail configuration $(HV_l)_{trap}$.

Figure 10.- Continued.

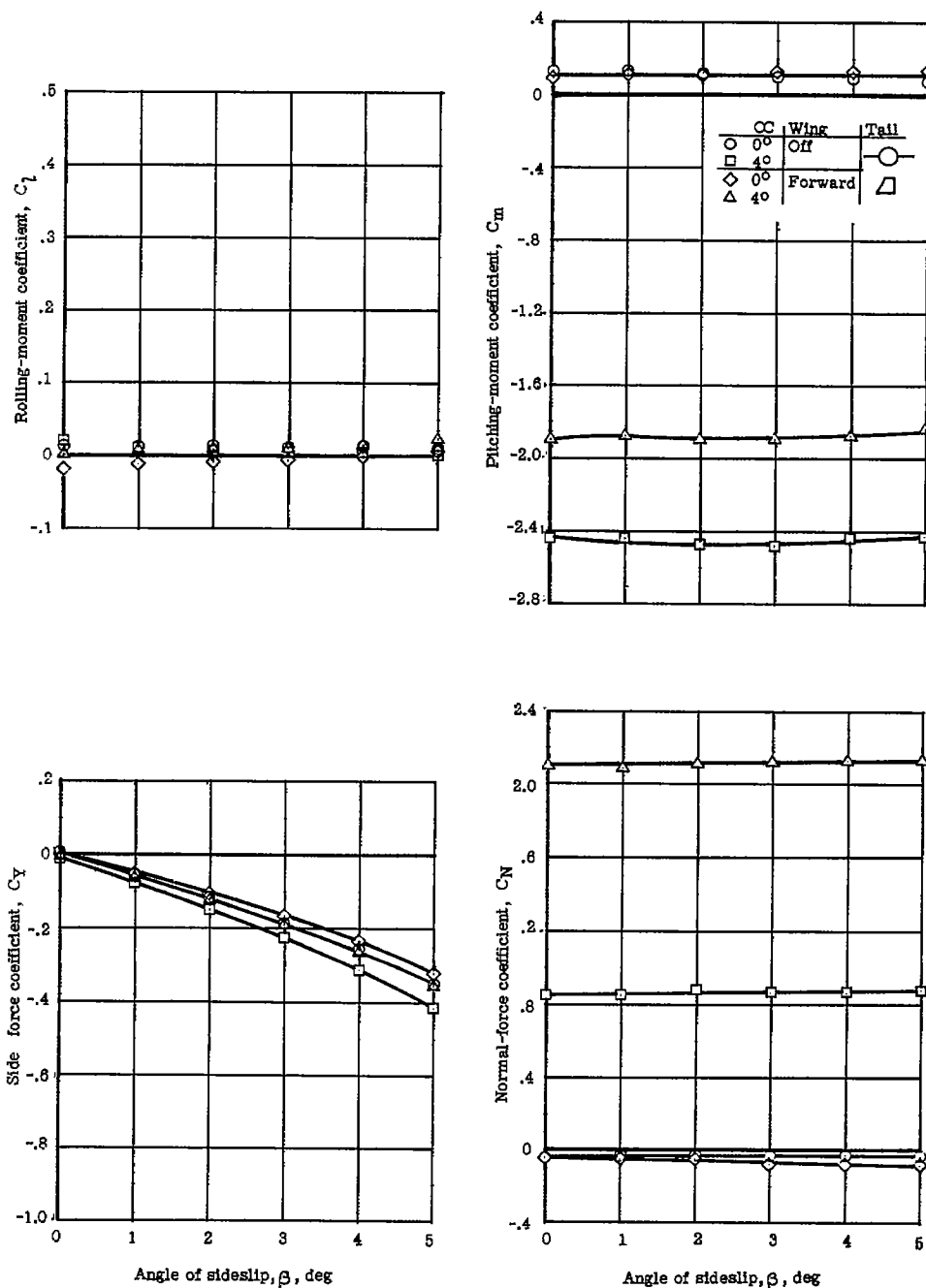
(d) Tail configuration $(H)_{trap}$.

Figure 10.- Continued.

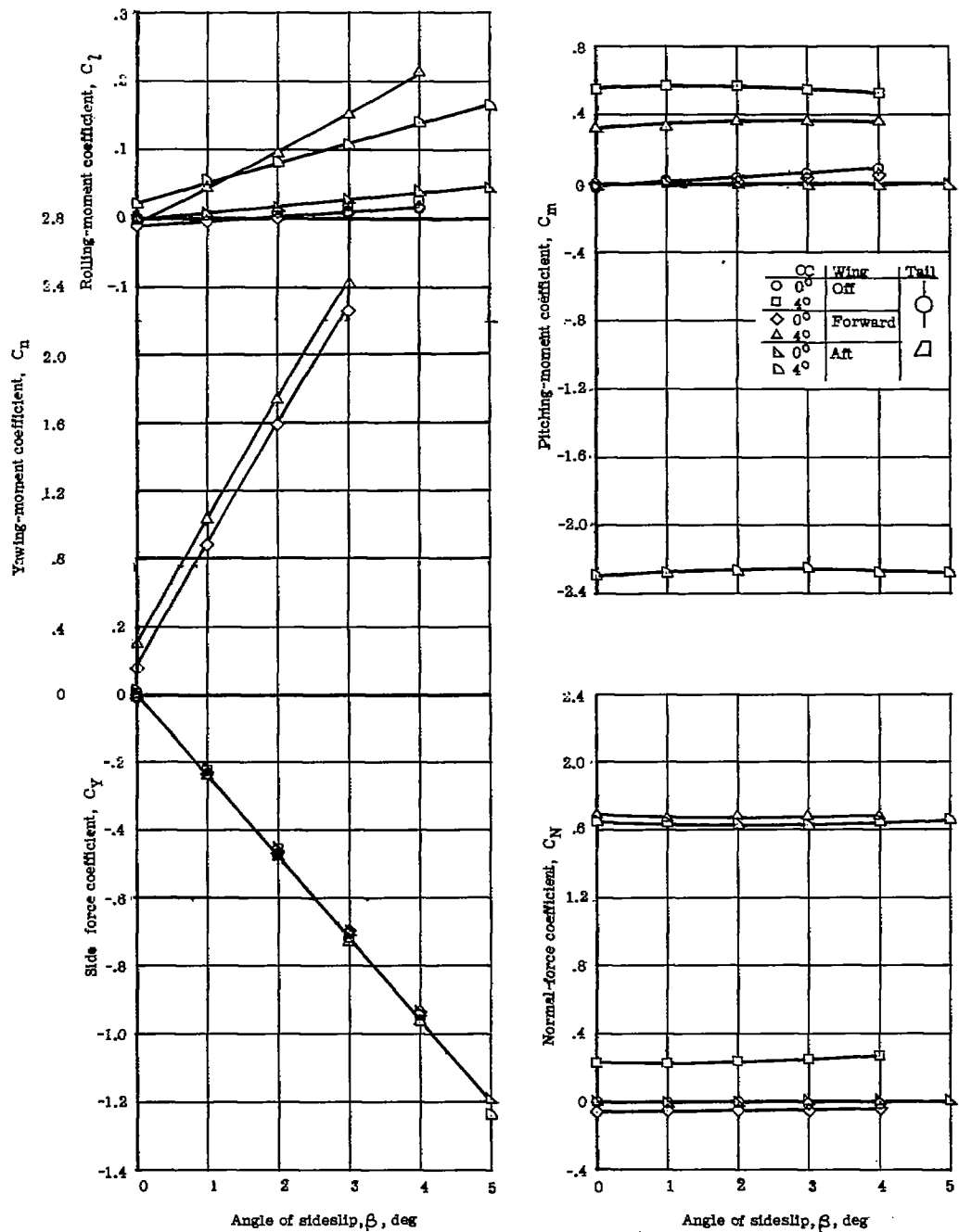
(e) Tail configuration $(V_u V_l)_{\text{trap}}$.

Figure 10.- Continued.

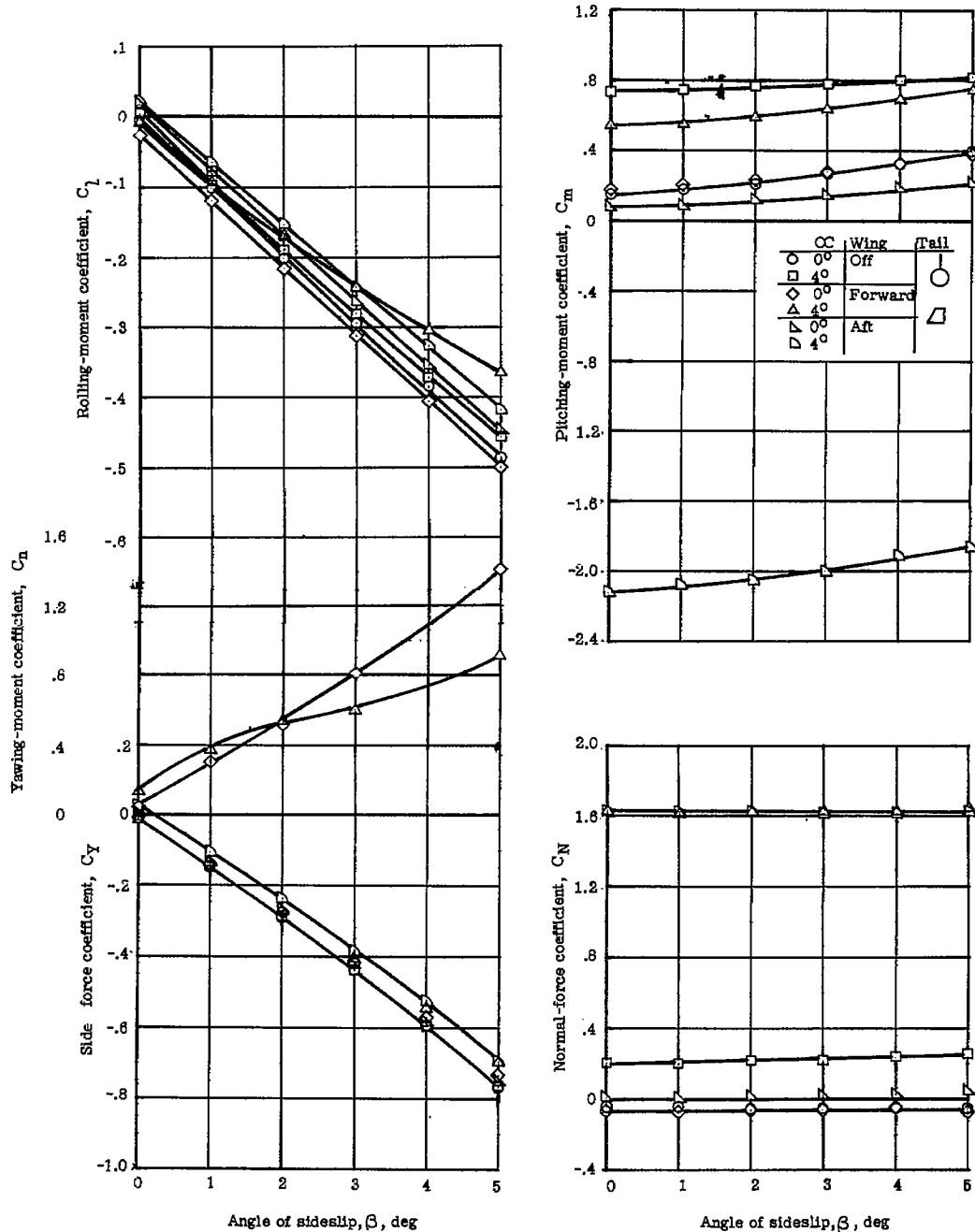
(f) Tail configuration $(V_u)_{trap}$.

Figure 10.- Continued.

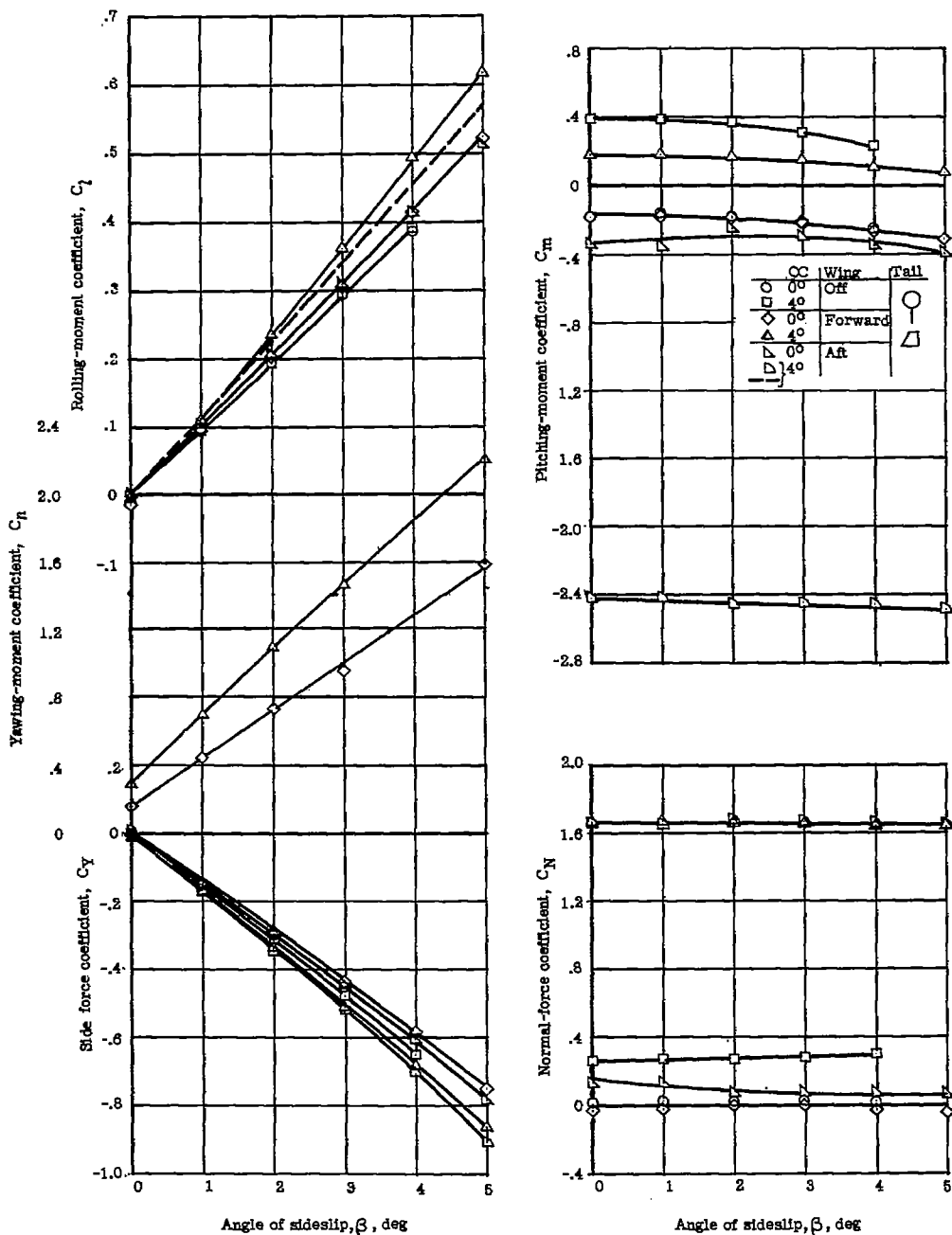
(g) Tail configuration $(V_l)_{trap}$.

Figure 10.- Concluded.

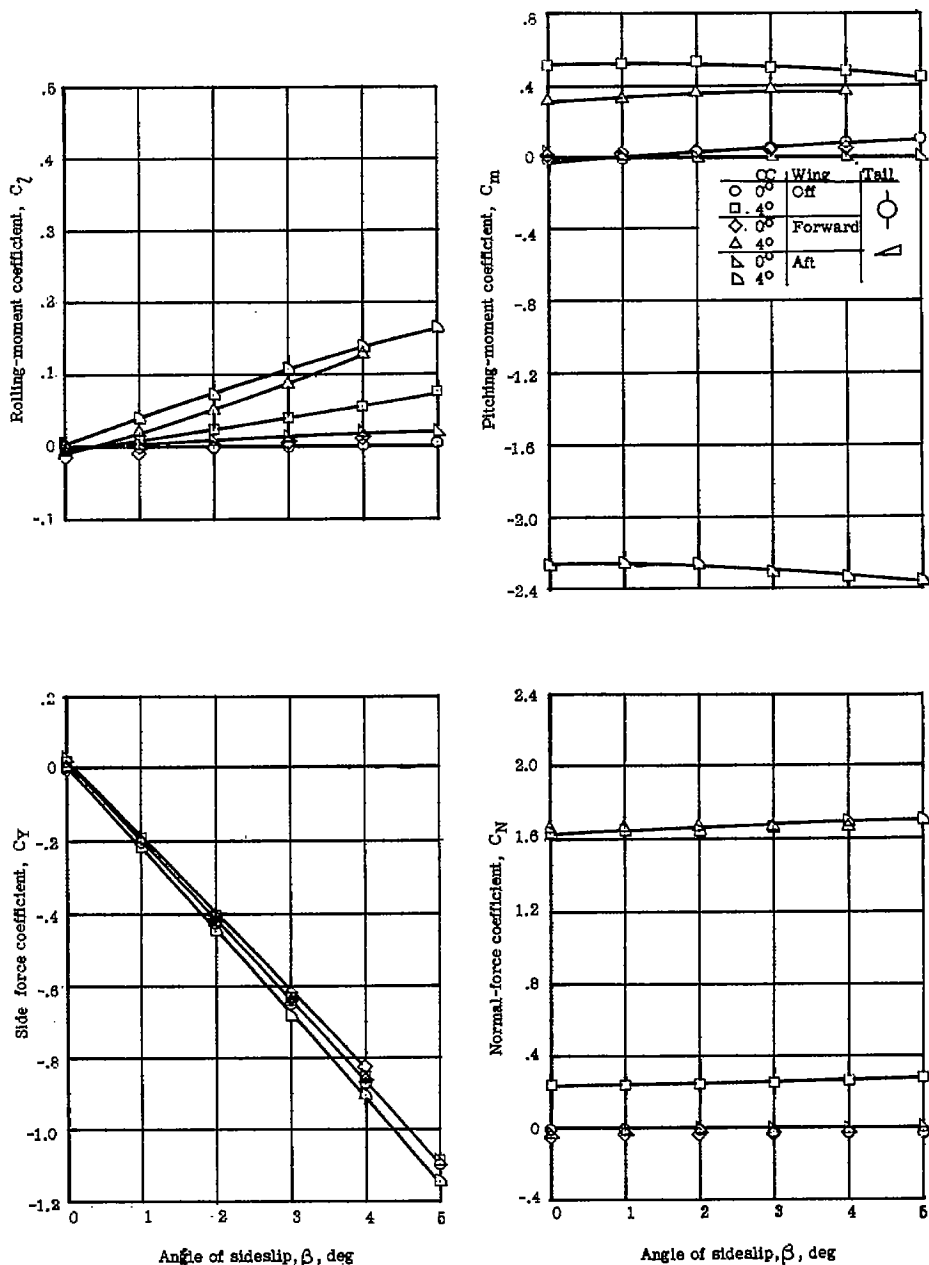
(a) Tail configuration $(V_u V_l)_{tri}$.

Figure 11.- Effects of angle of attack and wing position on the variation of aerodynamic characteristics with angle of sideslip for configurations with triangular tails.

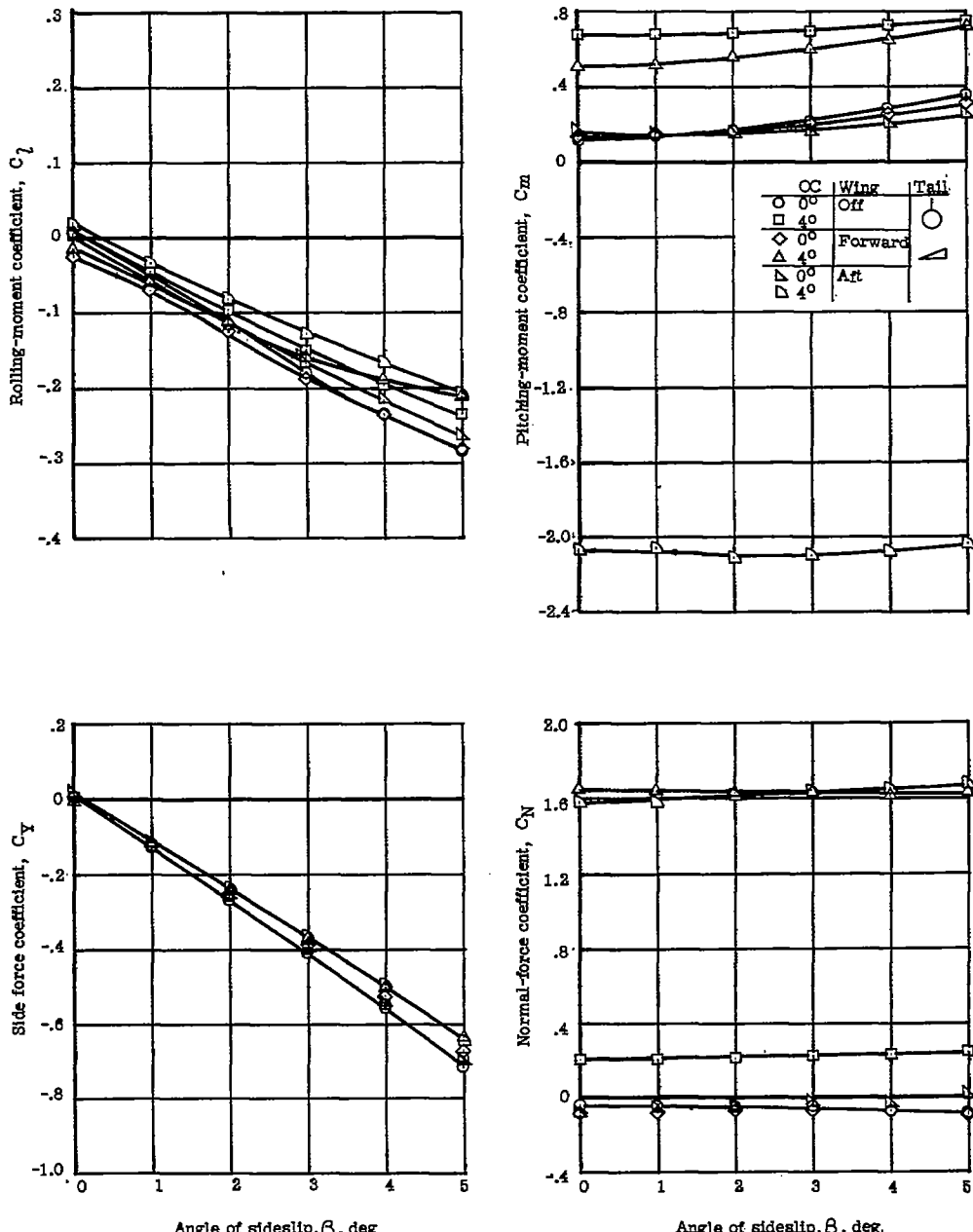
(b) Tail configuration $(V_u)_{tri}$.

Figure 11.- Continued.

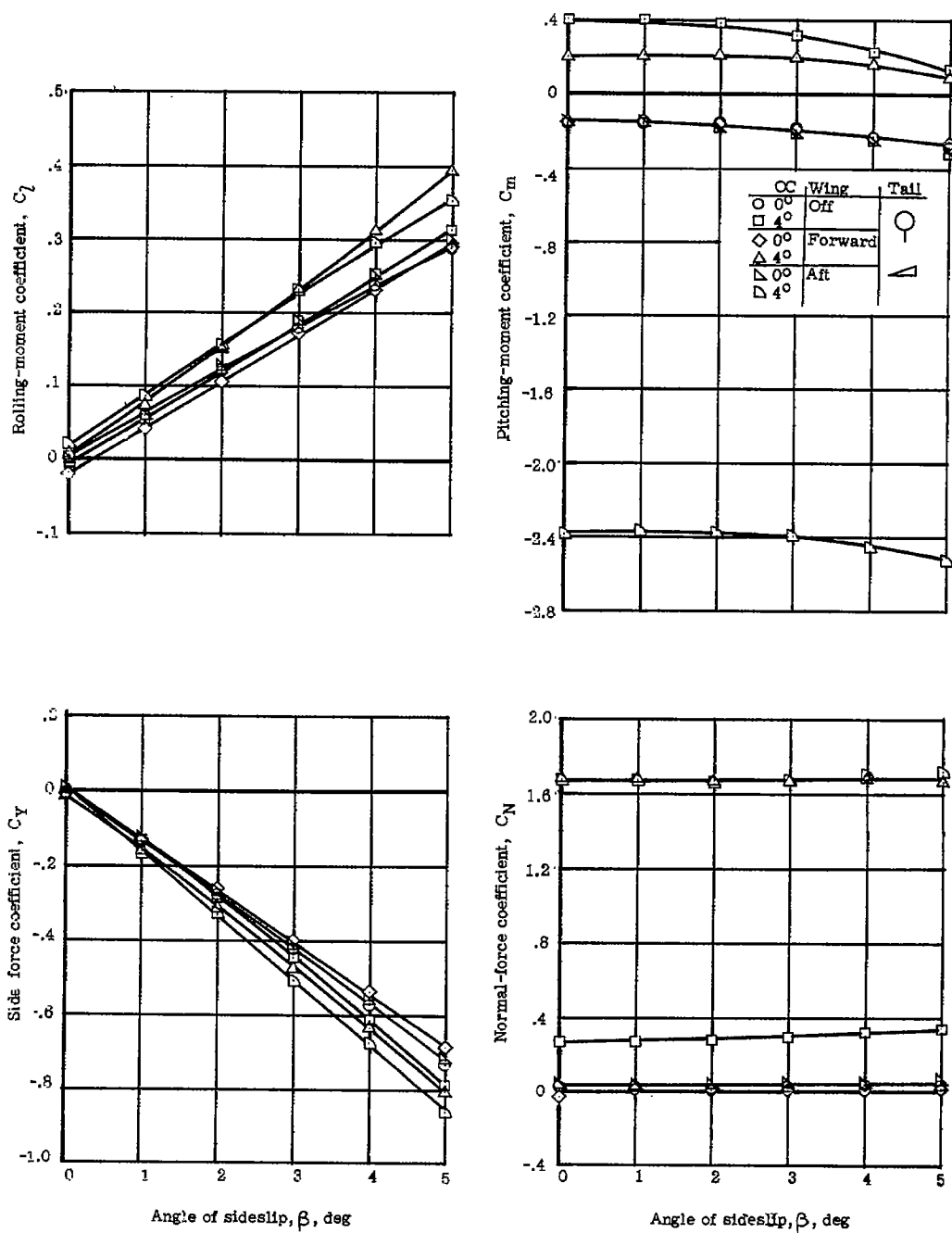
(c) Tail configuration $(V_l)_{tri}$.

Figure 11.- Concluded.

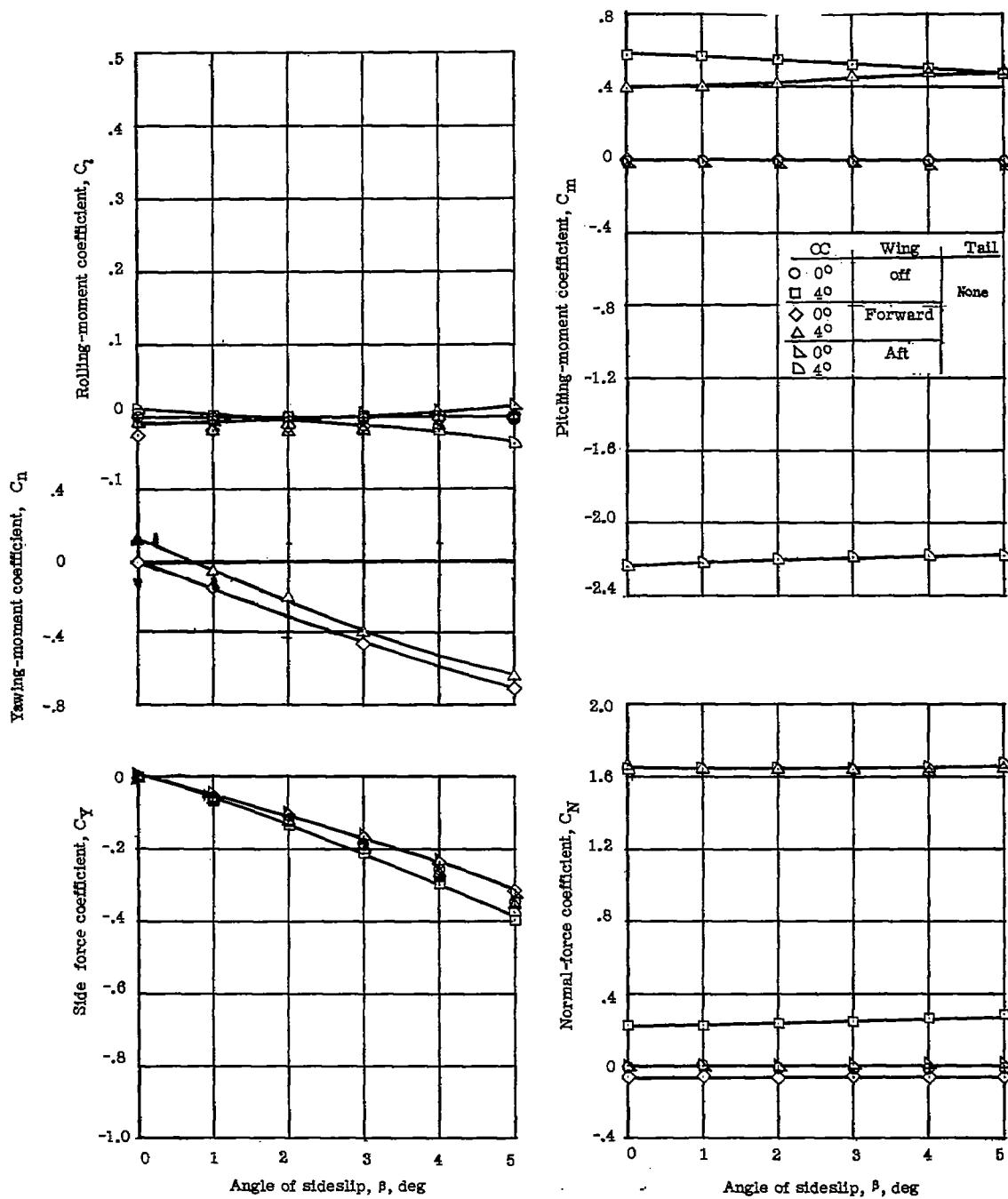
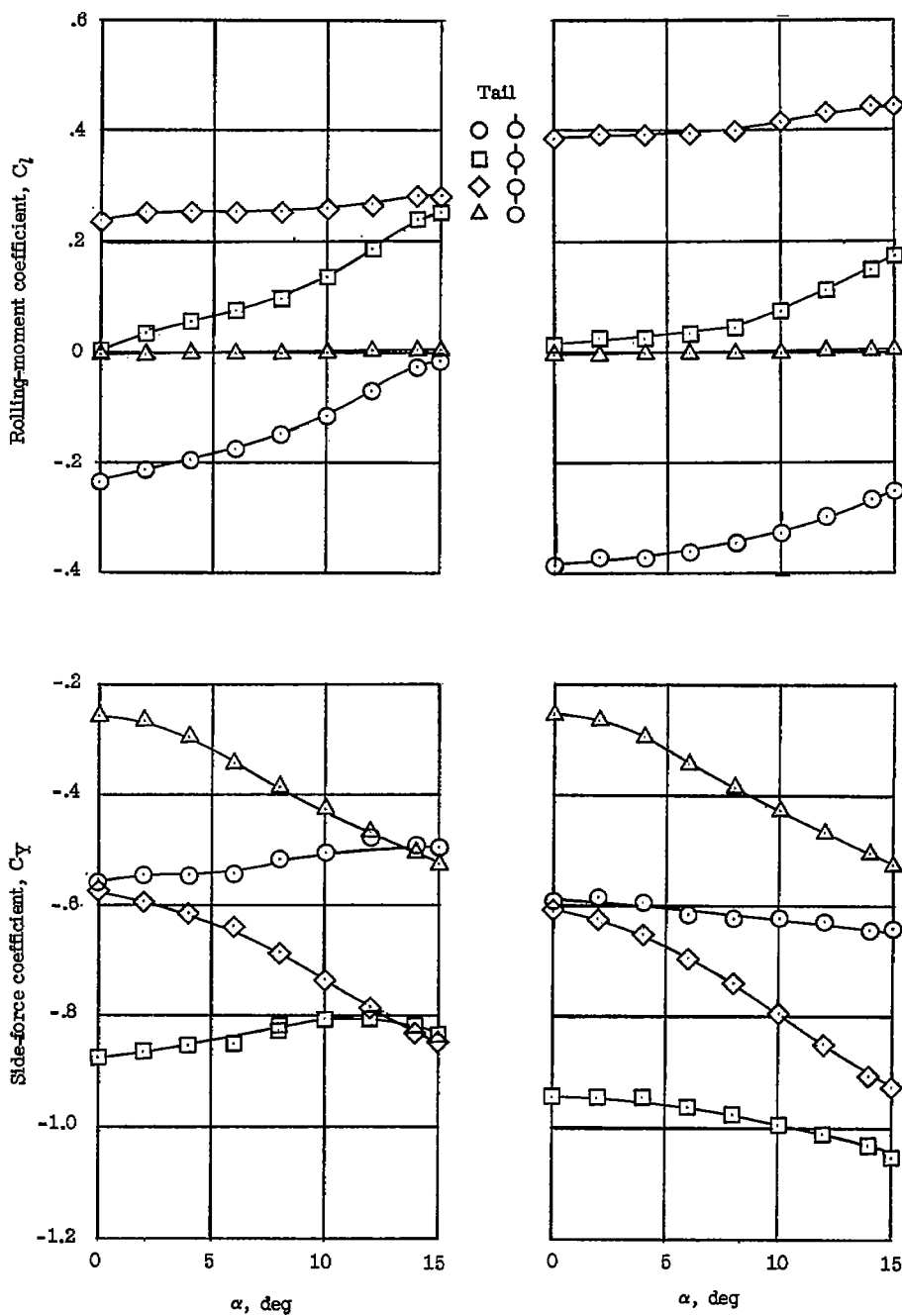


Figure 12.- Effects of angle of attack and wing position on the variation of aerodynamic characteristics with angle of sideslip for a configuration with no tail.

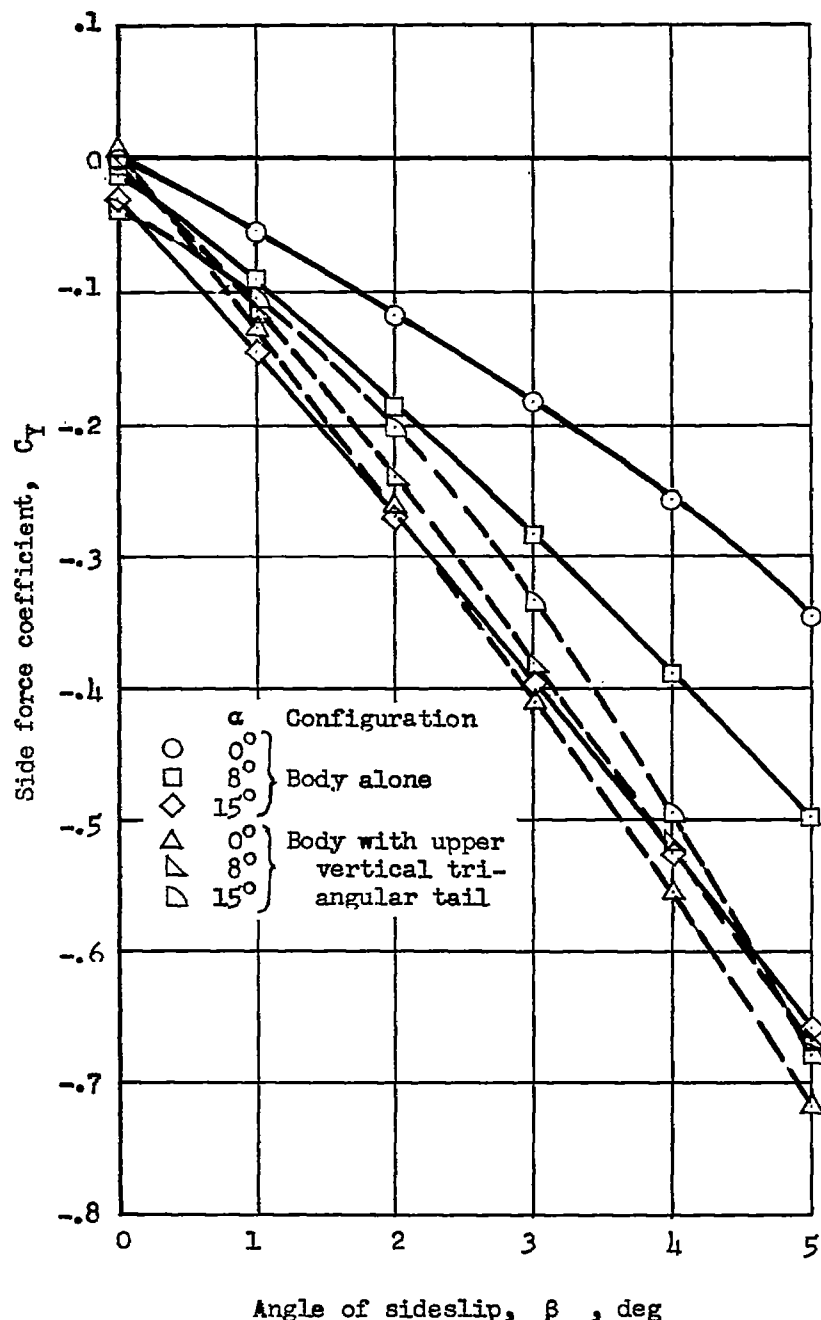
CONFIDENTIAL



(a) Triangular tails.

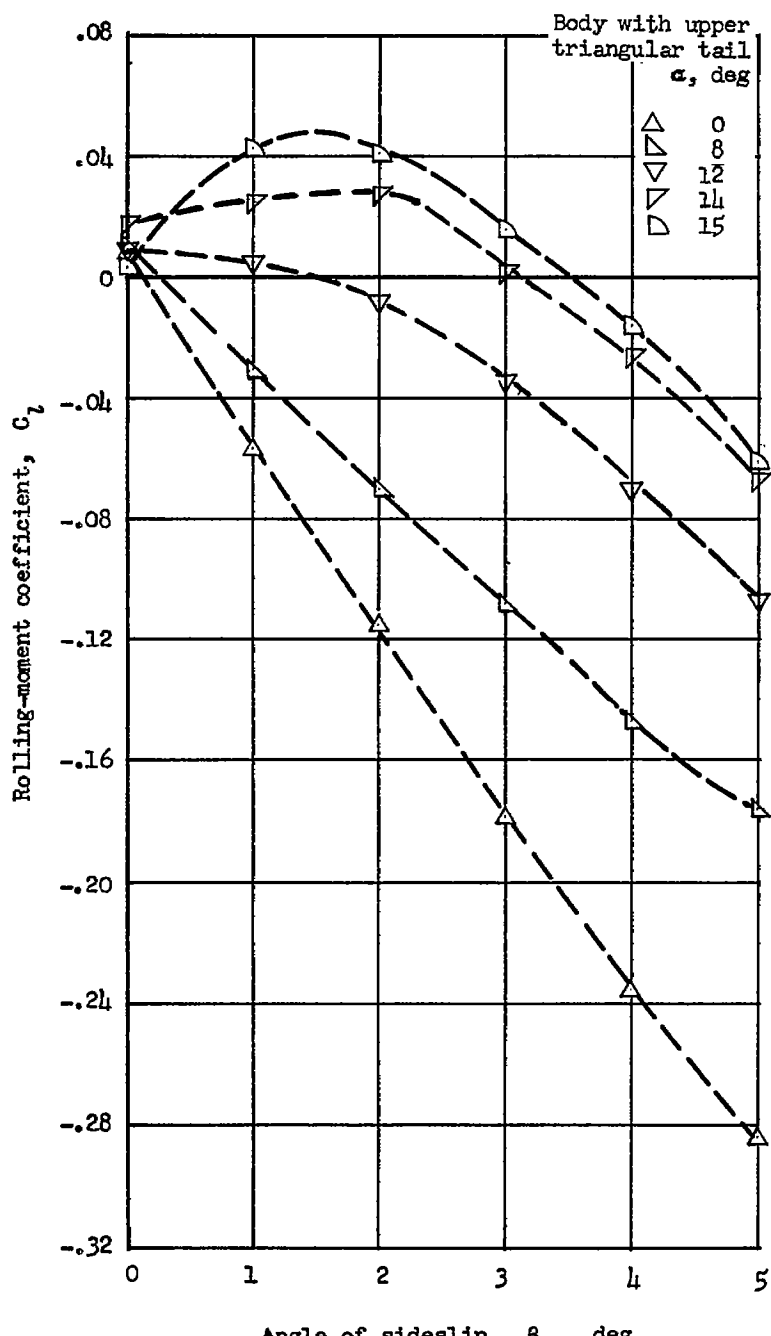
(b) Trapezoidal tails.

Figure 13.- Effect of angle of attack on the side force and rolling moments of a body with various tail configurations at $\beta = 4^\circ$.



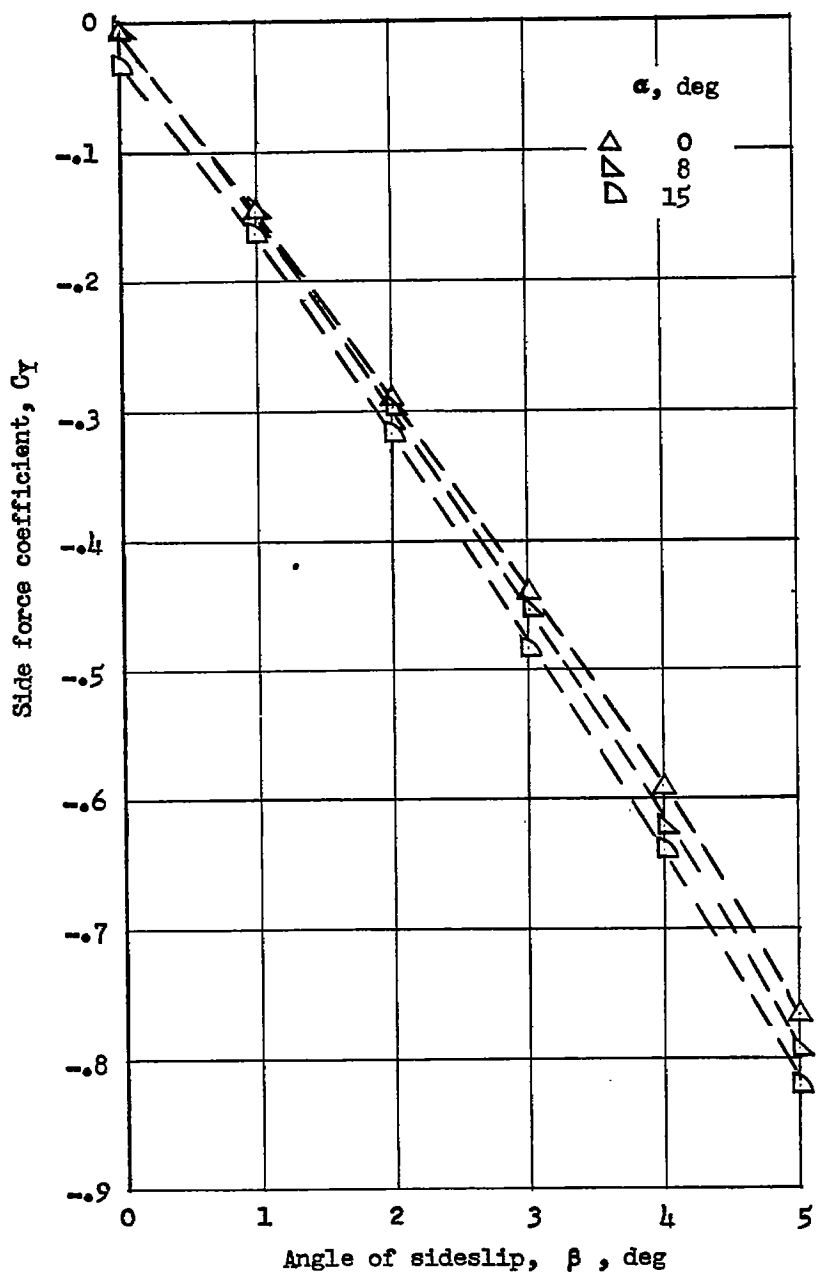
(a) Side-force coefficient.

Figure 14-- Effects of body vortices on an upper triangular tail in combination with an ogive-cylinder body.



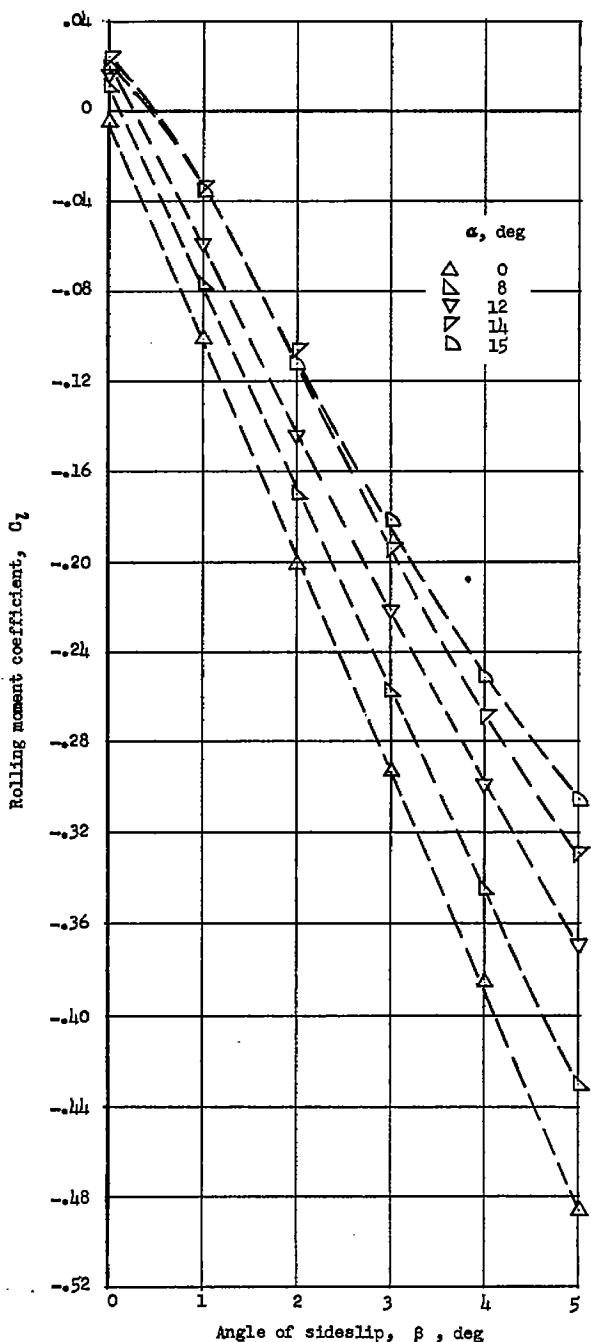
(b) Rolling-moment coefficient.

Figure 14.- Concluded.



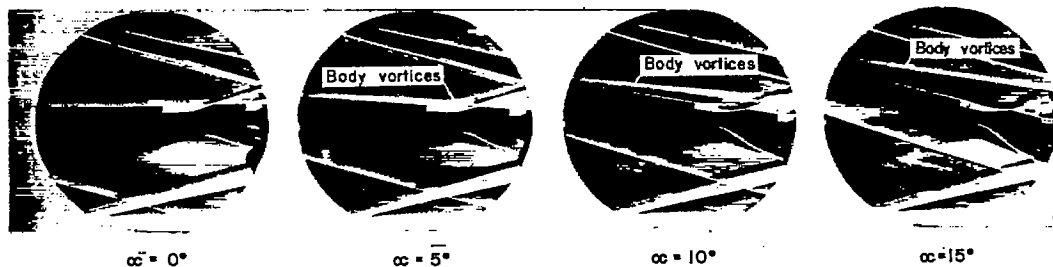
(a) Side-force coefficient.

Figure 15.- Effects of body vortices on an upper trapezoidal tail in combination with an ogive-cylinder body.

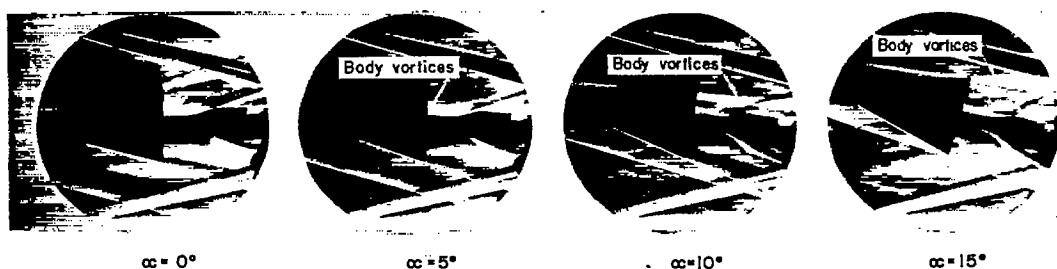


(b) Rolling-moment coefficient.

Figure 15.- Concluded.



(a) Configuration B.

(b) Configuration B($V_u V_l$)_{tri}.(c) Configuration BW_F.

I-58-1678

Figure 16.- Schlieren photographs of body vortices and wing flow fields.

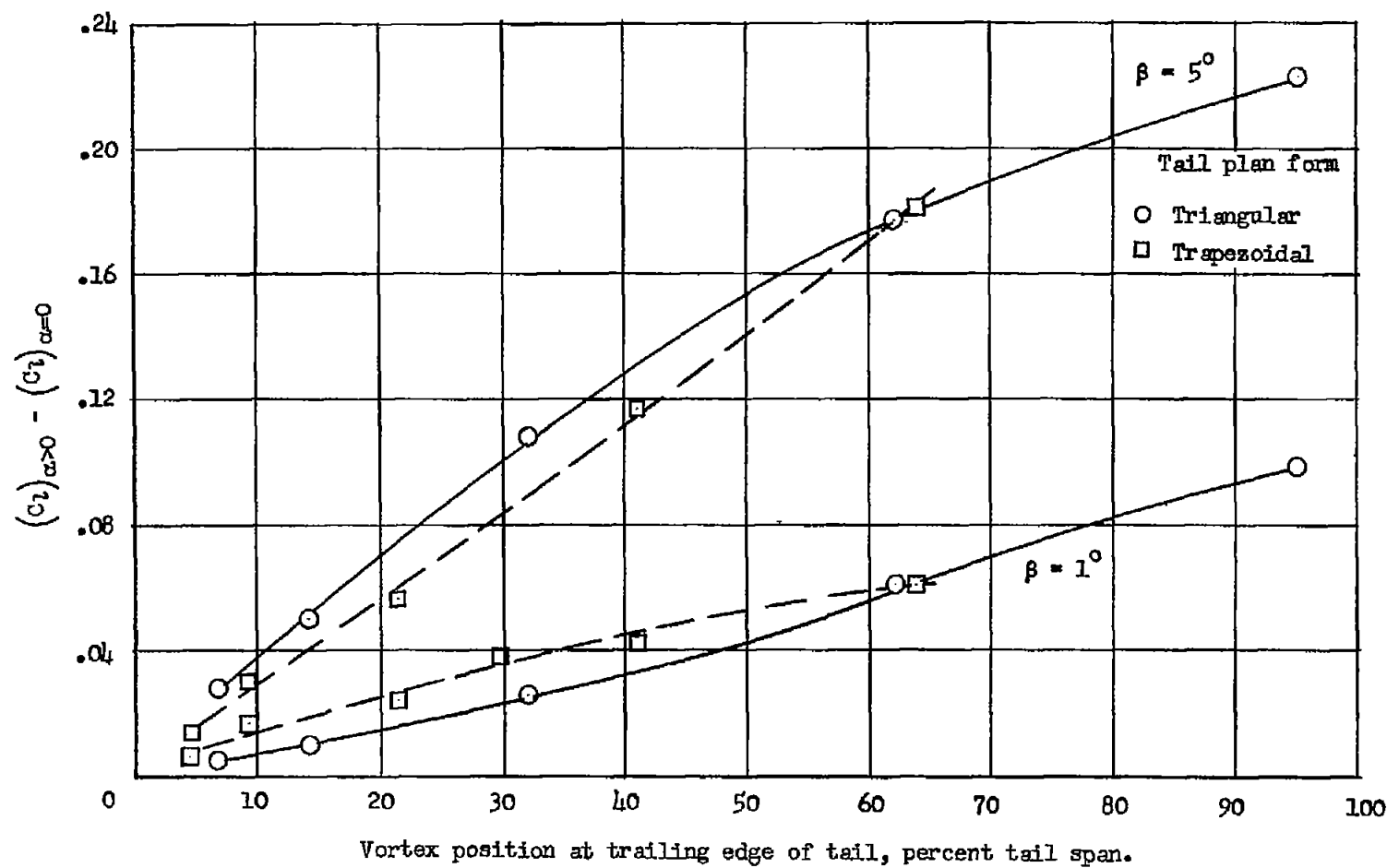


Figure 17.- Incremental rolling moment due to angle of attack plotted against vortex position for two configurations of body and upper vertical tail.

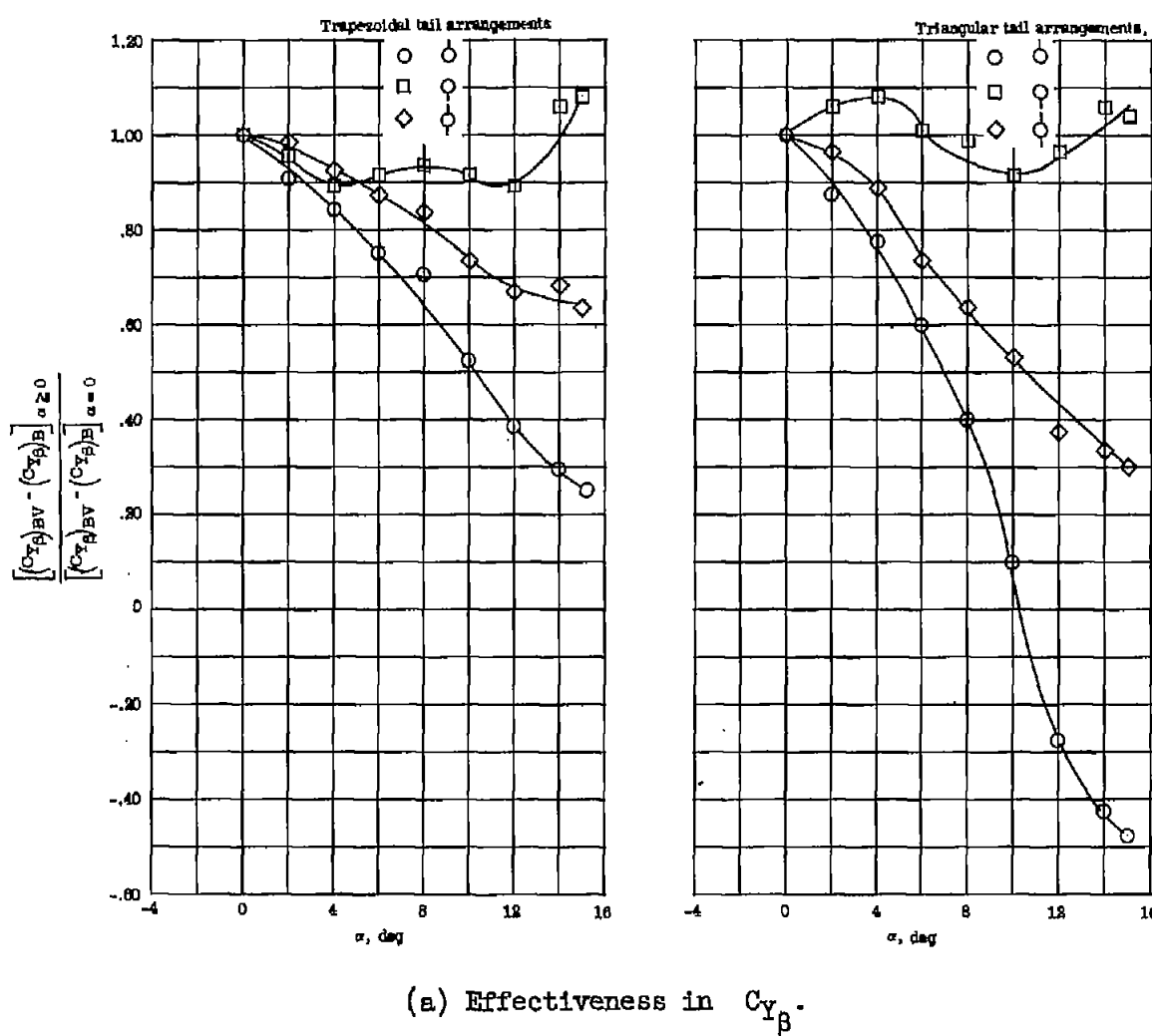


Figure 18.- Effectiveness in $C_{Y\beta}$ and $C_{l\beta}$ for several trapezoidal- and triangular-tail arrangements in combination with a body of revolution through an angle-of-attack range.

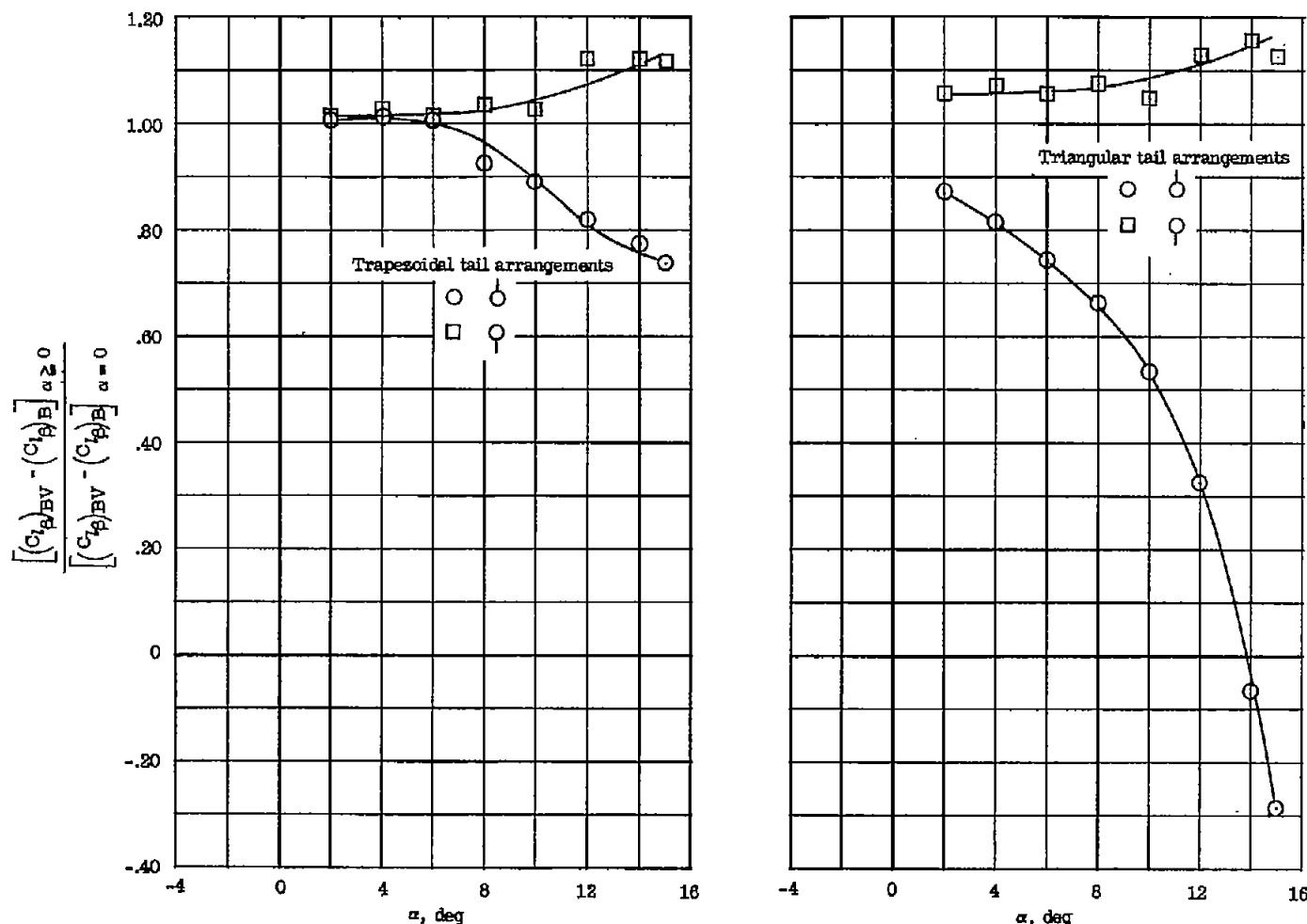
(b) Effectiveness in $C_{l\beta}$.

Figure 18.- Concluded.

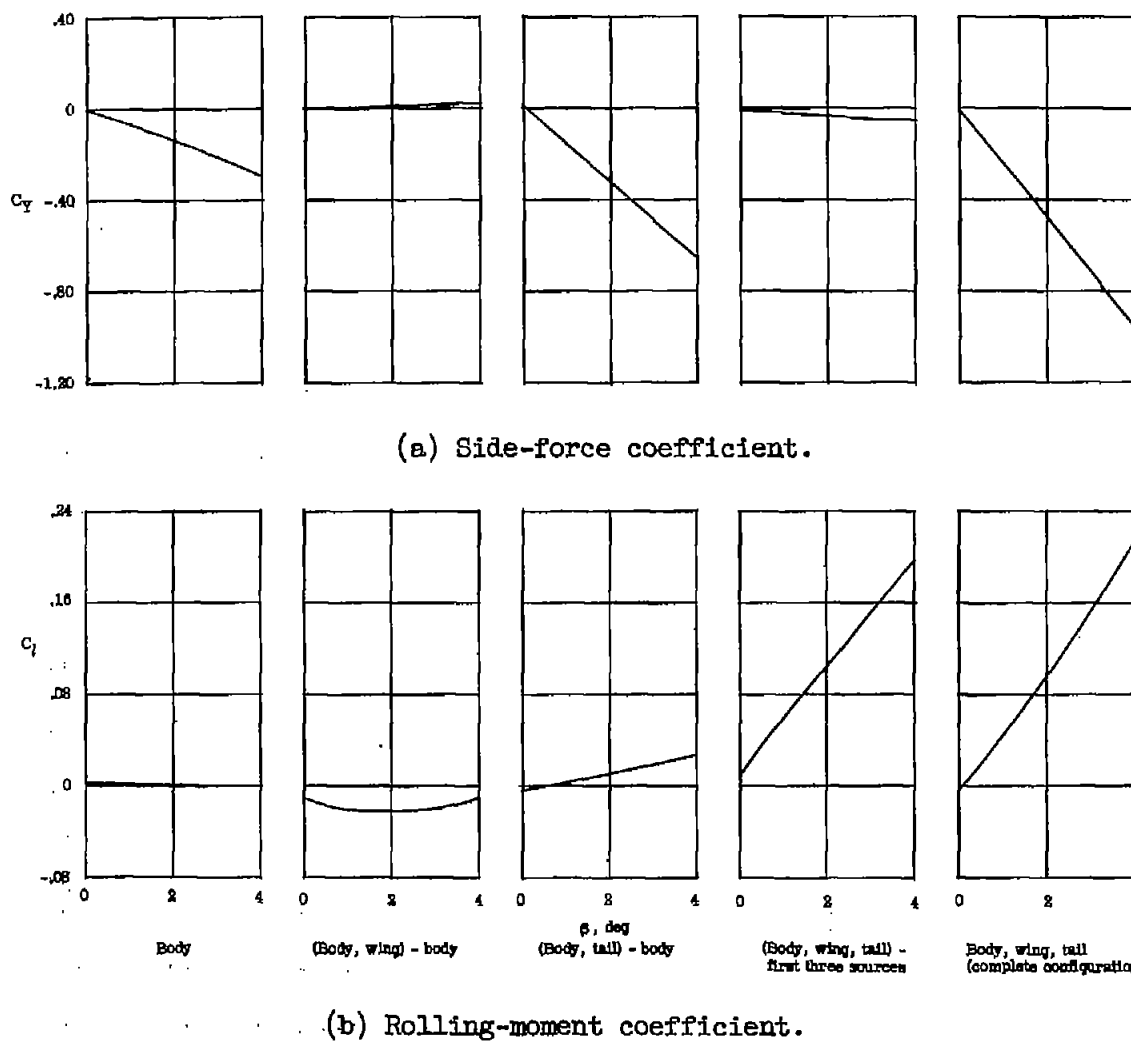
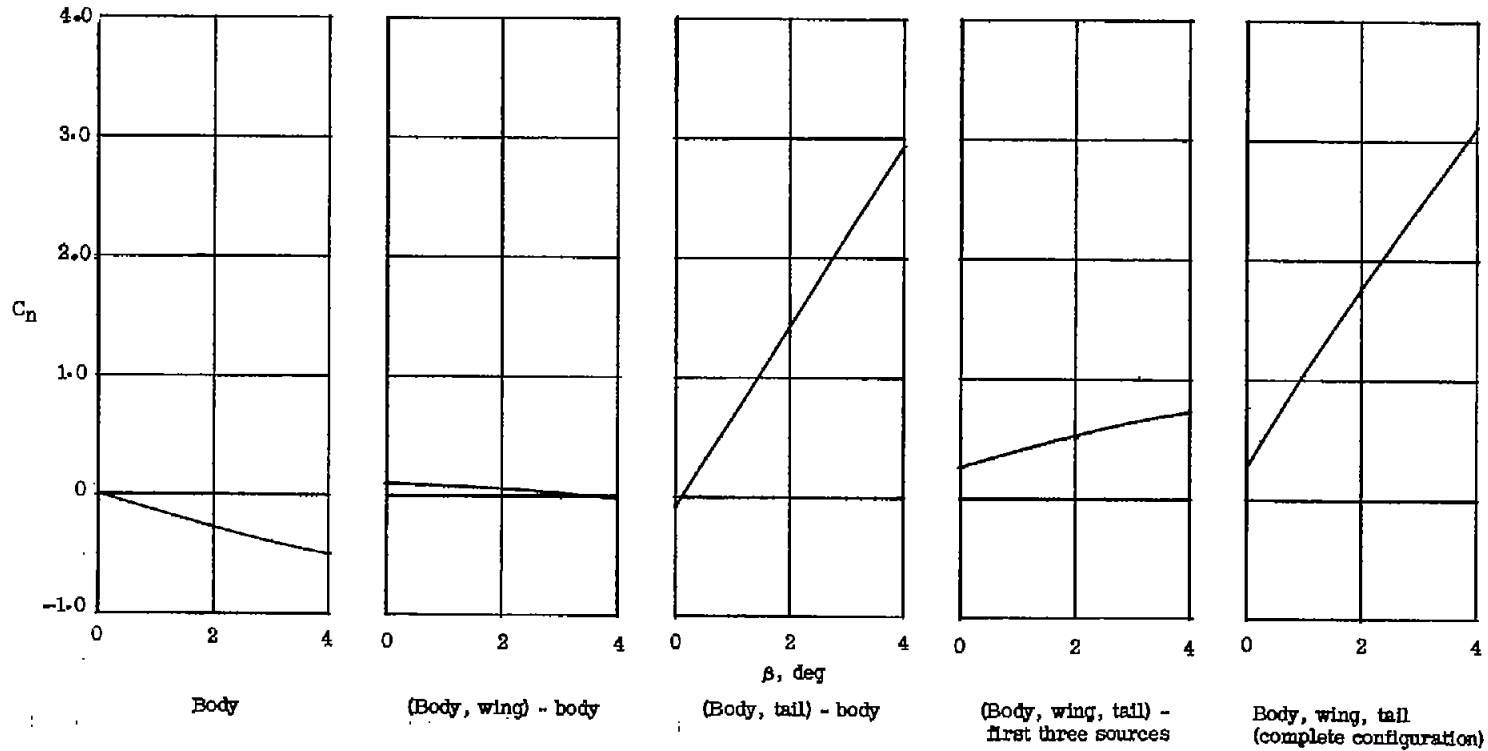
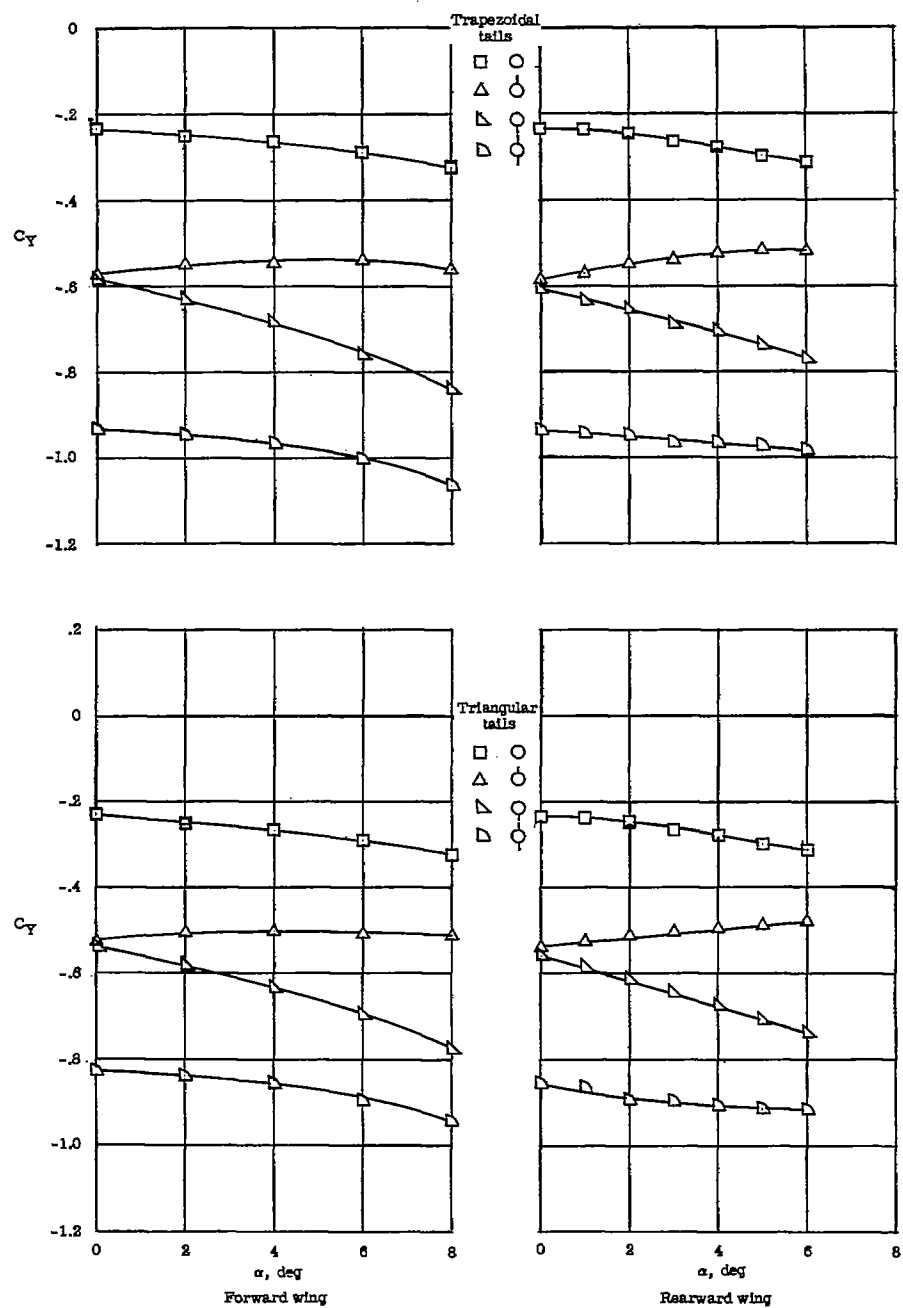


Figure 19.- Various sources of lateral forces and moments contributing to the resultant forces and moments of a body with forward wing and two vertical trapezoidal tails at $\alpha = 4^\circ$.



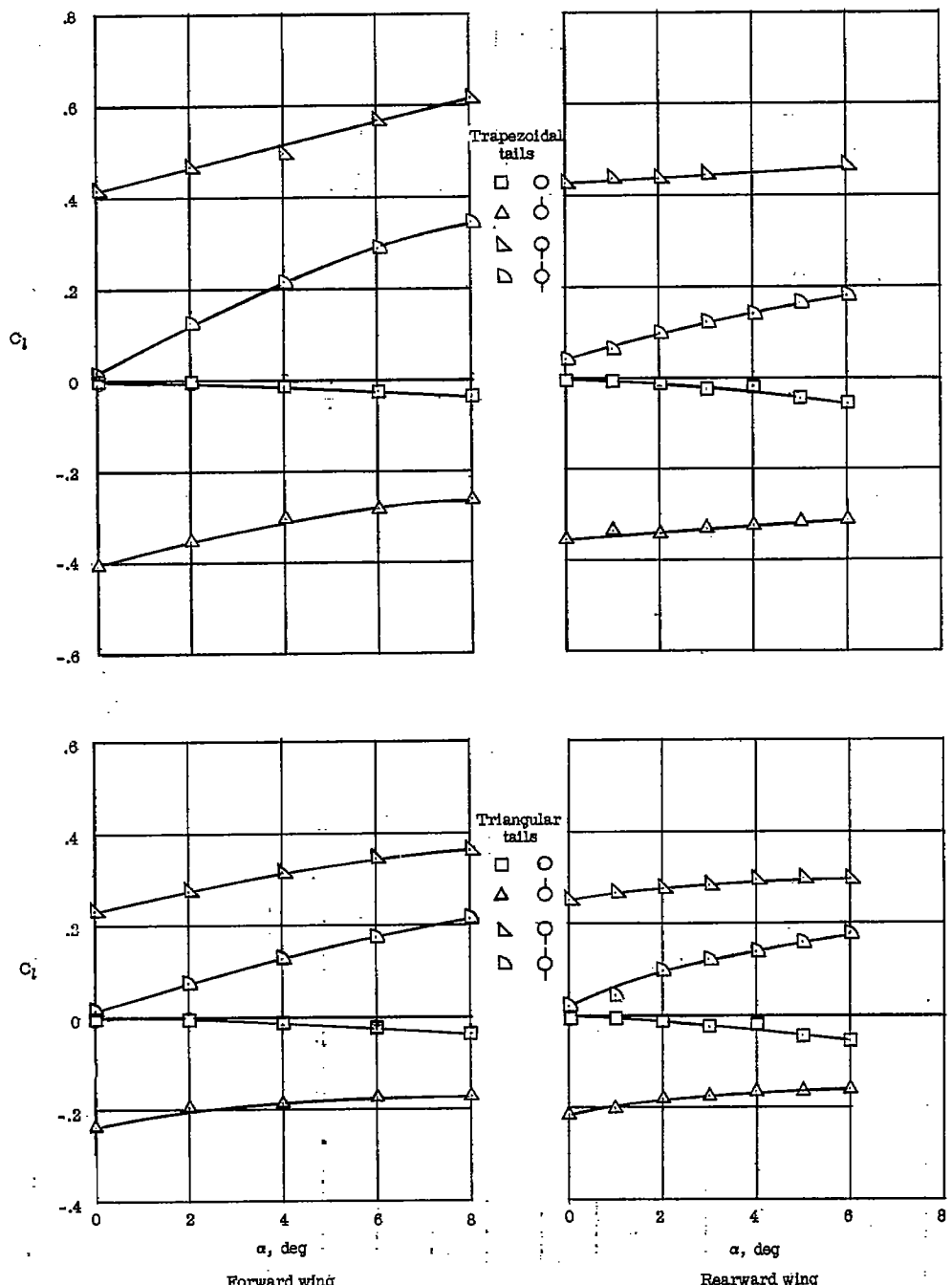
(c) Yawing-moment coefficient.

Figure 19.- Concluded.



(a) Side-force coefficient.

Figure 20.- Effect of angle of attack on C_y and C_l for a body-wing-tail configuration with various tail arrangements at $\beta = 40^\circ$.



(b) Rolling-moment coefficient.

Figure 20.- Concluded.

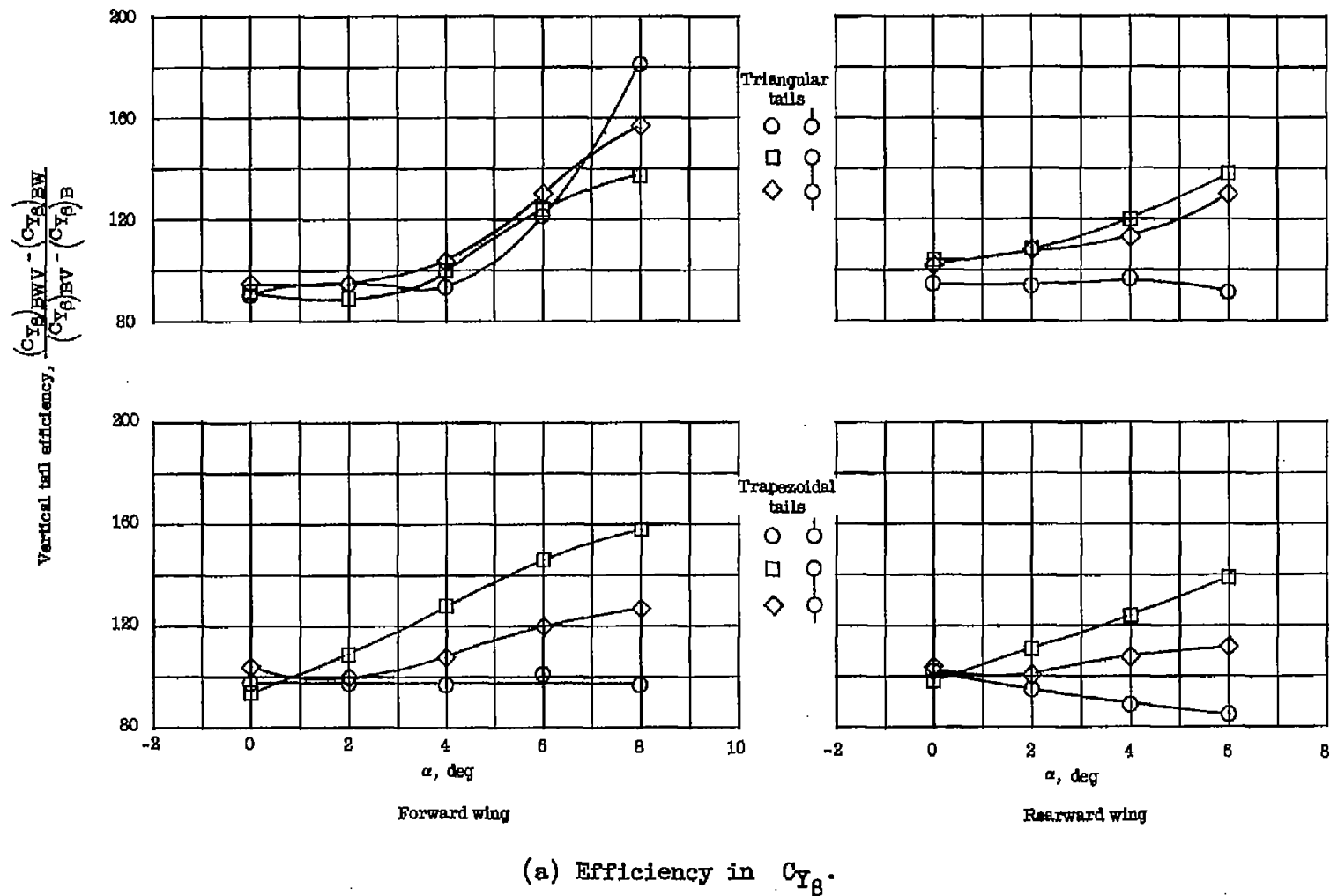


Figure 21.- Vertical-tail efficiency in $C_{Y\beta}$ and $C_{l\beta}$ for a number of vertical tails in combination with a body of revolution and a rectangular wing in two longitudinal positions.

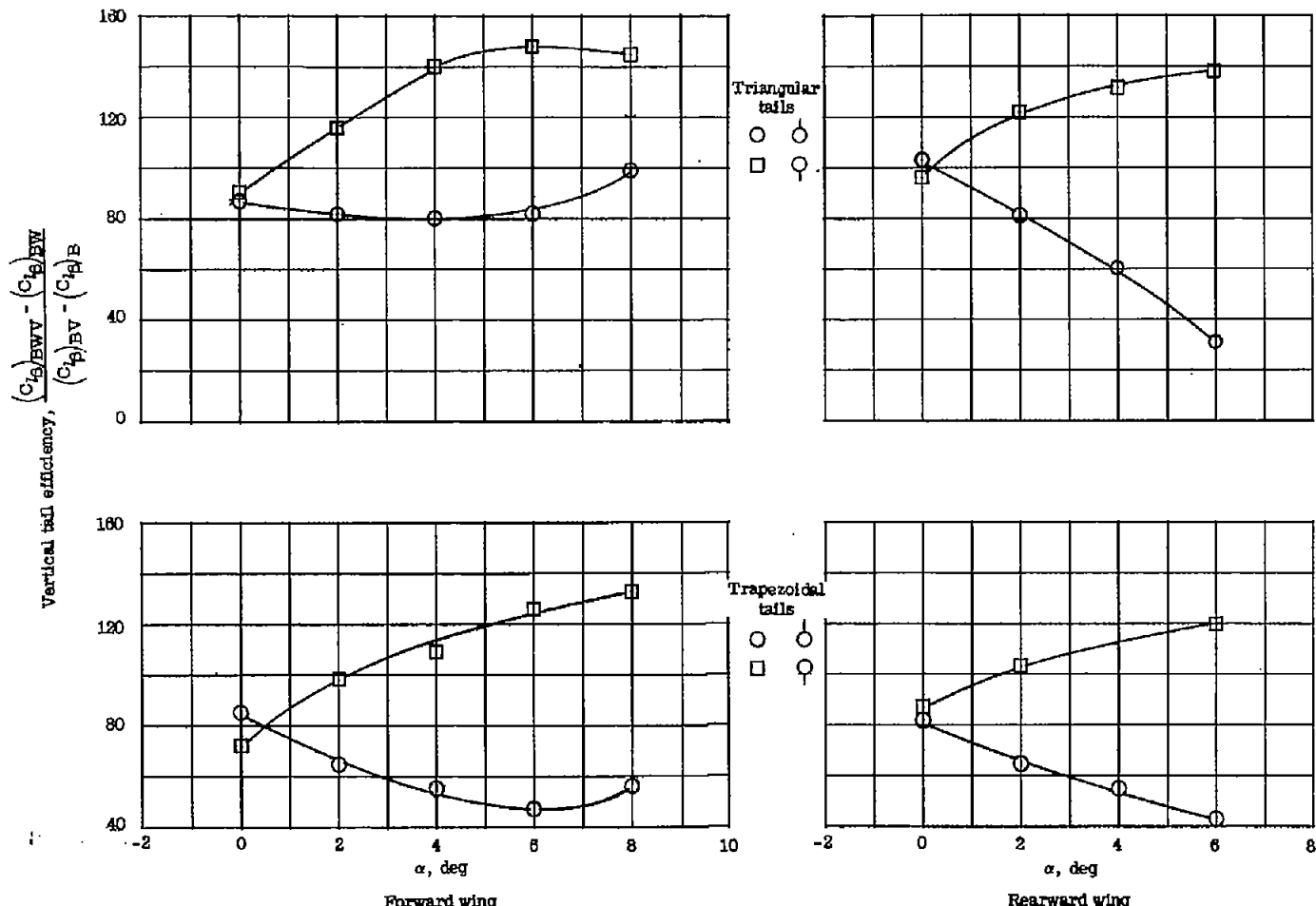
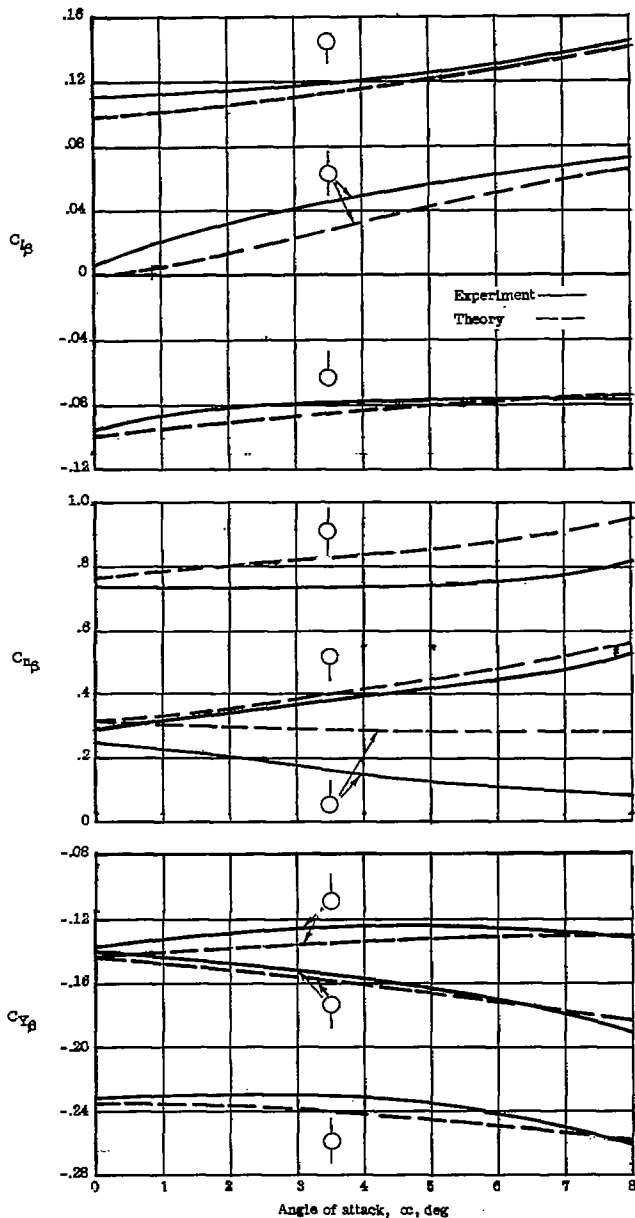
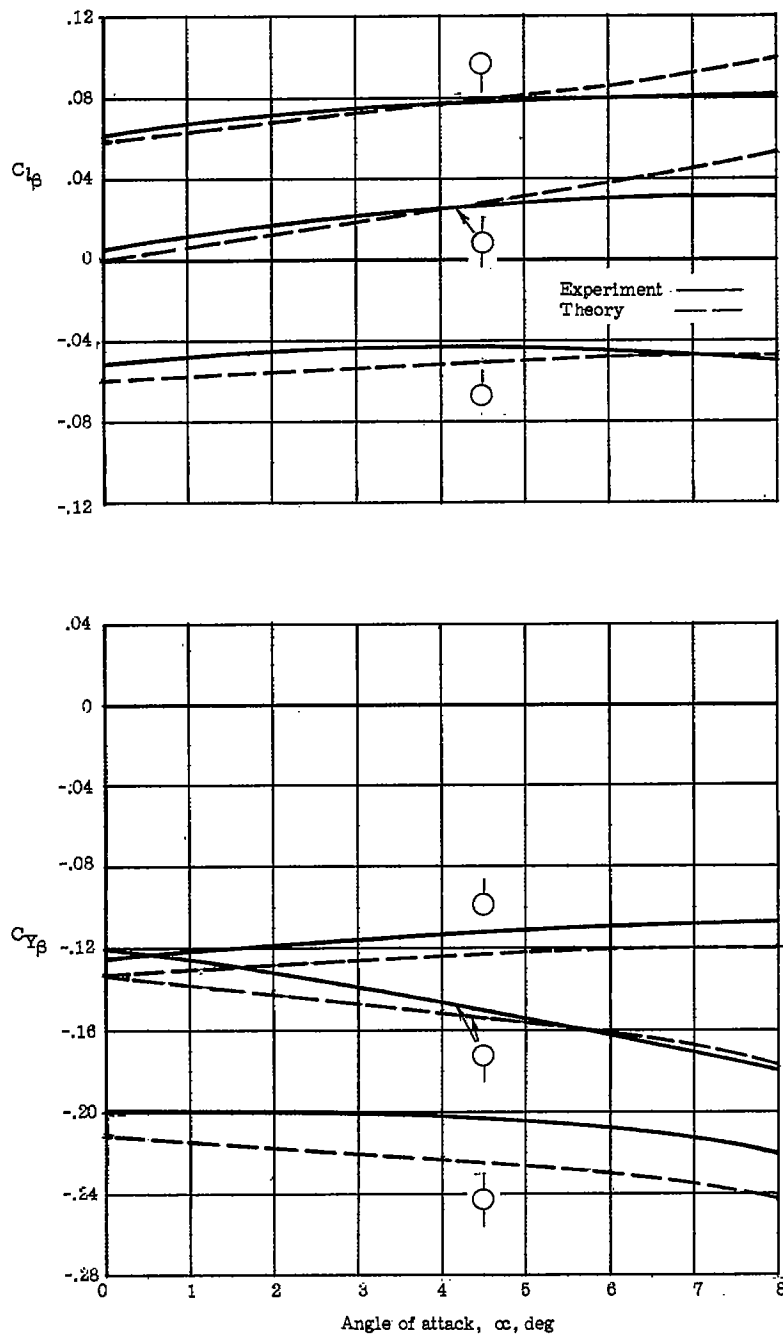
(b) Efficiency in C_{l_β} .

Figure 21.-- Concluded.



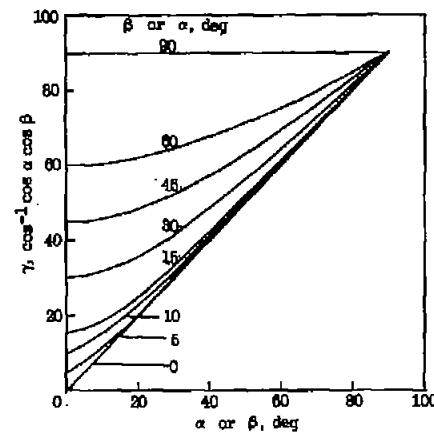
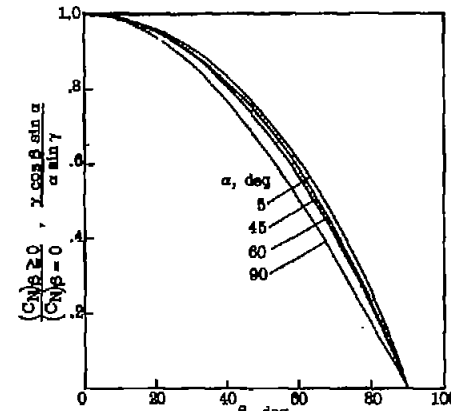
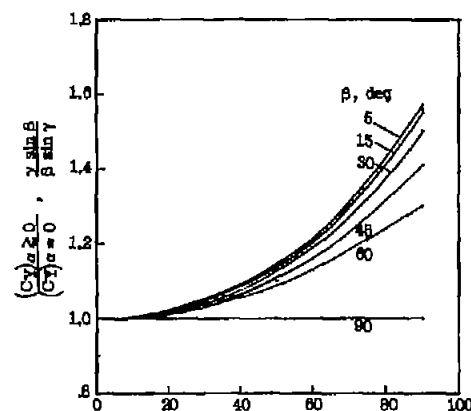
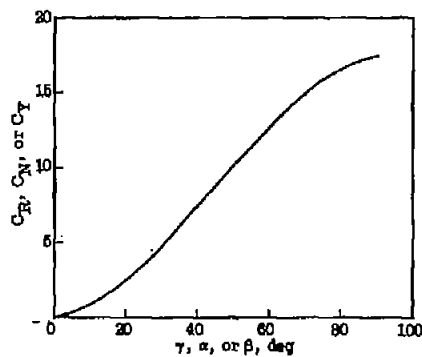
(a) Trapezoidal tails.

Figure 22.- Effect of angle of attack on the experimental and theoretical lateral stability parameters of several generalized missile configurations consisting of an ogive-cylinder body, a wing in the forward position, and various arrangements and plan forms of vertical tails.



(b) Triangular tails.

Figure 22.- Concluded.

(a) Resultant angles when α and β are combined.(b) Ratio of normal force for body at γ to that for body at α , assuming a linear force curve.(c) Ratio of side force for body at γ to that for body at β , assuming a linear force curve.

(d) Force curve from reference 2, showing more realistic nonlinearities of a body of revolution.

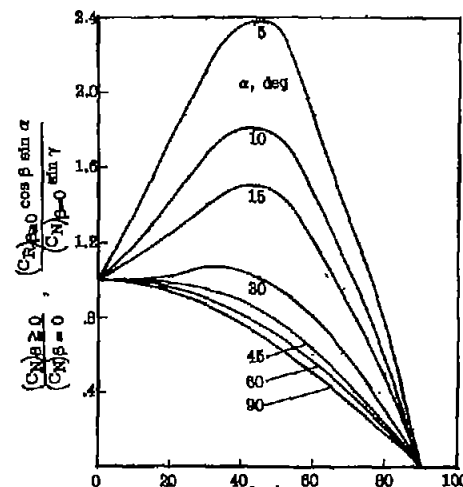
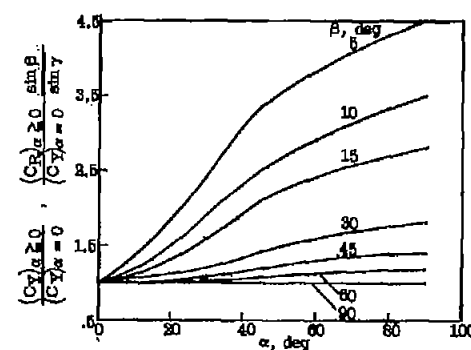
(e) Ratio of normal force for body at γ to that for body at α , assuming a more realistic nonlinear force curve.(f) Ratio of side force for body at γ to that for body at β , assuming a more realistic nonlinear force curve.

Figure 23.- Normal-force and side-force characteristics for a body of revolution at combined angles of attack and sideslip, illustrating equations contained in appendix B.